

Characterization of Pecan Shells for Value-added Applications

by

Brad Lavoy Littlefield

A thesis submitted to the Graduate Faculty of
Auburn University
in partial fulfillment of the
requirements for the Degree of
Master's of Science

Auburn, Alabama
August 9, 2010

Keywords: physical properties, flow properties,
thermal decomposition

Copyright 2010 by Brad Lavoy Littlefield

Approved by

Oladiran Fasina, Chair, Associate Professor of Biosystems Engineering
Joey Shaw, Alumni Professor of Agronomy and Soils
Sushil Adhikari, Assistant Professor of Biosystems Engineering
Brian Via, Assistant Professor of Forestry and Wildlife Sciences

Abstract

There is a growing need in the United States to decrease dependence on fossil fuels because of energy security and environmental concerns associated with their use. Energy derived from biomass is especially important to the southeast due to availability of vegetation and optimum climate conditions. Pecan shells, the by-product from the Pecan (*Carya illinoensis*) shelling process, are a potential biomass feedstock. In this study some of the physical characteristics of pecan shells (such as bulk, particle and tap densities, compressibility and flowability) that are important for its storage and process design were investigated. It was found that particle size and moisture content significantly affected the bulk, tap and particle densities. The porosity of pecan shells was significantly affected by particle size and moisture content as well. Hausner ratio was affected by particle size but not by moisture content. Mechanical compressibility was found to increase as particle size decreases and as moisture content increases. The mechanical compressibility of the samples increased with pressure and decreased particle size or increased moisture content. The flow behavior of pecan shells was not affected by particle size but moisture content indicated that lower moisture contents exhibited better flowability than pecan shells at higher moisture contents. Rate of moisture sorption was determined using the Page model and equilibrium moisture content and equilibrium relative humidity (EMC-ERH) relationships for pecan shells were sigmoidal in shape and best predicted by the Henderson and Chung-Pfost equations. The thermal decomposition

characteristics of pecan shells were examined in nitrogen and air atmospheres at heating rates of 5, 10, 20, 30, and 40 °C/min. Four main stages of mass loss were observed during the thermal decomposition of pecan shells: moisture evaporation, hemicelluloses decomposition, cellulose decomposition and lignin degradation. The moisture evaporation stage occurred within the temperature range of 30-150°C in both atmospheres. The thermal decomposition of pecan shells demonstrated mass loss rate peaks attributed to hemicelluloses decomposition (275-330°C and 270-331°C) and cellulose decomposition (348-386°C and 315-339°C) for nitrogen and air thermal decomposition, respectively, increasing with increased heating rate. The thermal decomposition of pecan shells was considered essentially complete at 600°C. Volatilized gases during thermal decomposition of pecan shells were analyzed using a Fourier-transform infrared spectrometer. Gaseous products volatilized during thermochemical conversion processes were identified and quantified by concentration. The major gases produced from nitrogen thermal decomposition of pecan shells were carbon dioxide (CO₂), carbon monoxide (CO), ethanol (CH₃CH₂OH) and acetic acid (CH₃COOH). The major gases produced from air thermal decomposition of pecan shells were carbon monoxide, carbon dioxide and methyl isocyanate (C₂H₃NO). A differential scanning calorimeter (DSC) was used to determine energy requirements at two temperature zones: moisture evaporation and thermal decomposition. It was found that the energy required to drive off moisture was more than the energy required to raise the pecan shells to thermal decomposition temperatures. The energy requirements at the two stages were not affected by heating rate. It was also found that the energy required in both temperature zones was about 30% of the energy contained in raw pecan shells.

Acknowledgements

First and foremost, I thank God for guiding me in the direction in which He knew was best for me. I would like to express my sincere gratitude to all of those in the Biosystems Engineering Department that helped, in any part, toward the finishing of my research. I was welcomed into the Department from my first day and I am very grateful to have been able to work in an environment that was always positive. I would like to especially thank those that served on my committee, Dr. Joey Shaw, Dr. Sushil Adhikari and Dr. Brian Via. I would also like to thank Dr. Oladiran Fasina for his guidance and providing the opportunity for me to earn my degree. I appreciate all the patience and knowledge that you shared with me during these past two years. I would also like to thank my wife, Laurel, without whom I would not have made it through these past few months. All of the love, support, understanding and patience you have given me during this endeavor was more than I could ever ask. Lastly, I would like to thank my parents (Brent and Gail) and the rest of my family and friends who have supported me throughout my academic career.

Table of Contents

Abstract	ii
Acknowledgements.....	iv
Table of Contents.....	v
List of Figures.....	ix
List of Tables	xi
Chapter 1. Introduction.....	1
Chapter 2. Literature Review.....	4
2.1. Bioenergy.....	4
2.2. Pecan Shells.....	6
2.3. Physical Characteristics.....	8
2.3.1. Particle Size	8
2.3.2. Bulk density	9
2.3.3. Particle density.....	10
2.3.4. Porosity	10
2.3.5. Hausner ratio.....	11
2.3.6. Compressibility.....	11
2.3.7. Flowability	12
2.3.8. Moisture sorption isotherms	17
2.3.9. Rate of Moisture Sorption.....	20
2.4. Thermochemical Conversion of Biomass.....	21
2.4.1. Chemical Composition of Biomass	21
2.4.2. Thermochemical Conversion Processes	23
2.4.2.1. Direct combustion	24
2.4.2.2. Gasification	24
2.4.2.3. Pyrolysis.....	25
2.4.2.4. Liquefaction	27
2.4.3. Thermo-analytical techniques for biomass thermochemical conversion	27
2.4.3.1. Thermogravimetric analysis.....	27
2.4.3.2. TGA-FTIR	28
2.5. Determination of Energy Requirement at Different Thermal Decomposition Temperatures	30
2.6. Summary.....	31
2.7 References.....	32

Chapter 3. Effect of Moisture and Particle Size on Physical Properties of Pecan Shells.....	40
3.1. Introduction.....	40
3.2. Materials and Methods	42
3.2.1. Preparation	42
3.2.2. Particle Size Distribution	42
3.2.3. Mechanical Separation of Pecan Shells	43
3.2.4. Compositional Analysis.....	45
3.2.4.1. Energy Content	45
3.2.4.2. Ash Content.....	45
3.2.4.3. Ultimate Analysis.....	46
3.2.4.4. Structural Carbohydrates.....	46
3.2.5. Poured Bulk Density	48
3.2.6. Particle Density	49
3.2.7. Tap Bulk Density	49
3.2.8. Hausner Ratio.....	50
3.2.9. Porosity	50
3.2.10. Mechanical Compressibility	51
3.2.11. Flowability	51
3.2.12. Rate of Moisture Sorption.....	53
3.2.13. Equilibrium Moisture Isotherm.....	55
3.2.14. Data Analysis.....	56
3.3. Results and Discussion	56
3.3.1. Particle Size Distribution	56
3.3.2. Chemical Composition Analysis.....	57
3.3.2.1. Energy and Ash Content	57
3.3.2.2. Ultimate Analysis.....	58
3.3.2.3. Structural Carbohydrates.....	59
3.3.3. Particle Size Effect on Physical Properties of Pecan Shells	60
3.3.3.1. Poured Bulk Density	60
3.3.3.2. Particle Density	61
3.3.3.3. Tap Bulk Density	62
3.3.3.4. Porosity	63
3.3.3.5. Hausner Ratio.....	63
3.3.3.6. Mechanical Compressibility.....	64
3.3.3.7. Flowability	65
3.3.4. Moisture Content Effect on Physical Properties of Pecan Shells	68
3.3.4.1. Moisture Adjustment.....	68
3.3.4.2. Particle Size Distribution	68
3.3.4.3. Poured Bulk Density	70
3.3.4.4. Particle Density	71
3.3.4.5. Tap Bulk Density	72
3.3.4.6. Porosity	73

3.3.4.7. Hausner Ratio.....	74
3.3.4.8. Mechanical Compressibility.....	75
3.3.4.9. Flowability	76
3.3.5. Rate of Moisture Sorption.....	79
3.3.6. Equilibrium Moisture Isotherm.....	83
3.4. Conclusions.....	87
3.5. References.....	89
Chapter 4: TG-FTIR analysis of pecan shells during thermal decomposition.....	93
4.1. Introduction.....	93
4.2. Methods and Materials	95
4.2.1. Sample Preparation	95
4.2.2. Thermal Decomposition Study	95
4.2.3. Fourier Transform Infrared Spectroscopy	96
4.2.4. Data Analysis	96
4.3. Results and Discussion.....	97
4.3.1. Thermal Decomposition of Pecan Shells in Nitrogen Atmosphere.....	97
4.3.2. Thermal Decomposition of Pecan Shells in Air Atmosphere.....	100
4.3.3. FTIR Analysis.....	104
4.3.3.1. Thermal Decomposition in Nitrogen Atmosphere.....	104
4.3.3.2. Thermal Decomposition in Air Atmosphere.....	109
4.4. Conclusions.....	114
4.5. References.....	116
Chapter 5. Determination of Energy Requirement at Different thermal degradation Temperatures.....	119
5.1. Introduction.....	119
5.2. Materials and Methods	120
5.2.1. Sample Preparation	120
5.2.2. Differential Scanning Calorimetry.....	120
5.2.3. Data Analysis	120
5.3. Results and Discussion	121
5.4. Conclusions.....	124
5.5. References.....	125
Chapter 6. Conclusion.....	126
Chapter 7. Future Work	129
Appendices.....	131
Appendix A. Effect of Particle Size Physical Property Data.....	132
Table A.1. Particle size distribution of pecan shells.....	132

Table A.2. Bulk density	133
Table A.3. Tap density	133
Table A.4. Particle density	133
Table A.5 Porosity	134
Table A.6. Hausner Ratio.....	134
Table A.7. Compressibility of pecan shells	134
Table A.8. Flow function data	135
Table A.9. Cohesion and angle of internal friction.....	135
Appendix B. Effect of moisture content on physical properties.....	136
Table B.1. Particle size distribution.....	136
Table B.2. Bulk density	136
Table B.3. Tap Density	137
Table B.4. Particle Density	137
Table B.5. Porosity	138
Table B.6. Hausner Ratio.....	138
Table B.7. Compressibility of pecan shells	139
Table B.8. Flow functions of pecan shells.....	140
Table B.9. Cohesion and angle of internal friction.....	141
Appendix C. Rate of Moisture Sorption of Pecan Shells	142
Figure C.1. Moisture change in pecan shells exposed to air at 25°C and relative humidity levels of 50, 65 and 80%.....	142
Figure C.2. Moisture change in pecan shells exposed to air at 35°C and relative humidity levels of 50, 65 and 80%.....	142
Figure C.3. Moisture change in pecan shells exposed to air at 50% relative humidity and temperatures of 15, 25 and 35°C.....	143
Figure C.4. Moisture change in pecan shells exposed to air at 65% relative humidity and temperatures of 15, 25 and 35°C.....	143
Appendix D. Equipment Photos	144
Figure D.1. Annular shear cell.....	144
Figure D.2. Texture analyzer with compression cell and tight fitting piston	144
Figure D.3. Compression cell with tight fitting piston filled with fine, medium and coarse pecan shell samples (left to right)	145
Figure D.4. Thermogravimetric analyzer (right) connected to Fourier-transform infrared spectrometer (left) by heated Teflon tube.	145

List of Figures

Figure 2.1 – Schematic illustrations of mass-flow and funnel-flow designed storage silos.....	13
Figure 2.2 – Consolidation and shear of Jenike Shear cell.....	14
Figure 2.3 – Typical plot of Mohr circles, used to analyze Jenike shear cell experiments.....	15
Figure 2.4 – Flow function graph.....	16
Figure 2.5 – Hemicellulose, cellulose and lignin in plant cell wall.....	23
Figure 2.6 – Main processes, intermediate energy carriers and final energy products from the thermochemical conversion of biomass.....	24
Figure 3.1 – Ripe pecan (left) and cracked pecans with shell (right).....	40
Figure 3.2 – Particle size distribution of pecan shells.....	44
Figure 3.3 – Kason vibrating screen separator.....	45
Figure 3.4 – Schematic diagram of rate of set up for moisture sorption study.....	54
Figure 3.5 – Particle size distribution of pecan shells.....	57
Figure 3.6 – Effect of particle size and pressure on the mechanical compressibility of pecan shells.....	65
Figure 3.7 – Flow functions of pecan shells fractions.....	66
Figure 3.8 – Particle size distribution of pecan shells at different moisture contents.....	69
Figure 3.9 – Effect of moisture content on the poured bulk density of pecan shells.....	70
Figure 3.10 – Effect of moisture content on particle density of pecan shells.....	71
Figure 3.11 – Effect of moisture content on the tap bulk density of pecan shells.....	73
Figure 3.12 – Effect of moisture content on porosity of pecan shells.....	74
Figure 3.13 – Effect of moisture content and applied pressure on the mechanical compressibility of pecan shells.....	76
Figure 3.14 – Flow functions of pecan shells at different moisture contents.....	77
Figure 3.15 – Cohesive strength of pecan shells at different moisture contents.....	79

Figure 3.16 – Moisture change in pecan shells exposed to air at 15°C and relative humidity levels of 50, 65 and 80%	80
Figure 3.17 – Moisture change in pecan shells exposed to air at 80% relative humidity and temperatures of 15, 25 and 35°C.	81
Figure 3.18 – Moisture sorption isotherms for pecan shells at 10, 20, 35 and 50°C	83
Figure 4.1 – Mass loss from thermal decomposition of pecan shells at different heating rates with nitrogen as carrier gas.....	98
Figure 4.2 – Mass loss rate from the thermal decomposition of pecan shells at different heating rates with nitrogen as carrier gas.....	99
Figure 4.3 – Mass loss from the thermal decomposition of pecan shells at different heating rates with air as carrier gas	101
Figure 4.4 – Mass loss rate from the thermal decomposition of pecan shells at different heating rates with air as carrier gas	103
Figure 4.5 – Three-dimensional spectral plot of the gases produced from the thermal degradation of pecan shells in nitrogen atmosphere at a heating rate of 30°C/min	104
Figure 4.6 – Concentration of the major gases volatilized during nitrogen thermal decomposition of pecan shells at heating rates of 5-40°C/min.....	107
Figure 4.7 – Concentration of the minor gases volatilized during nitrogen thermal decomposition of pecan shells at heating rates of 5-40°C/min.....	108
Figure 4.8 – Three-dimensional spectral plot of the gases produced from the thermal decomposition of pecan shells in air atmosphere at a heating rate of 30°C/min.....	110
Figure 4.9 – Concentration of the major gases volatilized during air thermal decomposition of pecan shells at heating rates of 5-40°C/min.....	112
Figure 4.10 - Concentration of the minor gases volatilized during air thermal decomposition of pecan shells at heating rates of 5-40°C/min.....	113
Figure 5.1 – Heat flow (W/g) of pecan shells pyrolysis at different heating rates	121

List of Tables

Table 2.1 – Flowability predictions based on compressibility of bulk solids.....	12
Table 2.2 – Classification of powder flowability by flow index	17
Table 2.3 – Chemical Constituents of Several Types of Biomass.....	21
Table 2.4 - Range of the main operating parameters for pyrolysis processes	26
Table 3.1 – Geometric mean diameter and geometric standard deviation of pecan shells fractions	57
Table 3.2 – Energy and ash content (dry basis) of pecan shells fractions	58
Table 3.3 – Carbon, hydrogen and nitrogen contents (dry basis) of pecan shells fractions	59
Table 3.4 – Cellulose, hemicelluloses and lignin contents (dry basis) of pecan shells fractions	60
Table 3.5 – Poured bulk density of pecan shells fractions.....	61
Table 3.6 – Particle density of pecan shells fractions.....	62
Table 3.7 – Tap bulk density of pecan shells fractions.....	62
Table 3.8 – Porosity of pecan shells fractions	63
Table 3.9 – Hausner ratio of pecan shells fractions.....	64
Table 3.10 – Flow index of pecan shells fractions.....	66
Table 3.11 – Cohesive strength (kPa) of pecan shells fractions	67
Table 3.12 – Angle of internal friction (AIF, °) of pecan shell fractions	68
Table 3.13 – Geometric mean diameters and standard deviation of pecan shells at different moisture contents.....	69
Table 3.14 – Hausner ratio of pecan shells at different moisture content levels	74
Table 3.15 – Flow index of pecan shells at various moisture contents.....	78
Table 3.17 – Angle of internal friction (°) of pecan shells at different moisture contents	79
Table 3.17 – Estimated values of moisture sorption rate constant (k), constant n and equilibrium moisture content (Me) obtained from non-linear regression analysis using Equation 3.20 for pecan shells	82

Table 3.18 – Model coefficients and values for the standard error of estimate (SEE), mean relative deviation (MRD) and coefficient of determination (R ²) for the temperature range of 10-50°C.....	86
Table 4.1 –Temperature (°C) peaks in mass loss rate for the main chemical constituents of pecan shells when thermally degraded in nitrogen and air	103
Table 4.2 – Effect of heating rate on the concentration (ml) of gases produced during thermal decomposition of pecan shells in nitrogen atmosphere.....	109
Table 4.3 – Effect of heating rate on the concentration (ml) of gases produced during thermal decomposition of pecan shells in air atmosphere.....	111
Table 5.1 – Energy requirements for moisture evaporation and thermal degradation of pecan shells at different heating rates.....	123

CHAPTER 1. INTRODUCTION

There is a growing need in the United States to decrease dependence on fossil fuel. National security, price stabilization, new government mandates placed on fossil fuel electricity producers and petroleum refineries and environmental concerns are primary reasons for the need to replace energy from fossil fuels with energy from renewable sources. Examples of environmental concerns include carbon dioxide emissions from fossil fuel power plants and the environmental effect of drilling (e.g. BP oil spill in Gulf of Mexico) and mining disasters (e.g. Upper Big Branch Mine (June 2010), West Virginia). Energy from biomass is an example of alternative energy that is applicable to the Southeast and has the potential to relieve some of the stress placed on fossil fuel energy production. Mean daily average temperatures of at least 10°C (50°F) and mean annual precipitation amounts of at least 114 cm (45 in.) create optimal conditions for producing biomass in the Southeast (Milbrandt, 2008). In addition, forest lands occupy at least 60% of the total land area in the states that are in the southeastern part of the United States (NASS, 2010). Energy by photovoltaic panels are not best suited due to government regulations which prohibit solar panels from existing on lands where minimum insolation values of six kilowatt-hours per square meter per day ($\text{Kwh/m}^2/\text{day}$) can be achieved (NREL, 2009). Most of the Southeastern U.S., including Alabama, have insolation values of 5 $\text{kWh/m}^2/\text{day}$ (NREL, 2009). Wind power is available in the Southeast, however wind requirements of class 5 wind power (6.4 – 8.0

m/s, 14.3 – 17.9 mph) are only available on off-shore sites on the Atlantic coast or Gulf of Mexico (DOE, 2008). New sites for hydropower have virtually been exhausted in Southeastern rivers and lakes (INL, 2006). Thus, biomass is the only viable renewable energy resource for the Southeastern part of the U.S.

Biomass is defined as organic materials that are plant or animal based (ASABE, 2006). A few examples of biomass are energy and agricultural crops, forestry and wood residues, food, feed, and fiber crop residue and agricultural wastes. Pecan shells are waste products obtained from shelling Pecan (*Carya illinoensis*). They can therefore be categorized as a secondary biomass feedstock (ASABE, 2006). Pecan shells have been utilized in a variety of applications, such as a source of activated carbon (Paraskeva et al., 2008), mulch (Brison, 1974) and smokeless fuel briquettes (Blesa et al., 2001).

Pecan shells are, however, a bulk solid. Characterization of the physical properties of pecan shells is required for efficient design and selection of handling, processing and storage equipment and facilities (Woodcock and Mason, 1987). This information is currently lacking for pecan shells.

In addition, thermal behavior of pecan shells during thermal decomposition must be quantified to assess the possibility of utilizing pecan shells as a feedstock for thermochemical processes (e.g. gasification or pyrolysis). These processes are used to convert biomass feedstocks such as pecan shells into value-added products.

Therefore, the main objective of this study is to quantify the properties of pecan shells that are essential for process design and value added utilization. To achieve this, the following tasks were carried out:

- (1) Quantify the effect of particle size and moisture content on the physical properties (particle size distribution, bulk density, tap bulk density, particle density, porosity, Hausner ratio, compressibility, flowability, moisture sorption rate and equilibrium moisture content) of pecan shells,
- (2) Determine the rate of thermal decomposition and quantify the composition of gas volatilized at temperatures of 30 – 800°C; and
- (3) Determine the energy required to thermally decompose pecan shells.

CHAPTER 2. LITERATURE REVIEW

2.1. Bioenergy

The last decade has proven to the United States and other countries around the world that are fossil fuel dependent that renewable and sustainable sources of fuel and energy are needed. Rising transportation fuel costs, environmental implications of greenhouse gas emissions and energy security are the motivation for increased renewable energy research. Bioenergy is one form of renewable energy that is derived from biomass or organic materials that are plant or animal based (ASABE, 2006). Other examples of renewable energy are solar, hydro, geothermal and wind. However, biomass is the only source of carbon in which the conversion to solid, liquid and gaseous energy sources can be produced (McKendry, 2002a). Economic considerations, environmental issues, specifically greenhouse gas emissions, energy security and price stabilization are all well known advantages of renewable energy. Recently, the United States government has introduced new policies and incentives for renewable energy research and development to try and alleviate some of the environmental and economic issues caused by the dependence on foreign sources of fossil fuels, such as renewable portfolio standards (RPS). RPS is a regulation that requires the increased production of energy from renewable energy sources, such as wind, solar, biomass or geothermal. The RPS mechanism generally places an obligation on electricity production companies to produce a specified fraction of their electricity from renewable energy sources. July 2008 marked

the highest crude-oil per barrel cost at \$137.11 (www.eia.doe.gov). Despite the oil prices falling again to roughly \$70 per barrel, the need for renewable energy remains.

Worldwide, the demand for energy and its resources is increasing exponentially with outgrowth of population and urbanization. Since 1973 the energy resources have doubled in developed countries but the demand remains higher. World energy demand is expected to increase approximately 2.5 times the present level by the year 2030 (Goyal et al, 2008; EIA, 2008). The depletion of fossil fuels and the greenhouse gas emissions dilemma suggest that future energy supplies must come from renewable and sustainable sources.

Biomass is regarded the renewable energy source with the highest potential to contribute to the energy needs of modern society for both developed and developing economies world-wide (Bridgwater, 2003). In contrast to other forms of renewable energy, biomass can be a substitute for all fossil-fuel based products, using a wide variety of technologies for conversion into solid, liquid and gaseous products. In addition, biomass is used in traditional ways, such as the burning of biomass for heat and cooking (EIA, 2008). In 2007 the United States produced approximately 102 quadrillion BTUs (10.7×10^{13} MJ) of energy and roughly 6.8 quadrillion BTUs (7.2×10^{12} MJ), or 7%, were from biomass (www.eia.doe.gov). The ‘Billion Ton Report’ was introduced in 2005 which outlined the ability of the United States to produce 1.36 billion tons of biomass for the production of bioenergy, which is sufficient enough to replace more than 30% of the petroleum fuel consumption in the country (Perlack et al., 2005).

Biomass stores energy during the process of photosynthesis. This energy can be recovered by thermochemical conversion processes into more usable forms, such as

ethanol, bio-oils and producer gases (Mani et al., 2004). Combustion, gasification and pyrolysis are three forms of thermochemical conversion processes in which biomass is converted to sources of energy. Direct combustion is the oldest form of energy where biomass is burned in an air atmosphere to convert chemical energy stored in biomass into heat, mechanical power or electricity (Demirbas, 2004; McKendry, 2002b). Combustion of biomass produces hot gases at temperatures at approximately 900-1000°C (McKendry, 2002b) Pyrolysis is the thermal degradation of biomass by heat in the absence of oxygen, which results in the production of charcoal (solid), bio-oil (liquid) and fuel gas products (Demirbas and Arin, 2002). Pyrolysis is usually conducted at temperatures ranging from 400-600°C (ASABE, 2006). Converting biomass into a combustible gas mixture by partial oxidation of biomass is the conversion process known as gasification and occurs at temperatures of 800-900°C (McKendry, 2002b). Thermochemical conversion processes of converting biomass to value-added energy products are discussed further in Section 2.4.2.

2.2. Pecan Shells

Pecan (*Carya illinoensis*) is a tree nut crop grown primarily in the southern and eastern portions of the United States, Mexico, Israel and Australia. The United States is responsible for more than 80% of the world's production (Geisler, 2009). Pecans are the only native tree nuts grown for commercial use in the U.S. and are considered the most important tree nut crop due to their export potential (Wood et al., 1994). In 2008, the U.S. exported approximately 52.4 million kilograms of pecans valued at \$238.5 million dollars (Geisler, 2009). Top pecan production states include Georgia, New Mexico,

Texas, Arizona and Oklahoma. Alabama produced approximately 2.7, 5.4 and 3.6 million kilograms of pecans in the 2006-2008 crop years, respectively (NASS, 2009).

Pecans can be found growing in their original habitat and in a semi-domesticated form where wild trees have been cleared from competing trees and brush. These pecans are called wild or native and improved, respectively (Harris et al., 1986). Pecans also grow in orchards or dooryard plantings where they have been vegetatively propagated. The commodity value of improved varieties is higher than native or wild pecans because of the desired characteristics exploited by genetic manipulation. Pecans are sold as an agriculture commodity on an in-shell or shelled (nutmeat only) basis. Approximately 54.5 million kilograms of pecan shells are produced annually from shelling operations in the United States (USDA-NASS, 2009).

Pecan shells are currently only utilized in a few ways. For example, pecan shells are used for mulching due to their slow breakdown, relative permeability, tannic acid composition and they are relatively light-weight. Pecan shells added to soils can increase acidity levels specifically for vegetation that thrive in acidic soil, such as azaleas, camellias and magnolias (Brison, 1974). However, excessive applications of pecan shells to soil can kill grass, weeds and other vegetative plants that are sensitive to soil pH. Other known uses for pecan shells range from meat smoking in combination with hardwoods (i.e. hickory), charcoal briquettes, imitation fire logs, glue and soap abrasives. Pecan shells have also been utilized as a source of activated carbon for water filtration purposes (Ng et al, 2003; Bansode et al., 2003; Johns et al., 1999).

2.3. Physical Characteristics

Pecan shells, similar to other agricultural crops and residues, are a bulk solid. Bulk solids consist of many random particles or granules of different sizes, densities and perhaps chemical compositions grouped together (Woodcock and Mason, 1987). The design and selection of storage, handling and transportation facilities and equipment is dependent upon the bulk solid behavior. Efficient and proper use of processing equipment and facilities could result in savings in handling costs, reduction in waste materials and improved utilization of labor, machines and space (Shamlou, 1988). In order to define the bulk solid behavior of pecan shells, determination of the individual particles that form the bulk solid must be quantified. Particulate size, shape, density, size distribution and surface area are some of pecan shells particle properties that are influential of its bulk solid behavior. Bulk density, tap density, particle density, compressibility, porosity, flow properties and equilibrium moisture content and relative humidity are bulk properties needed to properly characterize pecan shells in bulk form.

2.3.1. Particle Size

Particle size is crucial to the behavior of bulk material (Paraskeva et al., 2008). This is because it is directly used to calculate properties such as surface area and volume of individual particles that make up the bulk material. Size is always represented as a distribution due to the shape and size variability throughout the bulk material. There are several determination methods to quantify particle size, including mechanical sieving, digital imagery and laser-length scattering method. Most researchers rely on the sieving procedure because of the relative ease of use, simple analysis and lower capital cost of

equipment. The ASABE standard S319.4 (ASABE, 2008) is often used to estimate the geometric mean diameter and standard deviation of agricultural materials.

2.3.2. Bulk density

Bulk density is defined as the ratio of bulk mass of a material to its bulk volume. There are three different types of bulk density: poured, tap and aerated. Bulk density of agricultural materials is a key parameter that not only is important for the economic impact on transportation costs, but also affects the design and operation of conveyors, storage silos, processing and heat equipment (Woodcock and Mason, 1987).

Poured bulk density is the most common measurement technique for determining bulk density. This is obtained by pouring a sample into a container of known volume. The ratio of the mass of the material that filled the container to the volume of the container is determined as poured bulk density (Barbosa-Canovas et al., 2005).

Tap bulk density, sometimes referred to as vibrational compressibility, is the ratio of mass of the material to the volume of the material after it has been dropped, or tapped, by its own weight from a height of 14 mm. Tap density can also be determined using tap density testers that use graduated cylinders for volume measurements. During measurements, the cylinders are systematically rotated with constant up and down tapping. This results in reduction in volume of material. The ASTM standard B527 is typically used for tap density determinations (ASTM, 2005). Tap density is important for transportation requirements for biological materials.

Aerated bulk density is a measure of the material's density when its particulates are at their most 'loosely packed' form. The procedure to measure aerated bulk density is

very complicated and thus most researchers usually do not measure bulk density using this technique (Barbosa-Canovas et al., 2005).

2.3.3. Particle density

There are two types of particle density; true and apparent. True particle density is calculated by taking the mass of the particulate and dividing by its volume, excluding open and closed pores. Apparent particle density is different only in that it includes the volume of closed pores on the surface of the particulate in the volume measurement (Woodcock and Mason, 1987). True density is often measured with a helium pycnometer (Colley et al., 2006) or by the toluene displacement method (Deshpande et al., 1993). Apparent particle density is best obtained from size measurements of the particles.

2.3.4. Porosity

Porosity is an indication of the voidage, or volume occupied by air spaces when particulate solids are placed in a container. Poured bulk density and true particle density are used in the calculation of porosity, using the following equation:

$$\varepsilon = 1 - \frac{\rho_b}{\rho_p} \quad (2.1)$$

Where ρ_b is bulk density and ρ_p is particle density. An average porosity calculation of 0.4 is normal for spheroid particles, whereas irregular shaped or very small particulates have higher porosity values (Woodcock and Mason, 1987).

2.3.5. Hausner ratio

The Hausner ratio is a function of the tap and poured bulk density (Equation 2.2).

$$H_R = \frac{\rho_t}{\rho_b} \quad (2.2)$$

Where, ρ_t is tap bulk density and ρ_b is bulk density. This ratio is important because it deals with properties relevant to moving, rather than static, powder (Barbosa-Canovas et al., 2005). Geldhart et al. (1984) proposed that Hausner ratios smaller than 1.25 are easily fluidized, while powders with Hausner ratios higher than 1.4 could present fluidization issues (Geldhart et al., 1984; Barbosa-Canovas et al., 2005)

2.3.6. Compressibility

Compressibility is a physical characteristic that is of significant importance during storage, handling and transportation of bulk materials. Unintentional compression can cause flow problems resulting from vibrations during transportation or by due to the compressive weight of the bulk material. Mechanical compressibility is a measure of the compressibility of a bulk solid caused by its own weight during storage. Mechanical compressibility (%) can be calculated by the relationships below:

$$Cm = 100 \left(\frac{V_i - V_f}{V_i} \right) = 100 \left(1 - \frac{\rho_{bi}}{\rho_{bf}} \right) \quad (2.1)$$

where, V_i is initial volume (cm^3), V_f is compressed volume (cm^3), ρ_{bi} is initial bulk density (kg/m^3) and ρ_{bf} is final (compressed) bulk density (kg/m^3). Fayed and Skocir (1997) used mechanical compressibility values to classify the flowability of materials, as shown in Table 2.1 below:

Table 2.1 – Flowability predictions based on compressibility of bulk solids (Fayed and Skocir, 1997)

Percent Compressibility	Bulk Solid Description	Flow
5 to 15	free-flowing granules	excellent flow
12 to 16	free-flowing powdered granules	good flow
18 to 21	flowable powdered granules	fair to passable flow
23 to 28	very fluid powders	poor flow
28 to 35	fluid cohesive powders	poor flow
33 to 38	fluid cohesive powders	very poor flow
> 40	cohesive powders	extremely poor flow

2.3.7. Flowability

Flowability of bulk solids is another characteristic that is important in the design of large scale storage silos and processing equipment. Flowability is a measure of the cohesiveness and adhesiveness of bulk solids and is influenced by other properties, such as bulk density, porosity and compressibility. Particles within bulk solids have a strong tendency to ‘stick’ to one another due to attractive forces between particles. Adhesion occurs when particles in storage silos or bins ‘stick’ to the walls or exterior surface of the storage container. Flowability tests are designed to quantify the cohesiveness or adhesiveness of bulk solids.

Silos are typically the main storage facility for agricultural materials. Usually, materials are gravity-discharged from the bottom of the silo. Funnel and mass flow are two types of flow that can dictate the design of storage silos (Figure 2.1). In mass flow, all the particles move downward when the outlet is opened resulting in uniform flow. During funnel flow, the material at the bottom of the silo and the material above the

outlet are the only particles that move while the rest of the particles remain still. Simply stated, mass flow results in ‘first in, first out’ sequence, whereas the funnel flow particle sequence is ‘first in, last out’. Funnel flow can result in flow problems such as ratholing, increased segregation and possible degradation of material over time for the stagnant material. Therefore, funnel flow designed silos are limited to coarse, free flowing and non-degradable bulk solids.

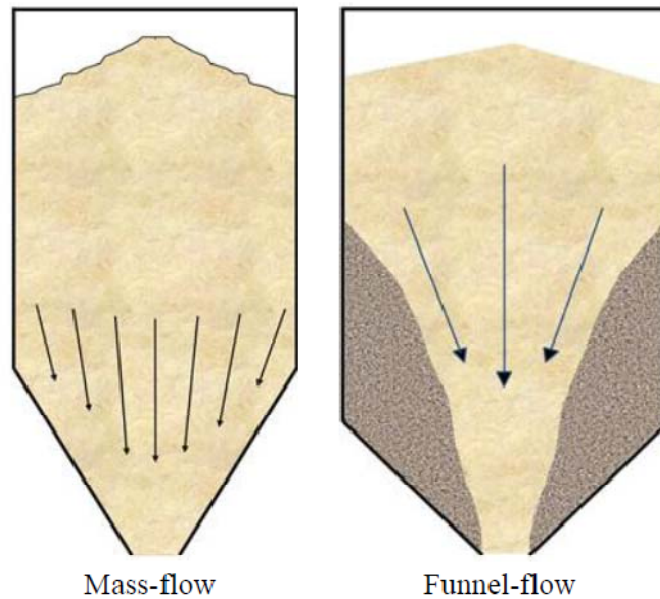


Figure 2.1 – Schematic illustrations of mass-flow and funnel-flow designed storage silos

Mass flow designed silos can have issues as well, such as channeling and arches that prevent discharge, known as ‘arching’. Arches can form via two different forces; mechanical and cohesive. Mechanical arches form from large particles interlocking with one another, whereas cohesive arches are caused by small particles consolidation to each other. Major flow complications (e.g. ratholing or arching) can result in damage to the silo or total structural failure. Flow problems can be averted if the materials flowability

characteristics are known and the storage silos, bins and hoppers are designed to prevent flow problems (Shamlou, 1988).

Flowability and cohesiveness of bulk solids is usually obtained by shear strength measurements, typically with the use of Jenike's tangential shear cell (Figure 2.2) developed in 1964 (Ganesan et al., 2008). Jenike's shear test measures the shear stress (τ) of a material while pressure (σ) is applied at various levels to the top of the material. At a specific normal force ($V = A\sigma$), the tangential force ($S = A\tau$) would increase until the material begins to fail or shear. The shear strength is obtained from the force required to fail the material.

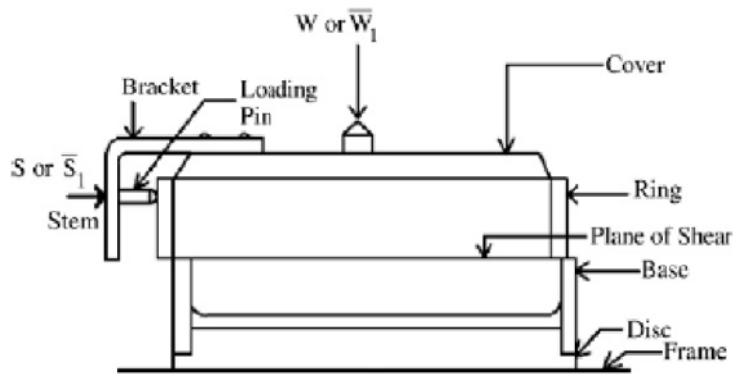


Figure 2.2 – Consolidation and shear of Jenike Shear cell (Ganesan et al., 2008)

The yield strength which a solid develops as it flows in a channel is an important criterion for determining the flowability of bulk solids. Yield locus (YL) is a plot of failure shear stress (τ , Pa or kPa) vs. normal stress (σ , Pa or kPa) for a given consolidating stress, as shown in Figure 2.3 below (Ganesan et al., 2008; Fitzpatrick et al., 2004):

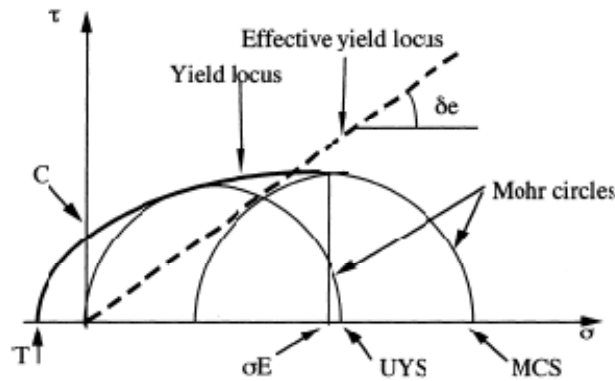


Figure 2.3 – Typical plot of Mohr circles, used to analyze Jenike shear cell experiments (Teunou et al., 1999).

Unconfined yield strength (UYS) is the compressive strength of a bulk solid and measured in units of pressure (Pa or kPa) (Schulze, 2006). UYS is a very important factor concerned with arching of bulk solids in silos (Jenike, 1964). The point of intersection of the Mohr circle (passing through the origin) and the normal stress (x-axis) determines UYS (Ganesan et al., 2008). Major consolidating stress (MCS) can also be determined from the Mohr circle, the point at which the circle passes through the steady state point and is tangent to the Yield Locus (YL), also measured in units of pressure (Pa or kPa). The effective angle of internal friction (AIF, δ_e) is a measure of the inter-particle friction as a bulk solid starts to slide itself at the onset of flow (Jenike, 1964), measured in degrees. Increases in pressure generally increase AIF, but not always (Ganesan et al., 2008). For any shearing to take place, the AIF of that material must be overcome. UYS and MCS are calculated by Equations 2.3 and 2.4 shown below:

$$UYS = \frac{2c(1 + \sin \varphi)}{\cos \varphi} \quad (2.3)$$

$$MCS = \left[\frac{A - \sqrt{A^2 \sin \varphi - \tau^2 \cos^2 \varphi}}{\cos^2 \varphi} \right] (1 + \sin \varphi) - \frac{c}{\tan \varphi} \quad (2.4)$$

Where, $A = \sigma + \frac{c}{\tan \varphi}$ and c is cohesion, defined as τ at $\sigma = 0$.

Flow function graphs are obtained by plotting the unconfined yield stress (Equation 2.3) vs. major consolidating stress (Equation 2.4) of a material, shown in Figure 2.4. This type of graph is very good at characterizing flow (Fitzpatrick et al., 2004; Teunou et al., 1999). The slope of the linear trendline (or line of best fit) is called flow function (FF). The inverse of the FF, called flow index (ff) is a dimensionless quantity used to classify materials flowability (Jenike, 1964). Classification of powder flowability by flow index developed by Jenike (1964) is shown in Table 2.2. All of the above properties are influenced not only by the physical nature of the particles themselves, but also by temperature, time of storage, moisture and chemical compositions (Ganesan et al., 2008).

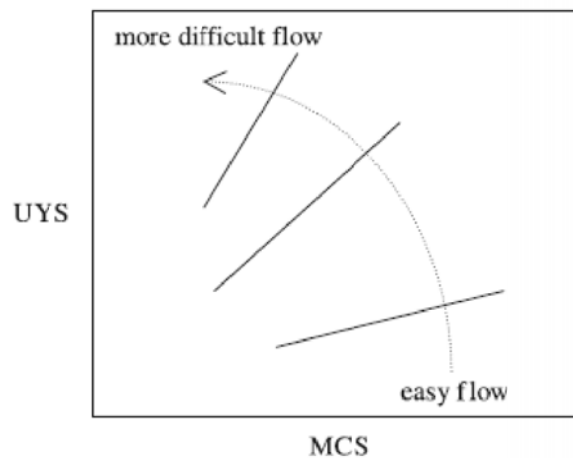


Figure 2.4 – Flow function graph (Fitzpatrick et al., 2004)

Table 2.2 – Classification of powder flowability by flow index (Jenike, 1964)

flow index (ff)	Flowability			
	Very cohesive ff < 2	Cohesive 2 < ff < 4	Easy flowing 4 < ff < 10	Free flowing Ff > 10

Although the use of Jenike’s shear cell is well established, its limitation is that the tests cannot be automated. This has led to the development of rotational shear testers, such as a ShearScan (Sci-Tec Inc., Worthington, Ohio).

2.3.8. Moisture sorption isotherms

Biological materials are hygroscopic in nature. Therefore, these materials have the ability to exchange moisture with the atmosphere (Colley et al., 2006). Knowledge of the equilibrium moisture content (EMC) and equilibrium relative humidity (ERH) relationship is crucial to the design of post harvest operations, such as storage, drying, aeration, handling, packaging and processing (e.g. shelling) of biological materials (Durakova et al., 2005; Pagano and Mascheroni, 2005; Erbas et al., 2005; Igathinathane et al., 2007). The equilibrium moisture content is the moisture content in which a hygroscopic material, such as pecan shells, is in equilibrium with the environment. The relative humidity of that environment is considered the equilibrium relative humidity. By plotting EMC vs. ERH at a particular temperature, moisture isotherm can be determined.

Moisture isotherm curves have been used to determine storage stability of biological materials when exposed to varying environmental conditions during storage and transportation (Erbas et al., 2005). They also provide a method for evaluation of

physical, chemical and microbiological parameters suitable and deteriorative reactions for the determination of stability of dry materials (Erbas et al., 2005; Leiras and Iglesias, 1991). EMC data can also determine the upper and lower limits of drying conditions for biomass (Labuza, 1984; Singh 2004). Singh (2004) determined the EMC of biomass briquettes at relative humidity ranges of 40-85% and reported that limited amounts of moisture are beneficial as the steam generated causes steam gasification reaction leading to better gas quality. However, high moisture in biomass briquettes can result in swelling, disintegration and prevention of application for thermochemical conversion (Singh, 2004)

In the drying of biological materials, the difference between the product's actual moisture content and the EMC is often used as a measure for the driving force (Banaszek and Sibenmorgen, 1993). Thermodynamic analysis of water sorption can also be determined from EMC-ERH data. Specific thermodynamic properties of biological materials that can be obtained from EMC-ERH relationships include the isosteric heat of sorption, free energy and entropy. Isosteric heat of sorption measures the binding energy or the force between water vapor molecules and the polar (active) sites of adsorbent surfaces, which is beneficial in estimating the heat requirement during drying and the state of absorbed water in the solid materials (Erbas et al., 2005; Labuza, 1984). The level of moisture at which the heat of sorption approaches the heat of vaporization of water is taken to be indicative of the amount of bound water in the material of interest. However, at moisture contents higher than this level, water is free in the void spaces of the system and readily available for microorganisms (Fasina and Sokhansanj, 1993).

There are more than 270 documented equations (theoretical, semi-empirical and empirical) have been documented to determine the EMC-ERH relationship of biological materials. Theoretical, or kinetic based, models are based on a monolayer or multilayer sorption where the material's physical properties are used as constants. Examples of theoretical isotherm models are the Langmuir, Brunauer-Emmet-Teller (BET) and Guggenheim-Anderson-deBoer (GAB). Empirical models require the use of non-linear regression from curve-fitting software to determine the model constants (Barbosa-Canovas et al., 2007). Traditional empirical isotherm models are the Halsey, Henderson, Chung-Pfost, Chen-Clayton and Iglesias-Chirife. However, no single equation accurately describes the relationship for all biological materials over a broad range of relative humidities and temperatures (Soysal and Oztekin, 1999). Models adopted as standard equations by the American Society of Agricultural and Biological Engineers (ASABE) are the modified Halsey, Modified Henderson, Modified Chung-Pfost, Modified Oswin and GAB (ASABE Standard D245.5, 2001). The Halsey equation was developed for food materials with high protein and oil contents whereas the Henderson and Chung-Pfost equations have been reported to be best suited for starchy foods (Fasina and Sokhansanj, 1993; Soysal and Oztekin, 2001). These equations have been utilized to model moisture sorption isotherms of various agricultural and biological materials such as amaranth grains (Pagano and Macheroni, 2005), medicinal and aromatic plants (Soysal and Oztekin, 2001), peanut hulls, kernels and whole pods (Correa et al., 2001), rapeseed (Sun and Byrne, 1998), rough rice, brown rice, corn kernels, corn cobs, soybeans and red beans (Chen, 2000), switchgrass pellets (Colley et al, 2006), pea seeds (Chen, 2003),

alfalfa pellets (Fasina and Sokhansaj, 1993), corn stover (Igathinathane, 2007), semolina and farina (Erbas et al., 2005) and poultry litter pellets (McMullen et al., 2005).

2.3.9. Rate of Moisture Sorption

In the previous section, it was mentioned that the hygroscopic nature of biological materials enables it to absorb or desorb moisture until equilibrium is reached with its environment. In this section, the rate at which moisture is absorbed or desorbed by biological materials is discussed. The Page empirical model, developed in 1949, has been widely used to describe the drying characteristics of various vegetables and fruits such as eggplant, red pepper, purslane and tomatoes (Doymaz and Pala, 2002; Doymaz, 2004; Kashaninejad and Tabil, 2004; Doymaz, 2007). Other mathematical models used to predict moisture sorption rate include: the Peleg model (Dadgar et al., 2004), exponential model (Colley et al, 2006; McMullen et al, 2005), two-term exponential model (Dadgar et al., 2004), Fick's diffusion model (Chhinnan, 1984; Dadgar et al., 2004). The Page model (Equation 2.5) was found to be best model for describing drying characteristics of rice kernel, tomatoes, field peas and apricots (Banaszek and Siebenmorgen, 1993; Doymaz, 2007; Dadgar et al., 2004; Akpinar and Bicer, 2004).

$$\frac{M-M_e}{M_i-M_e} = \exp(-kt^n) \quad (2.5)$$

where, t = time (min)

M = instantaneous moisture content (% w.b.)

M_i = initial moisture content (% w.b.)

M_e = equilibrium moisture content (% w.b.)

k = constant

n = constant

2.4. Thermochemical Conversion of Biomass

2.4.1. Chemical Composition of Biomass

Most biomass materials contain the same constituents; cellulose, hemicelluloses, lignin, ash and a small amount of other extractives. However, proportions of cellulose, hemicelluloses and lignin can vary drastically between materials. Table 2.3 below gives cellulose, hemicelluloses and lignin percentages (by mass) of several types of biological materials.

Table 2.3 – Chemical Constituents of Several Types of Biomass

Biological Material	Cellulose (%)	Hemicelluloses (%)	Lignin (%)
Birch Wood ^[a]	42.6	31.8	21.0
Fir ^[b]	48.9	11.9	31.2
White Pine ^[b]	53.3	12.3	26.7
Black Birch ^[b]	54.0	29.0	9.4
Poplar ^[b]	60.7	19.1	14.8
Rice Straw ^[b]	41.1	29.5	5.1
Corn Straw ^[b]	37.1	27.6	3.8
Olive Waste ^[a]	44.8	18.5	28.0
Wheat Straw ^[a]	43.6	27.3	21.7
Almond shell ^[c]	40.5	19.7	27.2
Hazelnut shell ^[c]	27.8	14.8	19.2
English walnut shell ^[c]	60.2	13.2	18.6
Macadamia nut shell ^[c]	25.8	11.7	47.6

^[a] Zanzi et al., 2003; ^[b] Liu et al., 2008; ^[c] Wartelle and Marshall, 2001

Cellulose, the most abundant polymer on earth, is a linear organic glucose polymer $(C_6H_{10}O_5)_n$, consisting of chains of (1,4)-D-glucopyranose units linked in the β -1,4-configuration with a molecular weight range of 300,000 to 500,000 Da (McKendry, 2002a). The crystalline portion of cellulose is insoluble and forms the skeletal structure of the cell (Yaman, 2004).

Hemicelluloses are shorter, complex polysaccharides containing several glucose chains that are also located with cellulose in the cell wall. Generally, hemicelluloses have the chemical formula $(C_5H_8O_4)_n$. Shorter chains of xylose, arabinose and galactose, 5-carbon monosaccharides, are connected in the hemicelluloses chains creating an amorphous branched polymer. Xylan is the most abundant hemicellulose polysaccharide in biological materials. The xylans exist in softwoods and hardwoods, composing of 10-30% of the dry weight of the species, respectively (Yaman, 2004). In contrast to cellulose, hemicelluloses are heterogenous branched polysaccharide that binds tightly (non-covalently) to the surface of the cellulose microfibril (McKendry, 2002a). Unlike cellulose, hemicelluloses are soluble in dilute alkaline solutions (Yaman, 2004).

Lignin is the second most abundant polymer on earth and the largest structure in the cell wall. Lignin is comprised of three carbon chains attached to six-carbon rings, called phenyl-propanes (Yaman, 2004). Lignin has several important functions in the cell wall, ranging from structure rigidity to water movement because of its hydrophobic nature. Woody plants species are typically composed of tightly bound fibers, giving a hard external surface from higher concentrations of lignin. Herbaceous plants are composed with more loosely bound fibers, indicating a lower proportion of lignin

(McKendry, 2002a). As shown in Figure 2.5, hemicelluloses, cellulose and lignin are the three main components that form a complex matrix in the plant cell wall.

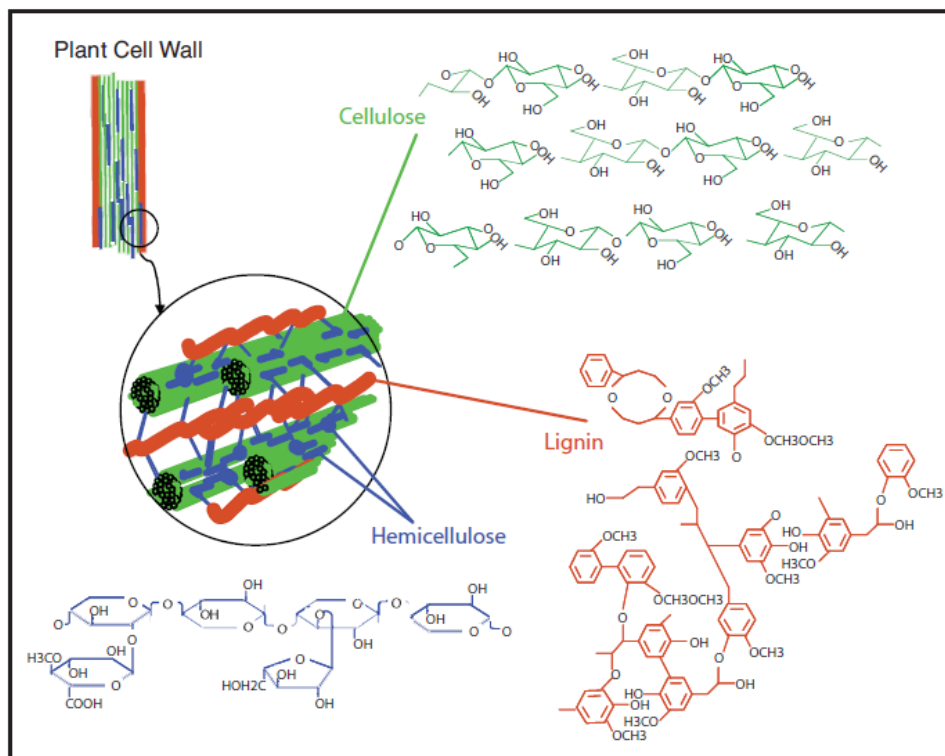


Figure 2.5 – Hemicellulose, cellulose and lignin in plant cell wall (Sierra et al., 2008)

2.4.2. Thermochemical Conversion Processes

Biomass can be converted to fuel, energy and value-added products by thermochemical processes, such as direct combustion, gasification, pyrolysis and liquefaction. The main processes, intermediate and final products that can be obtained from these thermochemical conversion processes can be found in Figure 2.6 below:

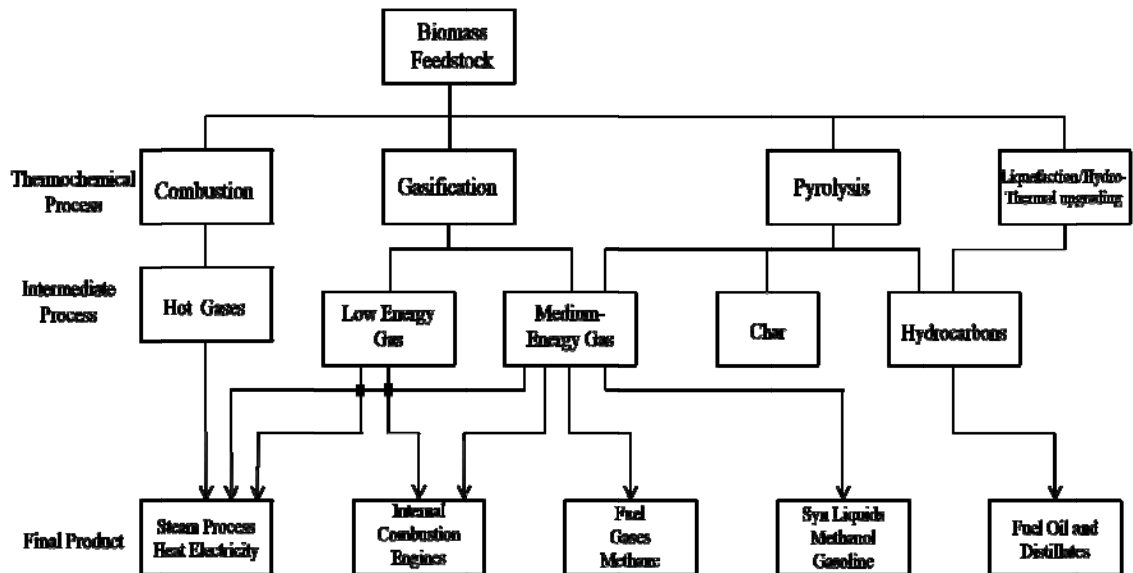


Figure 2.6 – Main processes, intermediate energy carriers and final energy products from the thermochemical conversion of biomass

2.4.2.1. Direct combustion

Direct combustion is defined as the burning of biomass in the presence of air so as to convert chemical energy stored in biomass into heat, mechanical power or electricity (ASABE, 2006; Goyal et al., 2008). Combustion of biomass produces hot gases at temperatures around 800-1000°C. It should be noted that combustion is feasible for any type of biomass with the condition that the moisture content of the material is less than 50% (wet basis) (Goyal et al., 2008). Volatile release, ash melting point, moisture content and thermal behavior of agricultural residues during combustion are important parameters for the design and operation of combustion systems (Werther et al., 2000).

2.4.2.2. Gasification

Gasification occurs at temperatures in the range of 750-850°C in an oxygen-deficient environment. The carbon-rich biomass is converted to a low calorific-value

gaseous fuel known as producer gas (ASABE, 2006). The producer gas is a mixture of carbon monoxide, hydrogen, carbon dioxide, methane and nitrogen which can be burned for heat or power, or further refined to form liquid fuels and chemicals (ASABE, 2006). The gas is regarded as more versatile than the original solid biomass and can be burned to produce heat or steam or used in gas turbines to produce electricity (Demirbas, 2001). Commercial gasifiers are available in a range of sizes and types utilizing a variety of materials, including wood, charcoal, coconut shells and rice husks (Demirbas, 2001).

2.4.2.3. Pyrolysis

Pyrolysis is carried out in the absence of oxygen at temperatures ranging from 400-600°C (ASABE, 2006). This process produces solid (bio-char), liquid (bio-oil) and gas compounds (methane, carbon dioxide and carbon monoxide). According to many researchers, pyrolysis is regarded as the most suitable technique for the thermochemical conversion of biomass to liquid fuels (bio-oil), charcoal, acetic acid, acetone and methanol (Bahng et al., 2009; Demirbas, 2001; Goyal et al., 2008; McKendry, 2002b). The pyrolysis process can be further subdivided into three classes: conventional (slow) pyrolysis (carbonization), fast pyrolysis and flash pyrolysis. The range of the main operating parameters for pyrolysis processes are given in Table 2.4.

Conventional, or slow, pyrolysis occurs under very slow heating rates (0.1-1°C/min). The slow heating rates enable higher char proportions instead of liquid and gaseous products (Demirbas and Arin, 2002). Slow pyrolysis has been used for centuries for the production of charcoal from wood. Das et al. (2008) conducted slow pyrolysis on

poultry litter and pine wood. They report product yields of 35-58% wt% liquid, 30-45% wt% solid char and 12-21% wt% non-condensable gases.

Table 2.4 - Range of the main operating parameters for pyrolysis processes (Demirbas and Arin, 2002)

	Conventional pyrolysis	Fast pyrolysis	Flash pyrolysis
Pyrolysis temperature (°C)	275 - 675	575 - 975	775 - 1025
Heating rate (°C/min)	0.1 – 1	10 – 200	> 1000
Particle size (mm)	5 – 50	< 1	< 0.2
Solid residence time (s)	450-550	0.5 – 10	< 0.5

A higher yield of liquid product is achieved in the fast pyrolysis procedure. Rapid heating rates ranging from 10-200°C/min are used to obtain a high-grade bio-oil. The fast heating rate allows the conversion of thermally unstable biomass compounds to liquid before they have a chance to form undesirable char (Bahng et al., 2009; Goyal et al., 2008). According to Bridgwater (2002), the fast pyrolysis procedure produces 60-75% wt% of liquid fuel, 15-25% wt% of char and 10-20% wt% of noncondensable gases, depending on the feedstock used. Because the fast pyrolysis process takes from a few seconds to a few minutes, the chemical reaction kinetics, heat and mass transfer processes and phase transition phenomena affect product distribution (Bahng et al., 2009; Bridgwater, 2002).

Flash pyrolysis has very short reaction times due to extremely fast heating rates (> 1000°C/min) (Demirbas and Arin, 2002). Particle size is important in the flash pyrolysis procedure because of the high heating rates. Many researchers have used flash pyrolysis to produce higher yields of liquid and gaseous products (Goyal et al., 2008). Sun et al. (2010) report product yields of 2-10% wt% char, 10-38% wt% liquid and 60-85% wt%

gaseous products for the flash pyrolysis of sawdust. Gercel (2002) suggest that the particle size should be approximately 105-250 μm . Reactor design for flash pyrolysis is also imperative to achieve high efficiency of conversion.

2.4.2.4. Liquefaction

Liquefaction is the thermochemical conversion of biomass (in liquid phase) at low temperatures (250-350°C) and high hydrogen pressures (100-200 bar) into stable liquid hydrocarbons (McKendry, 2002b). Liquefaction and pyrolysis are similar in that they both convert biomass into liquid products; however, liquefaction requires the use of a catalyst, such as sodium carbonate, to decompose macro-molecules into lighter molecules that repolymerize into oily compounds (Balat, 2008). The complexity of the reactors and fuel-feeding systems and overall higher capital than for pyrolysis processes has caused interest in liquefaction to remain low (McKendry, 2002b; Goyal et al., 2008).

2.4.3. Thermo-analytical techniques for biomass thermochemical conversion

Thermo-analytical techniques include thermo gravimetric analysis (TGA), differential scanning calorimetry (DSC) and differential thermal analysis (DTA). The thermal behavior of biomass and the kinetic parameters of the thermal reactions are examined with the use of these techniques (Murugan et al., 2008; Bahng et al., 2009).

2.4.3.1. Thermogravimetric analysis

Thermogravimetric analysis instruments are equipped with a balance that is used to monitor weight of the material as it is being heated. Reina et al. (1998) used TGA to

determine degradation, oxidation and reduction reactions, evaporation, sublimation and other heat-changes that occur in biomass. Mothe and Miranda (2009) used DTA-TGA methods to determine the decomposition of sugarcane bagasse and coconut fibers. Both TG curves of sugarcane and coconut fibers showed moisture evaporation temperatures of 100°C and 50°C, respectively. Sugarcane demonstrated mass loss at temperatures of 250-380°C, indicating hemicelluloses and cellulose decomposition. Mass loss peaks at temperatures of 320°C and 330°C are attributed to the decomposition of hemicelluloses and celluloses in sugarcane bagasse, respectively. Lignin degradation was determined to continue to 800°C and pyrolysis was determined to be essentially complete at 600°C. Coconut fibers demonstrated mass loss in the temperature range of 250-370°C with peaks at 300°C and 350°C indicating hemicelluloses and cellulose decomposition, respectively. Similar to sugarcane, coconut fiber lignin showed degradation until 600°C. The pyrolysis of coconut fiber was considered essentially complete at 800°C with 20% residual char (of original weight) remaining versus 15% residual char of sugarcane (Mothe and Miranda, 2009).

2.4.3.2. TGA-FTIR

Fourier transform infrared spectroscopy in combination with a thermogravimetric analyzer, TG-FTIR, is a well-known analytical tool for compositional analysis of evolved gaseous products from biomass pyrolysis (Bahng et al., 2009; Bassilakis et al., 2001). TGA combined with FTIR is a useful tool in dynamic analysis because it monitors continuously both the mass of the non-volatile material and the time dependent evolution of gases (Souza et al., 2009). Quantitative data are routinely obtained on about 20

commonly evolved volatile species, including water, carbon monoxide, carbon dioxide, carbonyl sulfide (COS), sulfur dioxide (SO₂), methane (CH₄), ethylene (C₂H₄), hydrogen cyanide (HCN), ammonia (NH₃), acetic acid, acetaldehyde, formic acid, formaldehyde, methanol, phenol, acetone and levoglucosan (Bassilakis et al., 2001; Bahng et al., 2009). One approach for measuring concentrations of these gases is based on evaluation of the concentration from the measured spectra using molecular spectroscopic databases, like HITRAN or QASOFT (den Blanken, 2008; Lee and Fasina, 2009). This approach is novel for FTIR spectroscopy with an intermediate resolution (Bahng et al., 2009; den Blanken, 2008). The combination of TGA and FTIR coupled together is extremely advantageous in the study of the pyrolysis because of the ‘real-time’ gas analysis. In other words, as soon as the volatilization of biomass occurs during pyrolysis, the gases volatilized are captured, sent through a pre-heated Teflon tube and analyzed in a FTIR to quantify and identify volatile compounds. There has been much research conducted on cellulose and lignin pyrolysis coupled with FTIR (Wang et al., 2007; Li et al., 2001; Bassilakis et al., 2001; Liu et al., 2008). There has also been extensive research with other biomass types, such as dry distiller’s grains with solubles (DDGS) (Guintoli et al., 2008), chicken manure (Guintoli et al., 2008), wood lignin (Liu et al., 2008), switchgrass (Lee and Fasina, 2009), coconut shells (Souza et al., 2009; Mothe and Miranda, 2009), corn stalk (Souza et al., 2009), peanut shells (Souza et al., 2009), tobacco (Bassilakis et al., 2001), wheat straw (Bassilakis et al., 2001) and sugarcane bagasse (Souza et al., 2009; Mothe and Miranda, 2009; Bilba and Ouensanga, 1996).

2.5. Determination of Energy Requirement at Different Thermal Decomposition Temperatures

Differential scanning calorimetry (DSC) is another analytical tool used to determine heat capacities, phase transition and thermal behavior of biomass, such as the energy used for heating during pyrolysis. Temperature ranges of thermal decomposition can be determined using TGA, however, the use of a DSC enables the determination of specific kinetic parameters during thermoconversion of biomass. DSC instruments calculate specific heat by measuring the difference in amount of heat required to increase the temperature of the sample (in the sample cell) versus the reference cell, measured as a function of temperature (Murugan et al., 2008). Enthalpy of pyrolysis is defined as the energy required to raise biomass from room temperature to the reaction temperature and convert the solid biomass into gaseous, liquid and char products (Daugaard and Brown, 2003). This value is important to the efficient design of pyrolysis reactors. The design of the system may vary with respect to heat transfer or sizing of the reactor to handle multiple biomass feedstocks (Daugarrd and Brown, 2003). Several researchers have used DSC in determining kinetic parameters necessary to model the kinetics of pyrolysis of biomass, such as lignin (Murugan et al., 2008), wheat straw (Stenseng et al., 2001), corn stalk (Cai and Chen, 2008), beech wood and artichoke thistle (Gomez et al., 2009), cotton stalk, peanut shells and pine (He et al., 2006) and palm oil mill by-products (Garcia-Nunez et al., 2008). Daugaard and Brown (2003) determined the enthalpy of pyrolysis of oak, oat hulls, pine and corn stover to be 2.0, 1.5, 0.8, 1.6 and 1.4 MJ/kg (dry basis), respectively. Moisture content is another important parameter in the consideration of biomass for thermochemical conversion by pyrolysis. It is feasible to thermally

decompose any type of biological material with a moisture content less than 50% (wet basis) (McKendry, 2002b). However, pre-drying of biological materials before thermochemical conversion can take place has an economic impact on the overall net energy conversion. Much is known about the energy required to evaporate pure water, however, less is known about the energy required to remove water from materials with strong water affinity, such as biological materials (Park et al, 2007). Park et al. (2007) determined the energy required to remove moisture from softwood fibers to be 2.36 and 2.24 KJ/g at moisture contents of 16.8% and 21.5% (wet basis), respectively.

2.6. Summary

The use of pecan shells as a feedstock for the production of renewable fuels through several thermochemical conversion processes is very promising. Understanding the effect of particle size and moisture content on the physical properties of pecan shells is needed for the proper design of equipment and facilities needed to store, transport and handle the material. The thermal behavior of pecan shells is also important to the efficient design of pyrolysis reactors or gasifiers. This knowledge will eventually result in waste reduction and improved utilization of labor, machines and storage space. Furthermore, the development of a large scale biorefinery for pecan shells will be crucial to its value-added utilization in the bioenergy economy.

2.7 References

- Akpınar, E.K., Bicer, Y. 2004. Modelling of the drying of eggplants in thin-layers. *International Journal of Food Science and Technology* 39: 1-9.
- Altunaş, E., Yildiz, M. 2007. Effect of moisture content of some physical and mechanical properties of faba bean (*Vicia faba* L.) grains. *Journal of Food Engineering*. 78: 178-183.
- ASABE Standard. 2000. D245.5 Moisture relationship of plant based agricultural products. St. Joseph, MI: ASABE.
- ASABE Standard. 2006. S593 Terminology and definitions for biomass production, harvesting and collection, storage, processing, conversion and utilization. St. Joseph, MI: ASABE.
- ASABE Standard. 2008. S319.4 Method of determining and expressing fineness of feed materials by sieving. St. Joseph, MI: ASABE.
- ASTM Standards. 2005. B 527. Standard test method for determination of tap density of metallic powders and compounds. West Conshohocken, PA: ASTM.
- Aydin, C. 2002. Physical properties of hazel nuts. *Biosystems Engineering* 82(3): 297-303.
- Bahng, M.K., Mukarakate, C., Robichaud, D., Nimlos, M. 2009. Current technologies for the analysis of biomass thermochemical processing: a review. *Analytica Chimica Acta* 651: 117-138.
- Balat, M. 2008. Mechanisms of Thermochemical Conversion Processes. Part 3: Reactions of Liquefaction. *Energy Sources, Part A*, 30: 649-659
- Balasubramanian, D. 2001. Physical properties of raw cashew nut. *Journal of Agricultural Engineering Research*. 78(3): 291-297.
- Banaszek, M.M., Siebenmorgen, T.J. 1993. Individual rice kernel drying curves. *Transactions of the ASAE* 36(2): 521-528.
- Bansode, R.R., Losso, J.N., Marshall, W.E., Rao, R.M., Portier, R.J. 2003. Adsorption of volatile organic compounds by pecan-shells and almond-shells based granular activated carbons. *Bioresource Technology* 90: 175-184.
- Barbosa-Canovas, G.V., Ortega-Rivas, E., Juliano, P., Yan, H. 2005. *Food Powders: Physical Properties, Processing, and Functionality*. New York, NY: Kluwer Academic/Plenum Pub.

Bassilakis, R., Carangelo, R.M., Wojtowicz, M.A. 2001. TG-FTIR analysis of biomass pyrolysis. *Fuel* 80: 1765-1786.

Bilba, K., Ouensanga, A. 1996. Fourier transform infrared spectroscopic study of thermal degradation of sugar cane bagasse. *Journal of Analytical and Applied Pyrolysis* 38: 61-73.

Blahovec, J., Yanniotis, S. 2009. Modified classification of sorption isotherms. *Journal of Food Engineering* 91: 72-77.

Bridgwater, A.V. 2003. Renewable fuels and chemicals by thermal processing of biomass. *Chemical Engineering Journal* 91: 87-102.

Brison, F. 1974. *Pecan Culture*. Austin, TX: Capital Printing. 247-254.

Cai, J., Chen, S. 2008. Determination of drying kinetics for biomass by thermogravimetric analysis under nonisothermal conditions. *Drying Technology* 26: 1464-1468.

Chen, C. 2003. Moisture sorption isotherms of pea seeds. *Journal of Food Engineering* 58: 45-51.

Chhinnan, M.S. 1984. Evaluation of selected mathematical models for describing thin layer drying of in shells pecans. *Transactions of the ASAE* 27: 610-615.

Chum, H.L. 1991. *Polymers from biobased materials*. New Jersey, USA: Noyes Data Corporation.

Colley, Z., Fasina, O.O., Bransby, D., Lee, Y. 2006. Moisture effect of the physical characteristics of switchgrass pellets. *Transactions of the ASABE*. (49)6: 1845-1851.

Correra, P.C., Pinto, F.A.C., Queiroz, D.M., Afonso Jr., P.C. 2001. Equilibrium moisture content for peanut hulls, kernels and whole pods. An ASAE Meeting Presentation, Paper No. 01-6083, American Society of Agricultural Engineers, Annual International Meeting, July 30-August 1, Sacramento, CA.

Dadgar S., Tabil, L.G., Crerar, B. 2004. Moisture adsorption of field peas as a function of temperature and relative humidity during storage, An ASABE/CSAE Annual Meeting Presentation, Paper No. 046089, Sponsored by ASAE/CSAE, August 1-4, Ottawa, Ontario, Canada.

Das, K.C., Garcia-Perez, M., Bibens, B., Melear, N. 2008. Slow pyrolysis of poultry litter and pine woody biomass: Impact of chars and bio-oils on microbial growth. *Journal of Environmental Science and Health Part A* 43: 714-724.

- Daugaard, D., Brown, R. 2003. Enthalpy for pyrolysis for several types of biomass. *Energy and Fuels* 17: 934-939.
- Demirbaş, Ahyan. 1998. Kinetics for non-isothermal flash pyrolysis of hazelnut shell. *Bioresource Technology* 66: 247-252
- Demirbas, Ayhan. 2001. Biomass resource facilities and biomass conversion processing for fuels and chemicals. *Energy Conversion and Management* 42: 1357-1378.
- Demirbas, A., Gonenc, A. 2002. An overview of biomass pyrolysis. *Energy Sources* 24:471-482.
- Demirbaş, Ahyan. 2004. Combustion characteristics of different biomass fuels. *Progress in Energy and Combustion Science* 30: 219-230.
- den Blanken, I.R. 2008. Equivalent width method for quantitative FTIR analysis of Biomass Pyrolysis using HITRAN database. Master's Thesis, University of Technology of Eindhoven, TUE, Eindhoven, Netherlands.
- Deshpande, S.D., Bal, S., Ojha, T.P. 1993. Physical properties of soybean. *Journal of Agricultural Engineering Research*. 56(2): 89-98.
- DOE. 2008. 20% Wind Energy by 2030, Increasing Wind Energy's Contribution to the U.S. Electrical Supply. U.S. Department of Energy: Washington D.C.
- Doymaz, I. 2004. Effect of the pre-treatments using potassium metabisulphide and alkaline ethyl oleate on the drying kinetics of apricots. *Biosystems Engineering* 89: 281-287.
- Doymaz, I. 2007. Air drying characteristics of tomatoes. *Journal of Food Engineering* 78: 1291-1297.
- Doymaz, I., Pala, M. 2002. Hot-air drying characteristics of red pepper. *Journal of Food Engineering* 55: 331-335.
- Durakova, A.G., Menkov, N.D. 2005. Moisture sorption characteristics of chickpea flour. *Journal of Food Engineering* 68: 535-539.
- EIA. 2008. Annual Energy Outlook 2008. Washington, DC: DOE Energy Information Administration. Available at: <http://www.eia.doe.gov/piaf/aeo/index.html>. Accessed 12 April 2009.
- Erbaş, M., Ertugay, M., Certel, M. 2005. Moisture adsorption behaviour of semolina and farina. *Journal of Food Engineering* 69: 191-198.

- Fasina, O.O., Sokhansanj, S. 1993. Equilibrium moisture relations and heat of sorption of alfalfa pellets. *Journal of Agricultural Engineering Research* 56: 51-63.
- Fayed, M.E., Skocir, T.S. 1997. *Mechanical Conveyors: Selection and Operation*. Lancaster, PA: Technomic Publishing Company, Inc.
- Fitzpatrick, J.J., Barringer, S.A., Iqbal, T. Flow property measurement of food powders and sensitivity of Jenike's hopper design methodology to the measured values. *Journal of Food Engineering* 61: 399-405.
- Ganesan, V., Muthukumarappan, K., Rosentrater, K.A. 2008. Flow properties of DDGS with varying soluble and moisture contents using Jenike shear testing. *Powder Technology* 187: 130-137.
- Garcia-Nunez, J.A., Garcia-Perez, M., Das, K.C. 2008. Determination of kinetic parameters of thermal degradation of palm oil mill by-products using thermogravimetric analysis and differential scanning calorimetry. *Transactions of the ASABE* 51(2): 547-557.
- Geisler, Malinda. 2009. Pecans. Agriculture Marketing Resource Center, Iowa State University. Available at: <http://www.agmrc.org>. Accessed 3 May 2010.
- Geldhart, D., Harnby, N., Wong, A. 1984. Fluidization of cohesive powders. *Powder Technology* 37(1): 25-37.
- Gercel, H.F. 2002. Production and characterization of pyrolysis liquids from sunflower pressed bagasse. *Bioresource Technology* 85: 113-117.
- Gomez, C., Velo, E., Barontini, F., Cozzani, V. 2009. Influence of secondary reactions on the heat of pyrolysis of biomass. *Industrial Engineering and Chemical Research* 48: 10222-10233.
- Goyal, H.B., Seal, D., Saxena, R.C. 2008. Bio-fuels from thermochemical conversion of renewable resources: a review. *Renewable and Sustainable Energy Reviews* 12: 504-517.
- Guintoli, H., de Jong, W., Arvelakis, S., Spliethoff, H., Verkooyen, A.H.M. 2009. Quantitative and kinetic TG-FTIR study of biomass residue pyrolysis: dry distiller's grains with solubles (DDGS) and chicken manure. *Journal of Analytical and Applied Pyrolysis* 85: 301-312.
- Gupta, R.K., Das, S.K. 1997. Physical properties of sunflower seed. *Journal of Agricultural Engineering and Research* 66(1): 1-8.

- Harris, M.K., Cutler, B.L., Ring, D.R. 1986. Pecan nut loss from pollination to harvest. *Journal of Economic Entomology* 79(6): 1653-1657.
- He, F., Yi, W., Bai, X. 2006. Investigation on caloric requirement of biomass pyrolysis using TG-DSC analyzer. *Energy Conversion and Management* 47: 2461-2469
- Igathinathane, C., Womac, A.R., Sokhansanj, S., Pordesimo, L.O. 2007. Moisture sorption thermodynamic properties of corn stover fractions. *Transactions of ASABE* 50(6): 2151-2160.
- Jenike, A.W. 1964. Storage and flow of solids. Bulletin No. 123. University of Utah, Salt Lake City, Utah: Engineering and Experiment Station.
- Jenkins, B.M. 1989. Physical Properties of Biomass. In *Biomass Handbook*, 860-891. Amsterdam, Holland: Gordon and Breach Science.
- Johns, M., Marshall, W.E., Toles, C.A. 1999. The effect of activation method on the properties of pecan shells-activated carbons. *Journal of Chemical Technology and Biotechnology* 74: 1037-1044.
- Joshi, D.C., Das, S.K., Mukherjee, R.K. 1993. Physical properties of pumpkin seeds. *Journal of Agricultural Engineering Research* 54(3): 219-229.
- Kashaninejad, M., Tabil, L.G. 2004. Drying characteristics of purslane (*Portulaca oleraceae* L.). *Drying Technology* 22: 2183-2200.
- Kotwaliwale, N., Bruswitz, G.H., Weckler, P.R. 2004. Physical characteristics of pecan components: effect of cultivar and relative humidity. *Transactions of the ASAE* 47(1): 227-231.
- Labuza, T.P. 1984. *Moisture sorption: practical aspects of isotherm measurement and use*. Minneapolis, MN: American Association of Cereal Chemist.
- Lee, S-B, Fasina, O. 2009. TG-FTIR analysis of switchgrass pyrolysis. *Journal of Analytical and Applied Pyrolysis* 86: 39-43.
- Leiras, M.C., Iglesias, H.A. 1991. Water vapor sorption isotherms of two cake mizes and their components. *International Journal of Food Science* 26: 91-95.
- Li, S., Lyons-Hart, J., Banyasz, J., Shafer, K. 2001. Real-time evolved gas analysis by FTIR method: an experimental study of cellulose pyrolysis. *Fuel* 80: 1809-1817.
- Liu, Q., Wang, S., Zheng, Y., Luo, Z., Cen, K. 2008. Mechanism study of wood lignin pyrolysis by using TG-FTIR analysis. *Journal of Analytical and Applied Pyrolysis* 82: 170-177.

Luo, Z., Wang, S., Liao, Y., Zhou, J., Gu, Y., Cen, K. 2004. Research on biomass fast pyrolysis for liquid fuel. *Biomass and Bioenergy* 26: 455-462.

Market Data.2009. Commodity Futures - Brent Crude Futures. Available at: <http://www.bloomberg.com>. Accessed 4 April 2009.

McKendry, P. 2002a. Energy production from biomass (part 1): overview of biomass. *Bioresource Technology* 83: 37-46.

McKendry, Peter. 2002b. Energy production from biomass (part 2): conversion technologies. *Bioresource Technology* 83: 47-54.

McMullen, J., Fasina, O.O., Wood, C.W., Feng, Y. 2004. Storage and handling characteristics of pellets from poultry litter. *Applied Engineering in Agriculture* 21: 645-651.

Milbrandt, A. 2008. A geographic perspective on the current biomass resource availability in the United States. NREL TP-560-39181. DOE, Washington, D.C.

Mothe C.G., Miranda, I.C. 2009. Characterization of sugarcane and coconut fibers by thermal analysis and FTIR. *Journal of Thermochemical and Analytical Calorimetry* 97:661-665.

Murugan, P, Mahinpey, N., Johnson, K.E., Wilson, M. 2008. Kinetics of the Pyrolysis of Lignin Using Thermogravimetric and Differential Scanning Calorimetry Methods. *Energy and Fuels* 22: 2720-2724.

Ng., C., Marshall, W.E., Ramu, R., Bansode, R., Losso, J. 2003. Activated carbon from pecan shells: process description and economic analysis. *Industrial Crops and Products* 17: 209-217.

Nimkar, P.M., Chattopadhyay, P.K. 2001. Some physical properties of green gram. *Journal of Agricultural Engineering Research* 80: 183-189.

Ozarlan, C. 2002. Physical properties of cotton seed. *Biosystems Engineering* 82(2): 169-174.

Pagano, A.M., Mascheroni, R.H. 2004. Sorption isotherms for amaranth grains. *Journal of Food Engineering* 67: 441-450.

Paraskeva, P., Kalderis, D., Diamadopoulos, E. 2008. Production of activated carbon from agricultural by-products. *Journal of Chemical Technology and Biotechnology* 83(5): 581-592.

Park, S., Venditti, R., Jameel, H., Pawlak, J. 2007. Studies of the heat of vaporization of water associated with cellulose fibers characterized by thermal analysis. *Cellulose* 14: 195-204.

Perlack, R.D., Wright, L.L., Turhollow, A.F., Graham, R.L., Stokes, B.J. Erback, D.C. 2005. Biomass feedstock for a bioenergy and bioproducts industry: the technical feasibility of a billion ton annual supply. Available at: http://www.feedstockreview.ornl.gov/pdf/billion_ton_vision.pdf. Accessed 1 May 2010.

Reina, J., Velo, E. Puighaner, L. 1998. Thermogravimetric study of the pyrolysis of waste wood. *Thermochimica Acta* 320: 161-167.

Renne, D., George, R., Wilcox, S., Stoffel, T., Myers, D., Heimiller, D. 2008. Solar Resource Assessment. NREL TP-581-42301. DOE, Washington, D.C.

Schulze, D. 2006. Storage of powders and bulk solids in solos. Dietmar Schulze. Available at: <http://www.dietmar-schulze.de/storagepr.html>. Accessed 13 April 2010.

Sentorun-Shalaby, C., Ucak-Astarlioglu, M.G., Artok, L., Sarici, C. 2006. Preparation and characterization of activated carbons by one-step steam pyrolysis/activation from apricot stones. *Microporous and Mesoporous Materials* 88: 126-134.

Shamlou, P.A. 1988. *Handling of Bulk Solids: Theory and Practice*. London, UK: Butterworth-Heinemann.

Sierra, R., Smith, A., Granda, C., Holtzapple, M. 2008. Producing fuels and chemicals from lignocellulosic biomass. *Chemical Engineering Progress*, August 1, 2008: 10-18.

Singh, R.N. 2004. Equilibrium moisture content of biomass briquettes. *Biomass and Bioenergy* 26: 251-253.

Souza, B.S., Moreira, A.P., Teixeira, A.M. 2009. TG-FTIR coupling to monitor the pyrolysis products from agricultural residues. *Journal of Thermal Analysis and Calorimetry* 97: 637-642.

Soysal, Y., Östekin, S. 1999. Equilibrium moisture content equations for some medicinal and aromatic plants. *Journal of Agricultural Engineering Research* 74: 371-324.

Soysal, Y., Oztekin, S. 2001. Comparison of seven equilibrium moisture content equations for some medicinal and aromatic plants. *Journal of Agricultural Engineering Research* 78: 57-63.

- Stenseng, M., Jensen, A., Dam-Johnson, K. 2001. Investigation of biomass pyrolysis by thermogravimetric analysis and differential scanning calorimetry. *Journal of Analytical and Applied Pyrolysis* 58-59: 765-780.
- Sun, D., Byrne, C. 1998. Selection of EMC/ERH isotherm equations for rapeseed. *Journal of Agricultural Engineering Research* 69: 307-315.
- Sun, S., Tian, H., Zhao, Y., Sun, R., Zhou, H. 2010. Experimental and numerical study of biomass flash pyrolysis in an entrained flow reactor. *Bioresource Technology* 101: 3678-3684.
- Teunou, E., Fitzpatrick, J.J. 1999. Effect of relative humidity and temperature on food powder flowability. *Journal of Food Engineering* 42: 109-116.
- USDA-NASS. 2008. Noncitrus Fruits and Nuts Summary. Washington, DC.: USDA National Agricultural Statistics Service.
- Wang, S., Liu, S., Luo, Z., Wen, L., Cen, K. 2007. Mechanism study on cellulose pyrolysis using thermogravimetric analysis coupled with infrared spectroscopy. *Frontiers of Energy and Power Engineering in China* 1(4): 413-419.
- Wartelle, L.H., Marshall, W.E. 2001. Nutshells as granular activated carbons: physical, chemical and adsorptive properties. *Journal of Chemical Technology and Biotechnology* 76(5): 451-455.
- Werther, J., Saenger, M., Hartge, E.-U., Ogada, T., Siagi, Z. 2000. Combustion of agricultural residues. *Progress in Energy and Combustion Science* 26: 1-27.
- Wood, B., Payne, J., Grauke, L. 1994. An overview of the evolution of the U.S. pecan industry. In *Pecan Technology*, 1-11. New York, NY: Chapman and Hall.
- Woodcock, C.R., Mason, J.S. 1987. *Bulk Solids Handling: An Introduction to the Practice and Technology*. Glasgow, Scotland: Blackie and Son, Ltd.
- Worley, R. 1994. Pecan Production. In *Pecan Technology*, 12-38. New York, NY: Chapman and Hall.
- Yaman, Serder. 2004. Pyrolysis of biomass to produce fuels and chemical feedstocks. *Energy Conversion and Management* 45: 651-671.
- Zanzi, R., Sjoström, K., Bjornbom, E. 2002. Rapid pyrolysis of agricultural residues at high temperature. *Biomass and Bioenergy* 23: 357-366.

CHAPTER 3. EFFECT OF MOISTURE AND PARTICLE SIZE ON PHYSICAL PROPERTIES OF PECAN SHELLS

3.1. Introduction

Pecan (*Carya illinoinensis*) is a tree nut crop grown in most of the southern states of the country. Pecan is the only native tree nut grown for commercial use in the U.S. The country produces over 80% of the world's supply (USDA-ERS, 2003; Geisler, 2009).



Figure 3.1 – Ripe pecan (left) and cracked pecans with shell (right) (UGCE, 2008)

Pecan shells are obtained as by-product of the pecan shelling process. It is therefore an agricultural by-product that have current uses as value-added products, such as mulch, imitation fire logs, glue and soap abrasives and as a source of activated carbon for water filtration and commercial absorbents (Bansode et al., 2003; Ng et al., 2003; Guo and Rockstraw, 2007).

Pecan shells are however, a bulk solid. Bulk solids consist of many particles of different sizes randomly grouped together to form a bulk (Woodcock and Mason, 1987). The physical characteristics of a bulk solid are important to the efficient design and selection of equipment for its handling and storage (Woodcock and Mason, 1987). Several published studies have reported that moisture content and particle size have significant influences on the physical properties of bulk biological materials, such as raw cashew nut (Balasubramanian, 2001), switchgrass pellets (Colley et al., 2006), poultry litter (Berhart et al., 2008) and barley straws, corn stover and switchgrass (Mani et al., 2004).

Therefore, the objectives of this study were to:

- (a) Quantify the effect of particle size and moisture content on poured bulk density, particle density, tap bulk density, Hausner ratio and porosity of pecan shells;
- (b) Quantify the effect of particle size, moisture content and applied pressure on the compressibility of pecan shells;
- (c) Measure the flowability, cohesion and internal angle of friction of pecan shells at the different particle sizes and different moisture levels; and
- (d) Determine the equilibrium moisture isotherm and rate of sorption of moisture by pecan shells.

3.2. Materials and Methods

3.2.1. Preparation

The pecan shells used in this study were obtained from the Louisville Pecan Company (Louisville, AL). Before use, the shells were stored in the Biosystems Engineering process engineering laboratory that has an average temperature of approximately 25°C. Physical property experiments were performed at moisture contents of 4.42, 8.41, 14.73, 19.36 and 24.70% (w.b.). In order to reach the desired moisture content, the samples were either: a) placed in an oven set at 45-50°C (for moisture content reduction) or, b) sprayed with a known quantity of distilled water (to increase moisture content of samples). In both cases, the samples were allowed to equilibrate for at least 24 hours in an air-tight container before further use. After the 24 hour moisture equilibration period, sample moisture content was verified by duplicate moisture content determinations using a moisture analyzer (MB45, Ohaus Corporation, Pine Brook NJ). Initial moisture content of the pecan shell sample was 14.59% (w.b.). All moisture contents are reported in wet basis unless otherwise noted.

3.2.2. Particle Size Distribution

Particle size distribution was determined by mechanical sieving according to ASABE Standard S319.4 (ASABE, 2008). A Ro-Tap sieve shaker (W.S. Tyler Model RX-29, Mentor Ohio) was used for the sieving method. Approximately 100 grams of pecan shells were placed in the first (top) sieve and shaken in the Ro-Tap sieve shaker for fifteen minutes. After the shaking period, particle size distribution curves were obtained

from weights of samples retained on each sieve. Geometric mean diameter (d_{gw}) and geometric standard deviation (S_{gw}) of the samples were also calculated according to the ASABE Standard S319.4 (ASABE, 2008) (Equations 3.1 – 3.3).

$$d_{gw} = \log^{-1} \left[\frac{\sum_{i=1}^n (W_i \log \bar{d}_i)}{\sum_{i=1}^n (W_i)} \right] \quad (3.1)$$

$$S_{log} = \left[\frac{\sum_{i=1}^n W_i (\log \bar{d}_i - \log d_{gw})^2}{\sum_{i=1}^n (W_i)} \right]^{1/2} \quad (3.2)$$

$$S_{gw} = \frac{1}{2} d_{gw} \left[\log^{-1} S_{log} - (\log^{-1} S_{log})^{-1} \right] \quad (3.3)$$

where, d_{gw} = geometric mean diameter (or median size) of particles by mass (mm)

S_{log} = geometric standard deviation of log-normal distribution by mass in ten-based logarithm (dimensionless)

S_{gw} = geometric standard deviation of particle diameter by mass (mm)

W_i = mass on i^{th} sieve (g)

n = number of sieves plus one pan

$\bar{d}_i = [d_i \times d_{i+1}]^{1/2}$

d_i = nominal sieve aperture size of the i^{th} sieve (mm)

d_{i+1} = nominal sieve aperture size of the next larger than i^{th} sieve (mm)

3.2.3. Mechanical Separation of Pecan Shells

Initial particle size analysis of the pecan shell sample demonstrated three separate peaks in the particle size distribution curve at 0.11, 1.4 and 2.4 mm aperture openings (Figure 3.2).

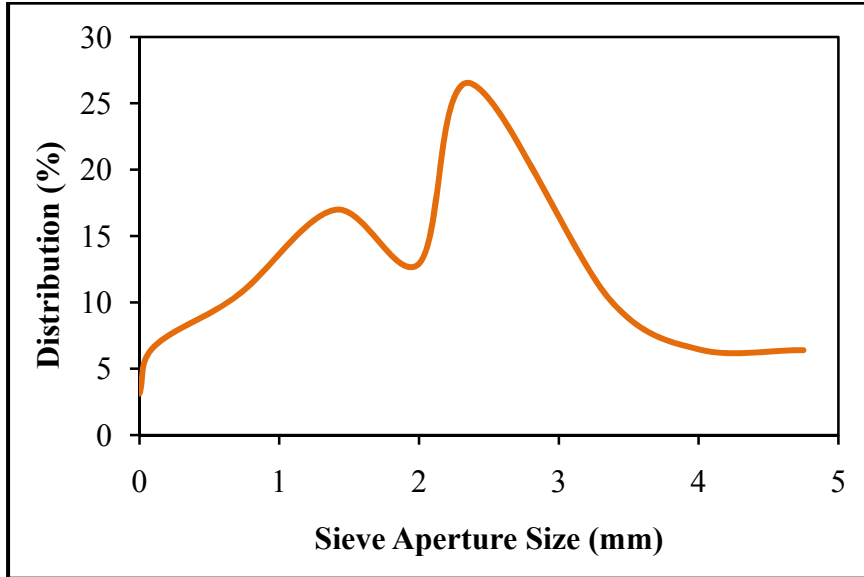


Figure 3.2 – Particle size distribution of pecan shells

The separation of the shells into the three distinct particle sizes observed in the initial sieve analysis was accomplished by the use of 30 inch Kason vibrating screen separator (Figure 3.3) (Kason Corporation, Millburn New Jersey). The following screens were used in the separation: #10 (1.885 mm aperture size) screen and #14 (1.295 mm aperture size). Pecan shells retained on the #10 screen were classified as ‘coarse’, those retained on #14 but passed through #10 were classified as ‘medium’ and those that passed through #14 screen were classified as ‘fine’. These three particle size fractions (coarse, medium and fine) and the raw sample (making a total of four samples) were used for further analysis.



Figure 3.3 – Kason vibrating screen separator

3.2.4. Compositional Analysis

3.2.4.1. Energy Content

Heating value of pecan shells was obtained with an IKA C200 calorimeter (IKA Works Inc., Wilmington, NC). To conduct measurements, approximately 0.5 g of sample was weighed and pressed into a pellet using IKA C21 pelleting press (IKA Works, Wilmington, NC). After pressing, the pellet was reweighed and placed in the bomb according to manufacturer guidelines. Energy content of pecan shells was determined in triplicate for the four samples.

3.2.4.2. Ash Content

Ash content of samples was determined using the National Renewable Energy Laboratory's (NREL) laboratory analytical procedure for the determination of ash in biomass (NREL, 2005). To conduct a test, approximately one gram of each sample was placed in a crucible and then transferred into a muffle furnace (Type-1500, Thermolyn Sybron Corp., Milwaukee, WI). Ashing of samples was carried out at $575^{\circ} \pm 25^{\circ}\text{C}$ for three hours. After the three hour period, the furnace was allowed to cool to 105°C . The

samples were then removed from the furnace and allowed to cool in a desiccator before they were re-weighed. Percent ash was calculated using Equation 3.4 and experiments were conducted in triplicate.

$$\% \text{ Ash} = \frac{\text{Weight}_{\text{crucible plus ash}} - \text{Weight}_{\text{crucible}}}{\text{Oven Dry Weight}_{\text{sample}}} \times 100 \quad (3.4)$$

3.2.4.3. Ultimate Analysis

Carbon, hydrogen and nitrogen were determined (in duplicate) for the samples using an elemental analyzer (Model 2400 Series II Perkin-Elmer, Shelton, CT). The samples were ground in a wiley mill to pass through a standard #40 screen before they were analyzed. Approximately 300 mg of sample was used. Helium was used as a carrier gas.

3.2.4.4. Structural Carbohydrates

Van Soest analysis was used to determine the hemicelluloses, cellulose and lignin fractions of the sample. In this process, the samples were separated progressively into neutral-detergent fiber (NDF), acid-detergent fiber (ADF) and acid-detergent-lignin (ADL). This method of analysis has been used for other biological materials, such as hazelnut shells, wood, rice straw and corn stover (Haykiri-Acma, 2006; Liu et al., 2008). NDF represents the insoluble matrix of the pecan shells cell wall, substances covalently linked and intimately associated through hydrogen bonding, crystallinity, or other intramolecular association that they are resistant to solutions within the range of physiological concentrations. ADF is considered as a rough estimate of the insoluble cell

wall, or cellulose, lignin, ash and acid insoluble ash (silica). ADL was determined using the Klason lignin methodology, which does not recover all of the true lignin, but by hydrolysis of cellulose in the cell wall, the residue not hydrolyzed is an effective approximation of lignin content in forages (Van Soest and Robertson, 1985). To determine NDF, ADF and ADL, the pecan shells were ground in a hammer mill to pass through a 1 mm screen. Approximately 1.0 g of pecan shells were weighed (Model AM50, DeltaRange, Mettler-Toledo, Heightstown, NJ), recorded and placed in a 600 ml beaker. Fifty milliliters of room-temperature solution (2% w/v amylase and deionized water) was added to the beaker containing the sample and placed on a hot plate and evenly boiled for 40 minutes. After 40 minutes, another 50 ml of enzyme solution was added to the beaker and replaced on the hot plate and boiled for another 20 minutes. After the hour of boiling, the enzyme solution was removed from the beaker, washed with deionized water in a filtering crucible (50 ml, 40-60 μm) and the solution of water and enzyme solution was removed via vacuum pump. The crucibles were dried overnight in a forced air oven set at 105°C (Precision Scientific, Chicago, IL). Then, the crucibles were removed, placed in a dessicator to cool, reweighed and recorded. NDF was determined for each particle size. For ADF determinations, approximately 1.0 dried and ground pecan shells were placed in a beaker and 100 ml acid-detergent solution was added. The beaker, containing solution and sample, was placed on a hot plate and boiled for 1 hour. Then the beaker was removed from the hot plate and the sample and solution mixture was rinsed with deionized water, filtered through a crucible and liquids removed via vacuum pump. The crucibles were dried overnight in an oven, allowed to cool, and weights recorded. ADL was determined using the residual of the ADF procedure.

Seventy-two percent (w/w 12M sulfuric acid and deionized water) was added to the crucibles (approx. 20 ml) and stirred using a glass stirring rod. The solution was stirred occasionally for 3 hours after which the crucibles were placed in a vacuum manifold and residue was washed with deionized water, rinsing off crucible sides, etc. to make sure that no fiber was left unfiltered. The crucibles were dried in a forced oven set at 105°C overnight. The crucibles were removed from the oven, allowed to cool in a dessicator and weights recorded. ADL was considered lignin composition whereas cellulose and hemicelluloses were calculated using the following Equations (3.5-3.6):

$$\% \text{ cellulose} = \%ADF - \%ADL \quad (3.5)$$

$$\% \text{ hemicelluloses} = \%NDF - \%ADF \quad (3.6)$$

NDF, ADF and ADL were conducted in duplicates.

3.2.5. Poured Bulk Density

Poured bulk density was determined by a bulk density measurement apparatus (Burrows Co., Evanston, IL) and according to ASABE Standard S269.4 (2002). This procedure involves pouring the bulk solid into a container of known volume (947 mm³) via a funnel placed above the container. The material was then leveled off the top of the container and weighed. The bulk density (ρ_b) of the pecan shells were calculated by dividing the mass of sample in the container (m_c) by the volume of the container (V_c) (Equation 3.7). This procedure was done in triplicate and the average value was reported.

$$\rho_b = \frac{m_c}{V_c} \quad (3.7)$$

3.2.6. Particle Density

Particle density of pecan shell samples was measured by gas comparison pycnometry (Model AccuPyc II 1340, Micrometrics Instrument Corp., Norcross, GA) that involves the use of known quantity of inert gas under pressure (helium) that is allowed to flow from a previously known reference volume into a cell containing a sample of pecan shells. By applying the ideal gas law to the pressure change from the reference cell to the sample cell, the pycnometer calculates the volume of the material in the sample cell. True particle density (ρ_p) was taken as the ratio of the mass of material in the sample cell (m_p) to the volume (V_p) measured by the pycnometer (Equation 3.8). Sample mass was obtained with a digital balance accurate to 0.001 grams (Model AR3130, Ohaus Corp., Pinebrook, NJ). This procedure was carried out in triplicate.

$$\rho_p = \frac{m_p}{V_p} \quad (3.8)$$

3.2.7. Tap Bulk Density

Tap bulk density of pecan shell samples were measured using an automated tap density tester (Model TD-12, Pharma Alliance Group Inc., Valencia, CA) that is based on ASTM Standard B 527 (ASTM, 2005). A 250 ml graduated cylinder was filled (to 250 ml) with a sample and weighed using a balance accurate to 0.01 g (Model PE3600 DeltaRange, Mettler-Toledo, Heightstown, NJ). The cylinder was then placed in the tap density tester. The tester taps the graduated cylinder in two steps. For the first step, the cylinder was tapped 500 times at a rate of 300 taps per minute. The volume of the material in the cylinder was measured after the first tapping. This was followed by tapping of the cylinder for 750 times at the rate of 300 taps per minute. After this step,

the new volume was measured. The tap bulk density (ρ_t) of the pecan shells was calculated as the mass of sample in the cylinder (m_c) divided by the final tap volume of the sample (V_t) (Equation 3.9). This procedure was carried out in triplicate.

$$\rho_t = \frac{m_c}{V_t} \quad (3.9)$$

3.2.8. Hausner Ratio

Hausner ratio is a function of the tap and poured bulk density. The Hausner ratio is often used to indicate how easily a powder is fluidized (Geldhart et al., 1984). It is mathematically defined by Equation 3.10 and was calculated as the ratio of tap bulk density (ρ_t) and poured bulk density (ρ_b).

$$H_r = \frac{\rho_t}{\rho_b} \quad (3.10)$$

Powders that are easily fluidized have Hausner ratios less than 1.25, whereas powders with fluidization problems have Hausner ratios greater than 1.40 (Geldhart et al., 1984).

3.2.9. Porosity

Porosity is the percentage of a bulk solid that is occupied by air spaces (Woodcock and Mason, 1987). Porosity is mathematically defined by Equation 3.11 and was calculated using the bulk and particle densities that were obtained in the previous sections.

$$\varepsilon = \left(1 - \frac{\rho_b}{\rho_p}\right) \times 100 \quad (3.11)$$

3.2.10. Mechanical Compressibility

A texture analyzer (Model TA-HD, Stable MicroSystems, Surrey, UK) was used to measure the mechanical compressibility of pecan shell samples. The measurement system consisted of a compression cell (internal diameter of 49.55 mm and internal height of 101.83 mm) and a tight-fitting piston (diameter of 49.00 mm) that was attached to the crosshead of the texture analyzer. For each test, a known mass of pecan shells (Model PM2000, DeltaRange, Mettler-Toledo, Heightstown, NJ, accurate to 0.01 g) was loaded into the compression cell. The piston compressed the sample (at a rate of 1 mm/s) inside the cell until a consolidating pressure of 1.5, 3, 6, 9, 12, or 15 kPa was reached. The software provided by the manufacturer of the analyzer recorded the force (or pressure) on the sample and the distance traveled (by compression of the sample) by the piston. This procedure was carried out in triplicate. Mechanical compressibility (Cm , %) was calculated as follows:

$$Cm = 100 \left(\frac{V_i - V_f}{V_i} \right) = 100 \left(1 - \frac{\rho_{bf}}{\rho_{bi}} \right) \quad (3.12)$$

where, V_i is initial volume (cm^3), V_f is compressed volume (cm^3), ρ_{bi} is initial bulk density (kg/m^3) and ρ_{bf} is final (compressed) bulk density (kg/m^3).

3.2.11. Flowability

An automated shear tester (ShearScan TS-12, Sci-Tec Inc., Worthington, Ohio) was used to quantify the flow behavior of pecan shells. The shear cell used in this procedure was of the annular ‘fixed’ cell type. The cell (height of 27 mm) consisted of a base ring attached to an inner (diameter of 109.6 mm) and outer ring (diameter of 55.0

mm), and to a cell lid. To run a sample, the space between the inner and outer rings was filled with a pecan shell sample. The cell lid was then placed on top of the sample between the inner and outer rings.

Using settings on the software provided by the manufacturer, a compression load was applied to the sample (in the cell) at a constant rate of 7.5 mm/min until the consolidating stress, or preset normal load, was reached. This was followed by twisting of load cell at 2.5 mm/min. Shear stress was determined by the shear cell load and increased until it reached the predetermined or programmed steady state point. When this point was reached, the load cell gradually lifted and decreased the load to a preset point. Shear action began once again until the sample failed due to shear stress. Consolidating stresses of 3, 6, 9, 12, 15 and 21 kPa were used for all samples. Each consolidating stress was run in triplicate. Maximum shear stress was recorded for six different loads (25, 35, 45, 55, 65 and 75% of the consolidating stress). Yield locus was obtained by plotting the maximum shear stress versus normal stress.

The software provided by the manufacturer was used to calculate ultimate yield stress (UYS) and major consolidating stress (MCS) (see Equations 3.13 and 3.14, respectively). The flow index was obtained as the inverse of the slope of the plot of UYS vs. MCS.

$$UYS = \frac{2c(1 + \sin \varphi)}{\cos \varphi} \quad (3.13)$$

$$MCS = \left[\frac{A - \sqrt{A^2 \sin^2 \varphi - \tau^2 \cos^2 \varphi}}{\cos^2 \varphi} \right] (1 + \sin \varphi) - \left(\frac{c}{\tan \varphi} \right) \quad (3.14)$$

$$\tau = c + \tan(\varphi) \sigma \quad (3.15)$$

Where:

τ = shear stress (kPa)

σ = normal stress (kPa)

φ = angle of internal friction ($^{\circ}$)

c = cohesion (kPa)

$A = \sigma + \frac{c}{\tan \varphi}$, and c is cohesion (defined as τ at $\sigma = 0$).

3.2.12. Rate of Moisture Sorption

Agricultural materials are hygroscopic in nature. Therefore, they have the ability to exchange moisture with the atmosphere (Singh, 2004; Igathinanthane et al., 2007). This experiment was designed to determine the rate at which pecan shells absorb or desorb moisture from an environment. Moisture sorption property of pecan shell samples was carried out in a chamber (0.9 m x 1.8 m x 0.9 m) that was supplied with conditioned air from a conditioner (Model #9221-2110, Parameter Generation and Control, Inc., Black Mountain, NC). The combination of temperatures and relative humidity levels used in this study were 15, 25 and 35°C ($\pm 1^{\circ}\text{C}$) and 50, 65 and 80°C ($\pm 3\%$) respectively. A schematic diagram of the test system is shown in Figure 3.4 below:

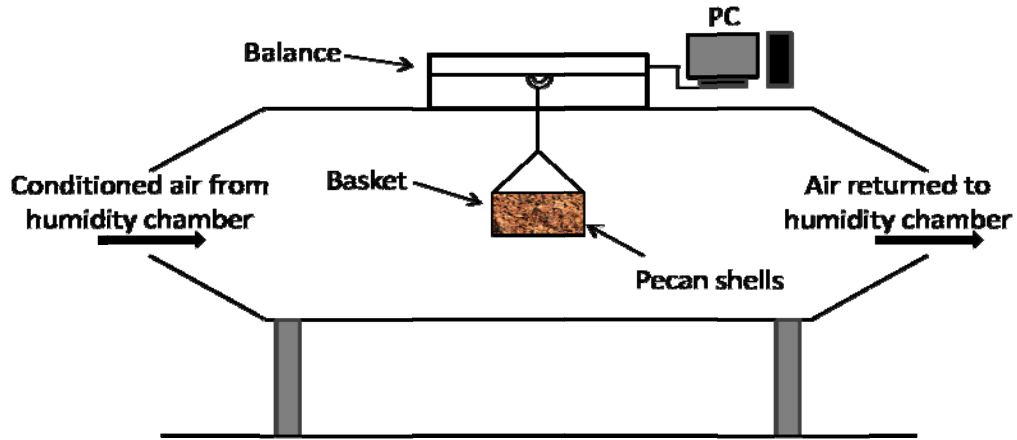


Figure 3.4 – Schematic diagram of rate of set up for moisture sorption study

To conduct a test, a thin layer of pecan shells (100-105 g) was placed in a wire mesh basket hung from a digital balance (Model PM4600, Mettler-Toledo, Columbus, OH) (accurate to 0.01g). Sample mass was monitored and continuously recorded on a personal computer at 10 minute intervals until equilibrium was reached (generally 48-60 hours, depending on the temperature and relative humidity of the conditioned air entering the chamber). A communication software (Windmill RS232, Windmill Software Ltd., Manchester, UK) was used to interface the balance to the personal computer. An experiment was considered complete when the mass of sample did not change by more than 0.01 g within a span of one hour. The moisture content of a sample after the end of each experiment was verified using a moisture analyzer (MB45, Ohaus Corporation, Pine Brook NJ). Experimentation at each temperature and relative humidity combination was performed in duplicate.

3.2.13. Equilibrium Moisture Isotherm

A water activity instrument (HygroLab 2 – H3, Rotronic Instrument Corp., Huntington, NY) was used to measure the equilibrium relative humidity of preconditioned pecan shell samples. To conduct a test, the conditioned sample was placed in the sample holder of the water activity instrument. The water activity probe was then placed on the top of the sample holder to form a sealed measurement system. A small fan, located in the probe, circulated air within the sample container and a thin film capacitance sensor measured relative humidity from 0 to 100% (with an accuracy of $\pm 1.5\%$) while a platinum RTD (resistance temperature detector) temperature probe (with an accuracy of $\pm 0.3^\circ\text{C}$) was used to measure temperature. The measurement probes and containers were placed into a temperature controlled-chamber (Model AA-5460A, Espec. Corp., Hudsonville, MI) set at 10, 20, 35, or 50°C . The pecan shells were adjusted to moisture content levels of 4.12, 7.06, 11.28, 14.56, 19.43, and 25.58% (wet basis), using the moisture content adjustment methods discussed previously. Relative humidity and dry-bulb temperature output from the water activity meter were continuously recorded on a personal computer until equilibrium was reached (usually less than 3 hours). Each combination of sample moisture content and chamber temperature were performed in triplicate. The equilibrium moisture content (EMC) and equilibrium relative humidity (ERH) were taken as the average of the three moisture contents and relative humidity combinations for each sample.

3.2.14. Data Analysis

Statistical analysis was performed on all data sets using SAS statistical software package (Version 9.1, SAS institute Inc., Cary, NC, 2009-2010). Microsoft Excel (Microsoft Office XP Professional, 2007) software was used for data analysis and data plotting.

3.3. Results and Discussion

3.3.1. Particle Size Distribution

Particle size analysis of the three fractions of pecan shells (fine, medium and coarse) was carried out by sieve analysis. Figure 3.5 shows that the raw sample was successfully separated into three sizes. The geometric mean diameter (d_{gw}) and geometric standard deviation (S_{gw}) of the three fractions and the raw pecan shell samples are given in Table 3.1 (Equations 3.1-3.3, ASABE 2008). Mechanical separation of raw pecan shells reduced the variability in particle size (based on the coefficient of variation values in Table 3.1).

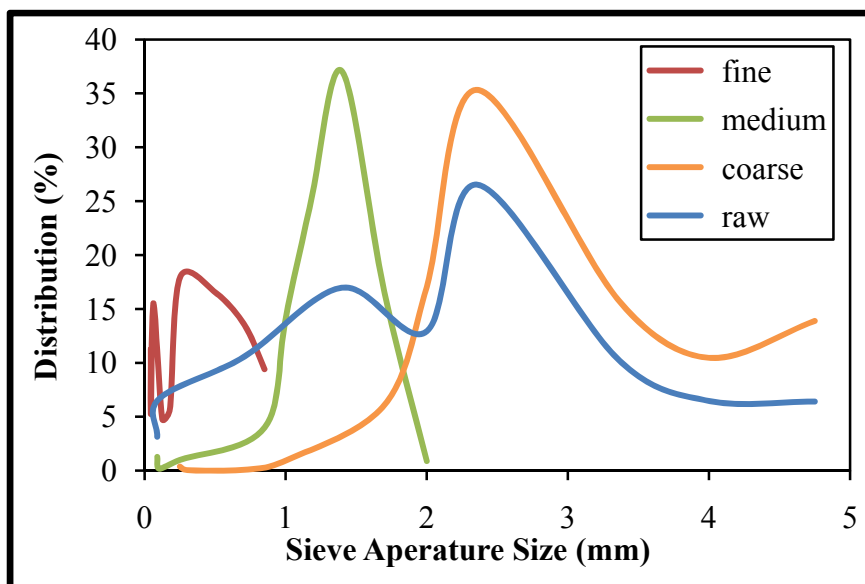


Figure 3.5 – Particle size distribution of pecan shells

Table 3.1 – Geometric mean diameter and geometric standard deviation of pecan shells fractions

	d_{gw} (mm)	S_{gw} (mm)	CV (%)
fine	0.212	0.244	115.09
medium	1.241	0.442	35.62
coarse	2.194	0.696	31.72
raw	1.200	2.262	188.50

3.3.2. Chemical Composition Analysis

3.3.2.1. Energy and Ash Content

The energy and ash contents of the four particle size fractions of pecan shells are given in Table 3.2. In general, energy content decreased as particle size increased, but the decrease was not significant except for the fine fraction. The heating values are comparable to values reported for other biomass feedstocks, such as switchgrass (19.22

MJ/kg), peanut hull (19.83 MJ/kg), almond shell (20.2 MJ/kg) and wood pellets (19.0 MJ/kg) (Fasina, 2007; Blesa et al., 2001; Biagini et al., 2006).

Ash content of the pecan shell fractions ranged from 3.02% in the fine fraction to 2.32% in the medium fraction. In general, the ash content of the pecan shell fractions are similar to that of other reported agricultural materials, such as almond shell (2.4%) and wood pellets (2.3%) (Di Blasi, 1999; Blesa et al., 2001). Table 3.2 gives the energy content (MJ/kg) and ash content (%) of the four particle size fractions of pecan shells. Statistical analysis of energy and ash content was performed using analysis of variance (ANOVA) and Tukey's multiple comparison tests (at $\alpha=0.05$) in SAS Version 9.3 (2009).

Table 3.2 – Energy and ash content (dry basis) of pecan shells fractions

Sample	HHV (MJ/kg)	St.dev.	Ash Content (%)	St.dev.
fine	20.50 ^[a]	0.09	3.02 ^[a]	0.06
medium	19.78 ^[b,c]	0.03	2.32 ^[c]	0.09
coarse	19.50 ^[c]	0.11	2.53 ^[b]	0.03
raw	20.06 ^[b]	0.03	2.49 ^[b]	0.01

samples (n=3) in each column with same letter are not significantly different (P<0.05)

3.3.2.2. *Ultimate Analysis*

Carbon, hydrogen and nitrogen contents of the pecan shells fractions are shown in Table 3.3. The fine fraction of pecan shells had significantly (P < 0.05) less carbon than the medium, coarse and raw fractions. As reported in the previous section, the fine fraction had the highest energy content (Table 3.2). There is no scientific explanation for the fine fraction to have the lowest carbon level even though it has the highest energy

content. However, it is postulated that the fine fraction contains soil particles from harvesting processes or pith particles (from the inside of the shell, between nut-halves). The pecan shell pith contains higher concentrations of phenolic compounds and tannins (compared to polysaccharide carbon chains) that have been extracted for the production of resins (McGraw, 1993; Hamud and Chung, 1989). Hydrogen percentages were not significantly affected by particle size in the four fractions. In terms of nitrogen (percentage by mass, dry basis), a trend of decreased nitrogen as particle size increased was observed. The carbon, hydrogen and nitrogen percentages are similar to other agricultural materials, such as cherry bay branch, cotton and maize straw and hazelnut shell (Hu et al., 2007; Haykiri-Acma, 2006).

Table 3.3 – Carbon, hydrogen and nitrogen contents (dry basis) of pecan shells fractions

Component	Fine	Medium	Coarse	Raw
Carbon (%)	42.38 ^[b] (0.778)	46.84 ^[a] (0.18)	46.14 ^[a] (0.35)	46.97 ^[a] (0.39)
Hydrogen (%)	5.55 ^[a] (0.01)	5.41 ^[a] (0.15)	5.67 ^[a] (0.08)	5.42 ^[a] (0.01)
Nitrogen (%)	0.60 ^[a] (0.06)	0.44 ^[a,b] (0.02)	0.23 ^[b] (0.10)	0.57 ^[a] (0.11)

Note: Standard deviations are notated in parenthesis below each measurement. samples (n=3) in each row with same letter are not significantly different (P<0.05)

3.3.2.3. Structural Carbohydrates

In general, the cellulose composition in pecan shells increased as particle size fractions increased. As expected from the ultimate analysis previously discussed, the fine fraction had significantly (P < 0.05) less cellulose and hemicelluloses than the medium,

coarse and raw particle size fractions (hence less carbon). There is no clear trend of an effect of particle size on hemicelluloses and lignin percentages. In general, the lignin composition of the samples was similar reported values of fir (31.2%), white pine (26.7%), olive waste (28.0%) and almond shell (27.2%) in Table 2.3. The structural carbohydrate analysis of particle size fractions of pecan shells is given in Table 3.4 below.

Table 3.4 – Cellulose, hemicelluloses and lignin contents (dry basis) of pecan shells fractions

Sample	Cellulose (%)^A	Hemicelluloses (%)^B	Lignin (%)^C	Extractives (%)^D
fine	9.53 ^[a]	7.38 ^[a]	26.53 ^[b]	56.56
medium	24.17 ^[b]	18.43 ^[c]	25.16 ^[a]	32.24
coarse	36.03 ^[c]	16.33 ^[b]	30.59 ^[d]	17.05
raw	35.56 ^[c]	16.73 ^[b]	29.78 ^[c]	17.93

samples (n=3) in each column with the same letter are not significantly different (P<0.05)

^A = Acid-detergent fiber (ADF) – acid-detergent lignin (ADL) (Eq. 3.5)

^B = Neutral-detergent fiber (NDF) – ADF (Eq. 3.6)

^C = ADL

^D = Extractives include lipids, proteins or non-structured carbohydrates (i.e. starch)

3.3.3. Particle Size Effect on Physical Properties of Pecan Shells

3.3.3.1. Poured Bulk Density

The poured bulk density of pecan shells ranged from 417.39 to 469.13 kg/m³ and decreased with an increase in particle size. Therefore, the volume required to store or transport (with identical mass) pecan shells is significantly increased as particle size increases. Mani et al. (2006) found that bulk and particle densities of wheat straw, barley straw, corn stover and switchgrass decreased with increased particle size. It should be mentioned that although the poured bulk density measurements were similar to other

biological materials (soybean – Deshpande, et al., 1993; faba bean – Altunaş and Yildiz, 2007; cashew nut – Balasubramanian, 2001; alfalfa cubes and pellets – Fasina and Sokhansanj, 1992), it is noticeably higher than some other bioenergy feedstocks, such as switchgrass and corn stover ($<200 \text{ kg/m}^3$) (Mani et al., 2006; Fasina, 2006; Bernhart and Fasina, 2009). The average poured bulk density (ρ_b) of pecan shell samples are shown in Table 3.5.

Table 3.5 – Poured bulk density of pecan shells fractions

Sample	Mean ρ_b (kg/m^3)	St. dev.
fine	459.93 ^[a]	7.02
medium	434.86 ^[b]	6.44
coarse	417.39 ^[c]	5.23
raw	469.13 ^[a]	6.09

samples (n=3) with same letter are not significantly different (P<0.05)

3.3.3.2. Particle Density

The particle density of pecan shells showed a significant decrease ($P < 0.05$) as particle size increased with particle densities ranging in value from 1498.51 to 1439.11 kg/m^3 . Therefore, the individual particles became less dense as the sample increased in size. It is postulated that the process of grinding or breaking of the particles removed some of the open pores within the particles. The particle density (ρ_p) of pecan shell samples is shown in Table 3.6 below.

Table 3.6 – Particle density of pecan shells fractions

Sample	Mean ρ_p (kg/m³)	St. dev.
fine	1498.51 ^[a]	2.40
medium	1456.98 ^[b]	4.24
coarse	1439.11 ^[c]	2.75
raw	1432.41 ^[c]	2.88

samples (n=3) with same letter are not significantly different (P<0.05)

3.3.3.3. Tap Bulk Density

The tap bulk density of pecan shells significantly decreased ($P < 0.05$) from 601.67 kg/m³ to 486.00 kg/m³ with an increase in particle size. It is postulated that the smaller size of the particles in the fine fraction made it easier to fill the voids during tapping. The larger sized samples have larger sized particles that cannot easily fill the void space during tapping. Similar trends have been reported for biological materials such as wheat straw, barley straw, corn stover and switchgrass (Mani et al., 2004; Lam et al., 2008). Statistical analysis showed that there was a significant effect ($P < 0.05$) of particle size on the tap bulk density of pecan shells. Table 3.7 shows the average tap bulk density (ρ_t) of pecan shell samples.

Table 3.7 – Tap bulk density of pecan shells fractions

Sample	Mean ρ_t (kg/m³)	St. dev.
fine	601.67 ^[a]	9.87
medium	546.33 ^[c]	5.03
coarse	486.00 ^[d]	2.65
raw	579.33 ^[b]	2.52

samples (n=3) with same letter are not significantly different (P<0.05)

3.3.3.4. Porosity

Porosity significantly increased ($P < 0.05$) from 0.672 to 0.710 as particle size increased from the fine to coarse fraction, respectively. These values are typical of extremely irregular-shaped particles that have cohesive tendencies (Woodcock and Mason, 1987). It is suspected that the hardness of the pecan shells and shelling process operations caused the irregularities in the particle shapes of pecan shells, hence the high porosity values. It should be noted that the porosity values of spherical particles is about 0.4. Increasing porosity values with increasing particle size has been reported for switchgrass and corn stover (Lam et al., 2008). High porosity values are a sign of logistical and economic problems that can be encountered during the storage and transportation of pecan shells, unless some form of densification is utilized (Fasina, 2007). Table 3.8 below gives the average porosity values of the pecan shell fractions.

Table 3.8 – Porosity of pecan shells fractions

Sample	Mean	St. dev.
fine	0.693 ^[b]	0.004
medium	0.702 ^[a,b]	0.004
coarse	0.710 ^[a]	0.003
raw	0.672 ^[c]	0.005

samples (n=3) with same letter are not significantly different ($P < 0.05$)

3.3.3.5. Hausner Ratio

Hausner ratio (H_R) values significantly increased ($P < 0.05$) with increase in particle size (Table 3.9). The values of Hausner ratio show that the coarse and raw

samples can be easily fluidized since their values are lower than 1.25. However, the fine and medium samples may present fluidization problems (Barbosa-Canovas et al., 2005).

Table 3.9 – Hausner ratio of pecan shells fractions

Sample	Mean H_R	St. dev.
fine	1.27 ^[a]	0.01
medium	1.28 ^[a]	0.02
coarse	1.15 ^[b]	0.01
raw	1.15 ^[b]	0.00

samples (n=3) with same letter are not significantly different (P<0.05)

3.3.3.6. Mechanical Compressibility

As expected, the compressibility of the samples decreased with increase in particle size. The percent compressibility of pecan shells ranged from 1.33% at applied pressure of 1.5 kPa to 10.5% at an applied pressure of 15 kPa for the coarse and fine samples, respectively. A trend of increased compressibility as particle size decreased and applied pressure increased is shown in Figure 3.6. The highest percentages of compressibility were obtained from the fine sample, which is indicative of its deformation property. The fine sample's consistency was similar to fine powders, whereas the larger particle size samples had larger particulates that were not able to deform as easily as the smaller particle size sample. The inability of the larger sized particles to fill the inter-particle void space (as was observed for tap bulk density) was also the reason for reduced compressibility values. High compressibility values can be associated with reduced flowing ability (Tabil and Sokhansanj, 1997; Barbosa-Canovas, 2005). According to Fayed and Skocir (1997), percent compressibility values ranging from 5 to 15% have excellent flow. Based on this and the values presented in Figure 3.6.,

pecan shells can be classified as free-flowing granules with excellent flow. Equation 3.21 was developed to show the relationship between mechanical compressibility (%), mean diameter particle size (mm) and pressure (kPa) of pecan shells.

$$C_M = 4.432 - 4.307*PS + 0.941*PS^2 + 4.917*\log(\sigma) , R^2 = 0.942 \quad (3.21)$$

Where, C_M is percent compressibility, PS is mean geometric particle size (mm) and σ is applied pressure (kPa).

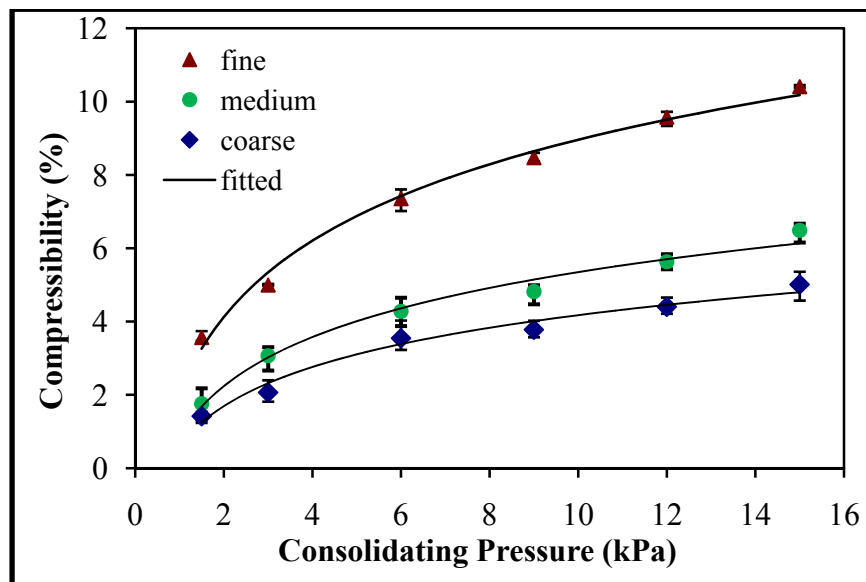


Figure 3.6 – Effect of particle size and pressure on the mechanical compressibility of pecan shells

3.3.3.7. Flowability

The flow function (FF) plots (Figure 3.7) or plots of the ultimate stress (UYS) vs. the major consolidating stress (MCS) indicate the flowability of the fine pecan shell sample is higher than that of the medium and coarse samples. This is confirmed from the values of the flow index (obtained from the inverse of the slope of the linear fit of the flow function graph; Table 3.10).

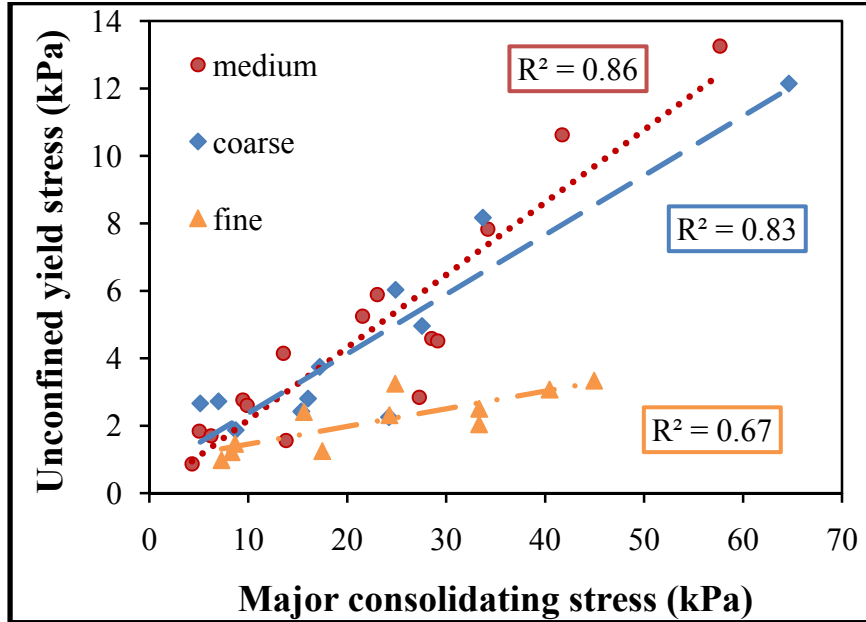


Figure 3.7 – Flow functions of pecan shells fractions

Table 3.10 – Flow index of pecan shells fractions

Sample	Flow Function (FF)	Flow Index (FI)	Flow Characteristic
fine	0.052	19.120	Free Flowing
medium	0.215	4.651	Easy Flowing
coarse	0.162	6.180	Easy Flowing

According to Jenike (1964) the fine sample can be classified as a free flowing material. The medium and coarse samples can be classified as easy flowing materials. Therefore, the fine sample has the best flow characterization of the pecan shells samples. The flow characterizations are expected from the results from the mechanical compressibility determinations in the previous section of this thesis. The flow properties of the pecan shell samples indicate that in storage silos or transportation equipment,

pecan shells separated into these particle sizes will most likely not need the use of flow aids or specialized discharge openings. Similar trends of flow behavior and particle size were reported for thirteen food powders by Fitzpatrick et al. (2004).

Cohesive strength and angle of internal friction (AIF) were also quantified. Cohesive strength increased as pressure increased for fine, medium and coarse particle size fractions (Table 3.11). The mean cohesive strength of the medium size fraction was significantly higher than those of fine and coarse fractions. In addition, analysis of variance indicated pressure had a significant effect ($P < 0.05$) on the cohesion of pecan shells at 9, 15 and 21 kPa.

Table 3.11 – Cohesive strength (kPa) of pecan shells fractions

Consolidating Pressure (kPa)	Fine	Medium	Coarse
3	0.26	0.40	0.44
6	0.49	0.58	0.67
9 [†]	0.77	1.49	1.40
12	0.72	0.90	0.97
15 [†]	0.78	2.16	0.66
21 [†]	0.40	2.85	2.33
Mean Cohesion (kPa)	0.57^[a]	1.40^[b]	1.08^[a]

*samples (n=3) in each column with same letter are not significantly ($P < 0.05$) different

[†] Comparisons of cohesion at that pressure are statistically different

Statistical testing also showed that the angle of internal friction (AIF) of the medium size fraction was significantly lower than those of the fine and coarse fractions. Pressure did not have a significant effect of the values of angle of internal friction for all particle size fractions. Average values for angle of internal friction for all pressures and particle size samples are shown in Table 3.12.

Table 3.12 – Angle of internal friction (AIF,°) of pecan shell fractions

Consolidating Pressure (kPa)	Fine	Medium	Coarse
3	43.49	34.97	35.63
6	44.63	37.85	42.14
9	43.74	40.90	42.74
12	44.59	39.47	44.98
15	45.81	35.27	43.14
21	46.98	38.08	44.61
Mean AIF (°)	44.87^[a]	37.76^[b]	42.21^[a]

* samples (n=3) with same letter are not significantly different (P<0.05)

3.3.4. Moisture content effect on physical properties of pecan shells

3.3.4.1. Moisture Adjustment

The study of the effect of moisture content on the physical properties of pecan shells was carried out with samples conditioned to five moisture content levels (4.42, 8.41, 14.73, 19.36 and 24.70%, wet basis). The initial moisture content of the shells was 14.59% (w.b.). Only the medium size sample (geometric mean diameter 1.241 mm) was used for the moisture content effect study.

3.3.4.2. Particle Size Distribution

The particle size distribution of the medium size fraction at different moisture contents is shown in Figure 3.8. The values of geometric mean diameter (d_{gw}) and geometric standard deviation (S_{gw}) (calculated according to ASAE S319.4) can be found in Table 3.13. Analysis of variance (ANOVA) and Tukey's multiple comparison test

indicated that moisture content had a significant effect ($P < 0.05$) on the geometric mean diameter of pecan shells. The increase in geometric mean diameter is a result of the additional moisture that caused the pecan shell particles to swell and increase in size.

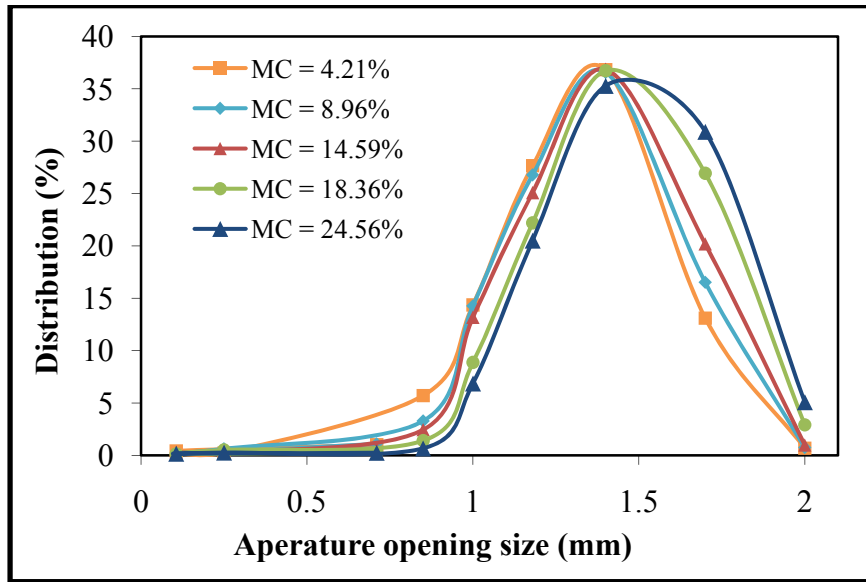


Figure 3.8 – Particle size distribution of pecan shells at different moisture contents

Table 3.13 – Geometric mean diameters and standard deviation of pecan shells at different moisture contents

Moisture Content (% w.b.)	d_{gw}	S_{gw}	CV (%)
4.21	1.219 ^[c]	0.459	37.65
8.96	1.243 ^[b,c]	0.464	37.33
14.59	1.284 ^[b]	0.421	32.79
18.36	1.356 ^[a]	0.384	28.32
24.56	1.404 ^[a]	0.381	27.14

samples (n=3) with same letter are not significantly different ($P < 0.05$)

3.3.4.3. Poured Bulk Density

Poured bulk density of pecan shells reduced from 460 kg/m³ to 396 kg/m³ as moisture content increased from 4.42% to 24.70% (Figure 3.9). This shows that the bulk material expanded volumetrically at a faster rate than the increased mass due to addition of moisture. Practical application of this is that when designing the storage, handling and transportation of shells, the volume necessary to store or move the shells (with identical mass) will increase as moisture content increases. Similar results have been documented for other biological materials (Balasubramanian, 2001; Nimkar and Chattopadhyay, 2001; Fasina and Sokhansanj, 1992; Deshpande et al., 1993; Mozammel et al., 2006; Altunataş and Yildiz, 2005; Bernhart and Fasina, 2009; McMullen et al., 2005; Colley et al., 2006). The following equation describes the relationship between poured bulk density (kg/m³) and moisture content (% w.b.).

$$\rho_b = 463.873 - 0.104 * MC^2, R^2 = 0.942 \quad (3.22)$$

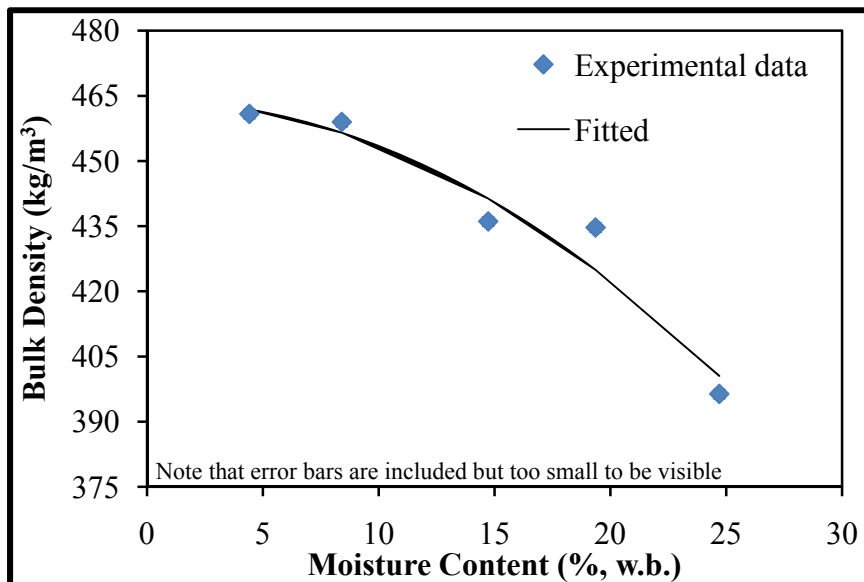


Figure 3.9 – Effect of moisture content on the poured bulk density of pecan shells

3.3.4.4. Particle Density

The particle density of pecan shells also decreased from 1429 kg/m³ to 1375 kg/m³ as moisture content increased from 4.42% to 24.7%, respectively (Figure 3.10). The decline in particle density is due to the volumetric expansion of the particles, occurring at a faster rate than the increase in mass of particles due to addition of moisture. Similar trends have been reported for other biological materials (Joshi et al., 1993; Deshpande et al., 1993; Colley and Fasina, 2006). Equation 3.23 explains the relationship between particle density (kg/m³) and moisture content (% w.b.) for pecan shells.

$$\rho_p = 1444.706 - 2.694 * MC, R^2 = 0.963 \quad (3.23)$$

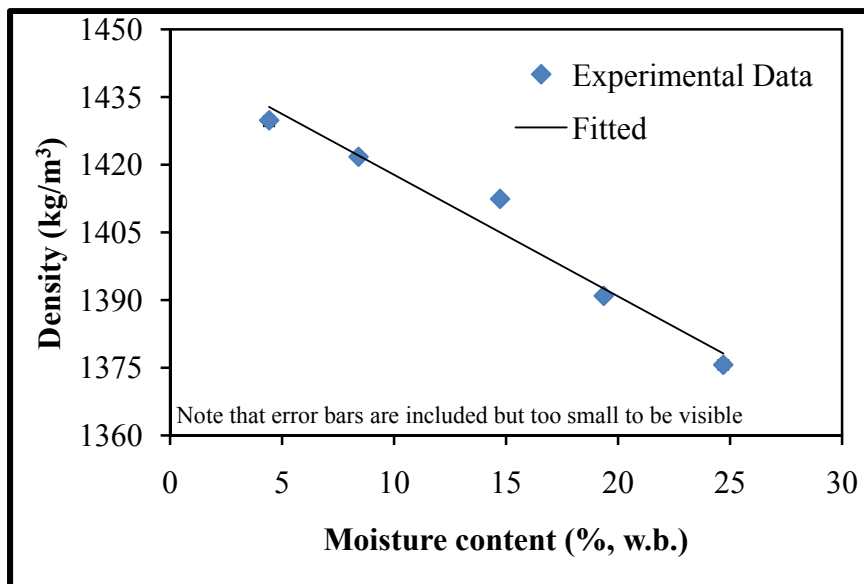


Figure 3.10 – Effect of moisture content on particle density of pecan shells

3.3.4.5. Tap Bulk Density

The tap bulk density of the pecan shells decreased with increased moisture content (Figure 3.11). A maximum value of 537 kg/m³ was obtained at the moisture content level of 4.42%. The decrease in tap density as moisture increases is indicative of the same moisture content – density relationship previously discussed in this thesis that showed that bulk and particle volume increased at a rate faster than the mass of the bulk. The overall higher values of tap bulk density versus poured bulk density is an implication that during the transport of pecan shells, the material will compact as a result of vibrations that could result in difficulties in unloading pecan shells from transportation vehicles. Similar trends have been reported for other biological materials (Lam et al., 2008; Bernhart and Fasina, 2009).

The following equation was developed to show the relationship of the effect of tap bulk density (kg/m³) and moisture content (% w.b.) for pecan shells.

$$\rho_t = 541.580 - 0.108*MC^2, R^2 = 0.942 \quad (3.24)$$

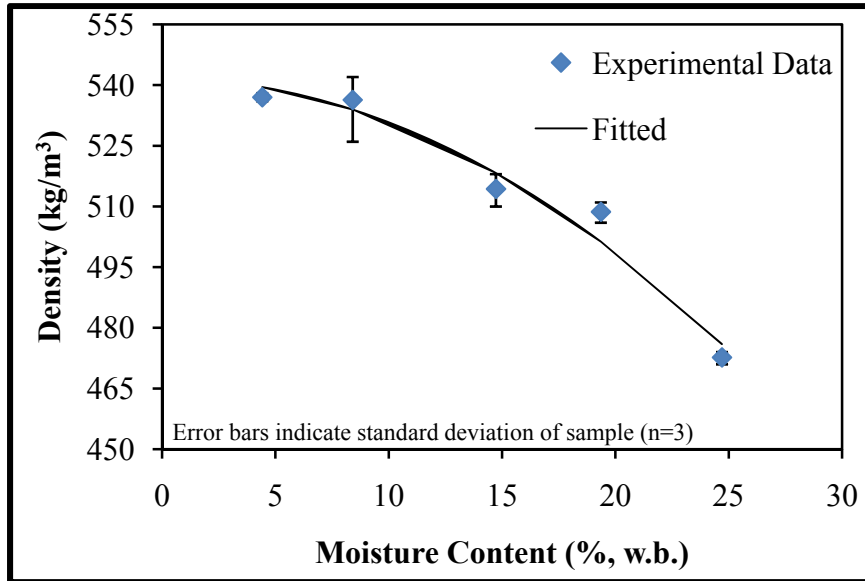


Figure 3.11 – Effect of moisture content on the tap bulk density of pecan shells

3.3.4.6. Porosity

Porosity increased from 0.677 to 0.712 as moisture content of pecan shells increased. Generally, as moisture content increased, an increase in porosity was observed. Figure 3.12 and Equation 3.25 demonstrate the linear relationship between porosity and moisture content. Similar trends have been obtained for other biological materials (Balasubramanian, 2001; Altunaş and Yildiz, 2007; McMullen et al., 2005; Suthar and Das, 1996; Gupta and Das, 1997; Aviara et al., 1999). The average porosity for spherical particles is 0.40. Non-spherical or irregular particles have higher porosity percentages (Woodcock and Mason, 1987). Therefore, the porosity values obtained in this study is indicative of the irregular shape of pecan shell particles.

$$\varepsilon = 0.675 + 0.000055*MC^2, R^2 = 0.858 \quad (3.25)$$

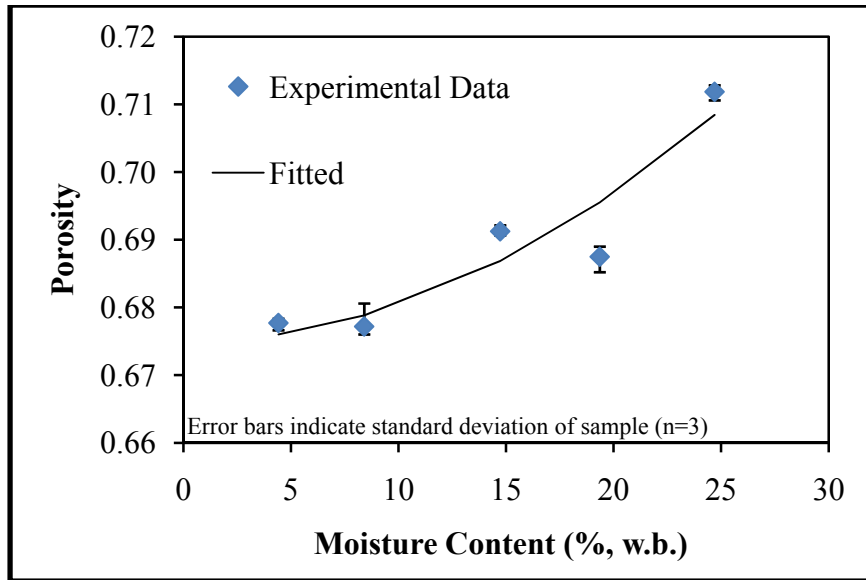


Figure 3.12 – Effect of moisture content on porosity of pecan shells

3.3.4.7. Hausner Ratio

In this study, statistical analysis of the Hausner ratio of pecan shells showed no significant effect ($P > 0.05$) of moisture content on Hausner ratio. The average Hausner ratio of pecan shells at different moisture contents was 1.144, less than the critical value of 1.25, therefore suggesting that pecan shells (with geometric mean diameter of 1.241 mm) can be easily fluidized at moisture content (% w.b.) levels ranging from 4.42% to 24.70% (Barbosa-Canovas et al., 2005).

Table 3.14 – Hausner ratio of pecan shells at different moisture content levels

M.C. (% w.b.)	Mean H_R	St. dev.
4.42	1.142 ^[a]	0.005
8.41	1.141 ^[a]	0.006
14.73	1.133 ^[a]	0.006

19.36	1.154 ^[a]	0.003
24.70	1.150 ^[a]	0.006

*samples (n=3) with same letter are not significantly different (P<0.05)

3.3.4.8. Mechanical Compressibility

The percent compressibility of pecan shells ranged from 0.78% to 10.02% within the range of moisture contents and applied pressures used in this study (Figure 3.13). As was observed for other biological materials (Bernhart and Fasina, 2009; Barbosa-Canovas et al., 2005), compressibility of pecan shells increased with moisture content and pressure. Increased compressibility with moisture content is due to moisture added that formed liquid bridges between particles thereby making them more cohesive (Teunou and Fitzpatrick, 1999). In addition, biological materials become softer when moisture is adsorbed, thus deformation of the material is greater at higher moisture contents (Bernhart and Fasina, 2009). Based on Fayed and Skocir's (1997) classifications, the compressibility values show that pecan shells have excellent flow, since the compressibility values are less than 15%. The following equation was developed to show the relationship of mechanical compressibility, applied pressure and moisture content:

$$C_M = 0.783 - 0.284*MC + 0.016*MC^2 + 4.961 \log(\sigma) , R^2 = 0.927 \quad (3.26)$$

Where C_M is compressibility (%), MC is moisture content (% w.b.) and σ is applied pressure (kPa).

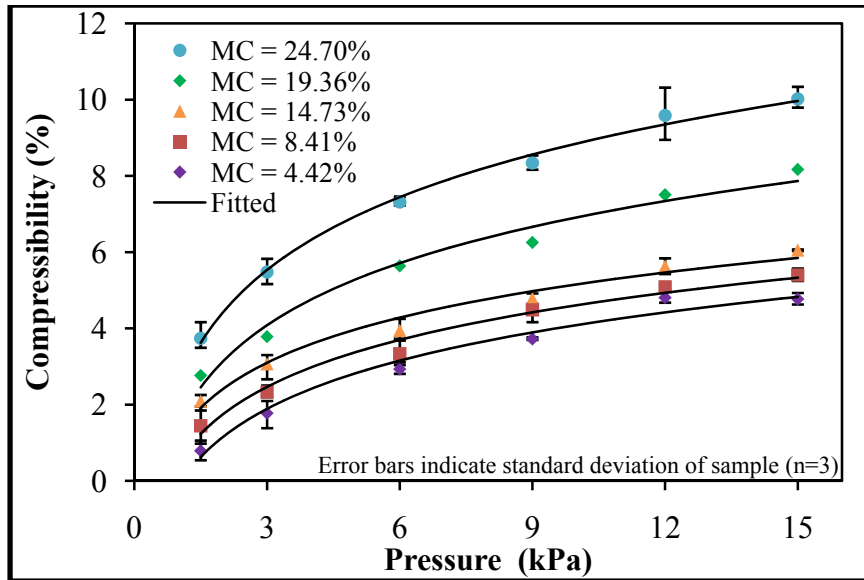


Figure 3.13 – Effect of moisture content and applied pressure on the mechanical compressibility of pecan shells

3.3.4.9. Flowability

The flow function plots of the ultimate yield stress (UYS) and major consolidating stress (MCS) (Figure 3.14) are fitted with linear best-fit lines that indicate that as moisture content increases, flowability decreases. Slopes of these lines that are lying towards the bottom of the graph (x-axis) represent easy flow, and more difficult flow is represented as the linear fit lines move upwards in a counter-clockwise direction (see Figure 2.4). Flowability of the pecan shells is further characterized by flow index (FI) values obtained from the inverse of the slope of the linear fit of the flow function plot (Table 3.15). Similar to the effect of moisture on mechanical compressibility discussed in the previous section, higher moisture content levels in pecan shells will compress more than lower moisture content shells. Therefore, at higher moisture

contents, the material is compressing more and the force required to shear the material is greater than the force required to shear lower moisture content samples that compress less at the same pressure. The general trend for reduction in flowability due to increase in moisture content observed in this study is similar to other biological materials (Ganesan et al, 2008; Zou and Brusewitz, 2002; Teunou and Fitzpatrick, 1999)

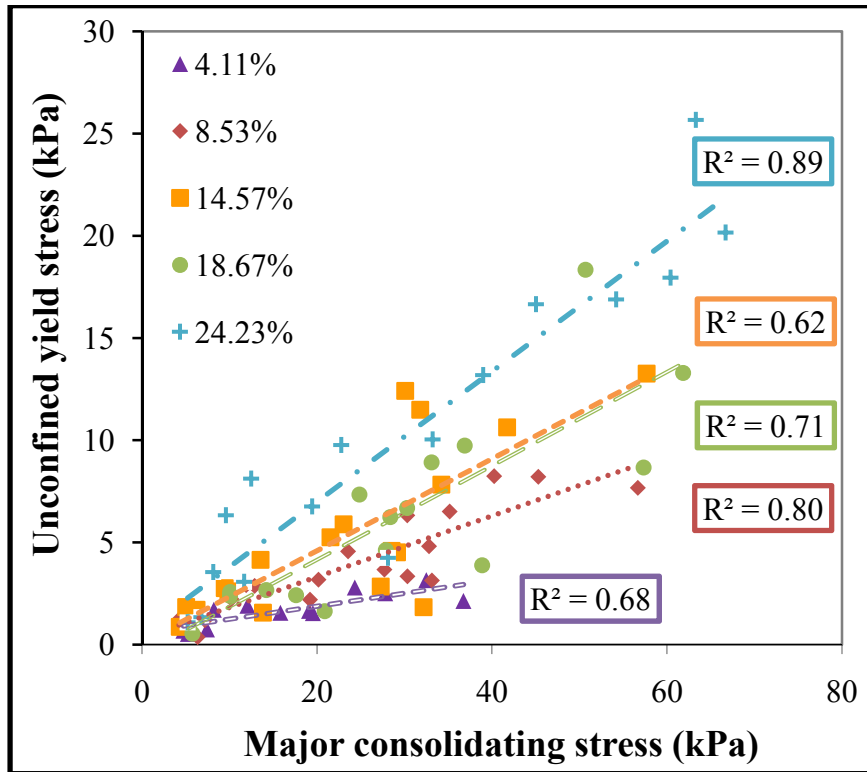


Figure 3.14 – Flow functions of pecan shells at different moisture contents

Utilizing Jenike’s classification of flowability by flow index, the reduction in flowability is confirmed as pecan shells at the lowest moisture content (4.11%, w.b.) is characterized

as free flowing and the 24.23% (w.b.) moisture content sample is classified as a cohesive material. The implication of the shift in flow behavior due to moisture content indicates that pecan shells at moisture contents above 24% (w.b.) will require flow aids during discharge from storage equipment.

Table 3.15 – Flow index of pecan shells at various moisture contents

M.C. (% w.b.)	Flow Function (FF)	Flow Index (FI)	Flow Characteristic
4.11	0.063	15.773	Free Flowing
8.53	0.150	6.676	Easy Flow
14.57	0.225	4.448	Easy Flow
18.67	0.230	4.352	Easy Flow
24.23	0.319	3.138	Cohesive

Figure 3.15 shows the cohesion at all pressures for all samples. As expected, cohesion increased with pressure. The cohesive strength of the 4.11% (w.b.) sample was significantly ($P < 0.05$) lower than that of the other samples whereas the angle of internal friction of the highest moisture content sample (24.23%, w.b.) was significantly higher than those of the other samples. Similar to cohesive strength, angle of internal friction also increased with increased pressure. Mean angle of internal friction at all pressures and moisture content levels are given in Table 3.16.

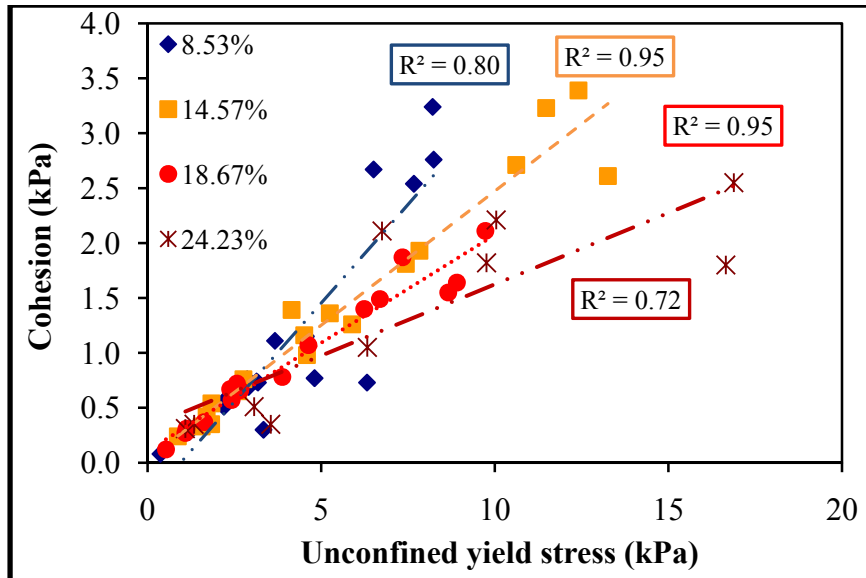


Figure 3.15 – Cohesive strength of pecan shells at different moisture contents

Table 3.17 – Angle of internal friction (°) of pecan shells at different moisture contents

Consolidating Pressure (kPa)	Moisture Content (% w.b.)				
	4.11	8.53	14.53	18.67	24.23
3	37.03	40.52	32.97	36.91	35.62
6	32.97	36.46	37.85	33.39	39.10
9	42.52	38.42	34.71	40.34	48.78
12	42.81	36.33	42.35	39.87	47.76
15	-	39.98	35.27	46.31	47.89
21	-	35.51	38.08	45.28	54.28
Mean (kPa)	38.83 ^[a]	37.87 ^[a]	36.87 ^[a]	40.35 ^[a]	45.57 ^[b]

*samples (n=3) with same letter are not significantly different (P<0.05)

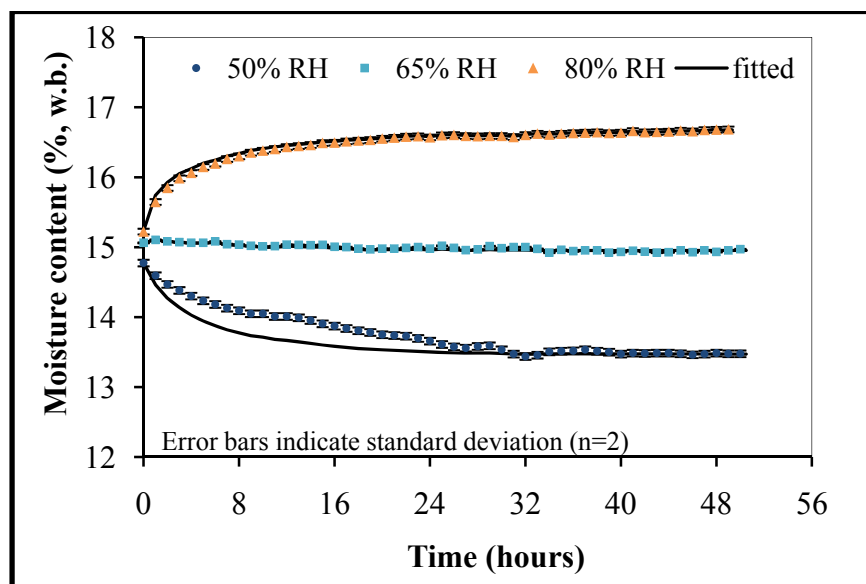
- denotes values that could not be determined

3.3.5. Rate of Moisture Sorption

The effect of air temperature and relative humidity on the rate of moisture sorption by pecan shells is shown in Figures 3.16 and 3.17. Overall, the rate of moisture sorption was affected by the environment that the samples were exposed to. Figure 3.16

demonstrates the effect of relative humidity for pecan shell samples exposed to a temperature of 15°C. At 50% relative humidity, the moisture content at the end of the experiment (13.47%, w.b.) decreased from the initial moisture content of 15.02% (w.b.). An increase in relative humidity to 80% (compared to 50% RH) resulted in an increase in final moisture content (16.68%, w.b.). Figure 3.17 demonstrates the effect of temperature on the rate of moisture sorption of pecan shells in the same relative humidity environment of 80%. The rate of moisture sorption increases with increased temperature (at 80% relative humidity). At 80% relative humidity, final moisture contents of 16.68, 16.92 and 17.62% (w.b.) were observed for temperatures of 15, 25 and 35°C, respectively. The implication of the data depicted in the two graphs is that air relative humidity and temperature will affect the moisture content of pecan shells during storage and transport and that these changes can occur in a period of two days or less.

Figure 3.16 – Moisture change in pecan shells exposed to air at 15°C and relative humidity levels of 50, 65 and 80%. Initial moisture content was 15.02% (w.b.)



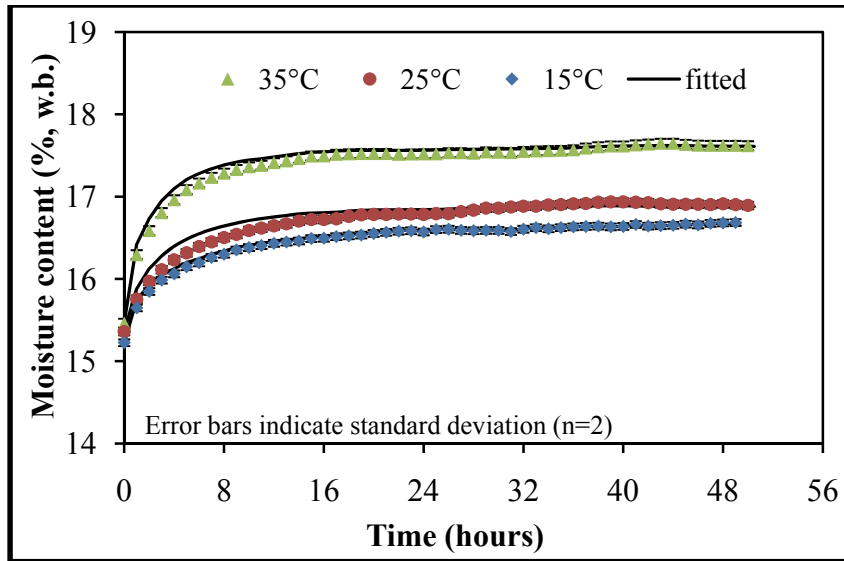


Figure 3.17 – Moisture change in pecan shells exposed to air at 80% relative humidity and temperatures of 15, 25 and 35°C.

The Page model (Equation 3.27) has been used to model the drying characteristics of biological materials and fruits (Dadgar, 2004; Doymaz, 2007; Kashinaninejad and Tabil, 2004; Akpinar and Bicer, 2004). Table 3.17 gives the estimates of rate of moisture sorption constants k and n and the equilibrium moisture content (M_e). A non-linear regression procedure in SAS (Version 9.3, 2008) was used to estimate the values of the constants.

$$\frac{M - M_e}{M_i - M_e} = \exp(-kt^n) \quad (3.27)$$

where, t = time (min)

M = instantaneous moisture content (% w.b.)

M_i = initial moisture content (% w.b.)

M_e = equilibrium moisture content (% w.b.)

k = constant

n = constant

Table 3.17 – Estimated values of constant (*k*), constant (*n*) and equilibrium moisture content (*M_e*) obtained from non-linear regression analysis using Equation 3.20 for pecan shells

Relative Humidity (%)	Temperature (°C)	<i>k</i>	<i>n</i>	<i>M_e</i>
50	15	0.1007	0.9349	13.47
	25	0.0337	1.3566	11.46
	35	0.2321	0.8449	9.86
65	15	0.0066	1.5464	15.05
	25	0.5131	0.5646	14.28
	35	0.2067	0.7429	14.20
80	15	0.3639	0.6389	16.68
	25	0.3008	0.7209	16.92
	35	0.5003	0.6223	17.62

Statistical analysis showed that estimated values of *k*, *n* and *M_e* were significantly ($P < 0.05$) affected by relative humidity and temperature. In general, *k* was lower for samples that desorbed moisture and higher for those that absorbed moisture. Overall, samples that did not absorb or desorb moisture had low *k* values and *n* values higher than 1. High coefficient of determination (R^2) values indicates that the model used to determine the constants were appropriate with values between 0.892 and 0.991. Standard errors of the model ranged from 0.0005 and 0.0052, giving further confidence that the model is acceptable in the determination of moisture sorption rate, constant *n* and equilibrium moisture content of pecan shells. Other biological materials have shown the similar relationships of *k*, *n* and *M_e* on relative humidity and temperature (Dadgar et al, 2004; Doymaz, 2007; Doymaz and Pala, 2002).

3.3.6. Equilibrium Moisture Isotherm

Typically, equilibrium moisture relationships for biological materials are represented in terms of dry basis, or grams of water per grams of dry material. Since most moisture content measurements have been reported in wet basis, equation 3.28 was utilized to convert wet basis (MC_{wb} , %) to dry basis (MC_{db} , %) (ASAE Standard D245.6, 2007).

$$MC_{db} = \frac{100 * MC_{wb}}{100 - MC_{wb}} \quad (3.28)$$

The equilibrium moisture content (EMC) – equilibrium relative humidity (ERH) curves are illustrated in Figure 3.18. The curves are type II (sigmoidal) in shape that is typically obtained for biological materials (Labuza, 1984; Erbas et al., 2005; Chen, 2003; Igathinathane et al., 2007).

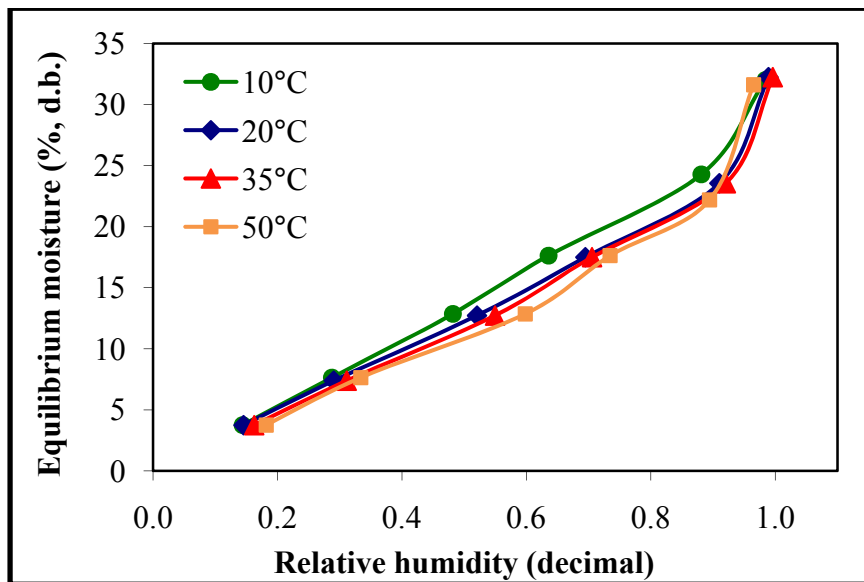


Figure 3.18 – Moisture sorption isotherms for pecan shells at 10, 20, 35 and 50°C

The EMC and ERH data were analyzed using the following four equations (Chen, 2008; Ajibola et al., 2003; Colley et al., 2006; Fasina and Sokhansanj, 1993):

$$\text{Modified Halsey equation: } ERH = \exp \left[-\frac{\exp(a+b*t)}{MC_{db}^c} \right] \quad (3.29)$$

$$\text{Modified Henderson equation: } ERH = 1 - \exp[-a * (t + c) * (MC_{db})^b] \quad (3.30)$$

$$\text{Modified Chung-Pfost equation: } ERH = \exp \left[-\frac{a}{t+c} \exp(-b * MC_{db}) \right] \quad (3.31)$$

$$\text{Modified Oswin equation: } ERH = \left[\left(\frac{a+bt}{MC_{db}} \right)^c + 1 \right]^{-1} \quad (3.32)$$

Where, ERH is equilibrium relative humidity (in decimal), MC_{db} is equilibrium moisture content (in dry basis), t is temperature ($^{\circ}C$) and a, b and c are model constants. The experimental data collected were fitted to the four isotherm equations using the NLIN procedure (SAS, 2008), that involves minimizing the sum of squares deviations in a series of iterations. The coefficient of determination (R^2), standard error of estimate (SEE) and mean relative deviation (MRD) were utilized to determine the goodness-of-fit for each isotherm prediction equation (3.22 – 3.24). The standard error of the estimate is defined as:

$$SEE = \frac{\sqrt{\sum_{i=1}^m (MC_{db} - \widehat{MC}_{db})^2}}{df} \quad (3.33)$$

Where, MC_{db} is the experimental data, \widehat{MC}_{db} is the estimated value, m is the number of data points and df is degrees of freedom on the regression model. Mean relative

deviation (MRD) gives insight of the mean divergence of the measured data from the predicted data, and is defined as:

$$MRD = \frac{1}{m} \sum_{i=1}^m \left(\frac{|MC_{db} - \overline{MC_{db}}|}{MC_{db}} \right) \quad (3.34)$$

The SEE value represents the fitting ability of a model in relation to the number of data points, however used alone is not able to provide direct visualization of the goodness-of-fit. Therefore, SEE is used in combination with MRD and R^2 in this study. In general, the best model has the smallest SEE and MRD values and highest R^2 value (Sun and Byrne, 1998). Multiple authors have reported the use of multiple statistical parameters to select the best moisture sorption isotherm equation (Chen, 2003; Fasina and Sokhansanj, 1993; Sun and Bryne; 1998; Colley et al., 2006). The model coefficients and statistics of fitting are located in Table 3.18. All of the models have R^2 values of 0.999. According to Pagano and Mascheroni (2005), isotherm equations that have MRD values less than 0.05 are considered to be a good fit. The Henderson and Chung-Pfost equations have SEE values and MRD values less than 0.05, and both could be used as isotherm equations for pecan shells. The Chung-Pfost and Henderson equations have also been reported as the best isotherm equation for other biological materials (switchgrass pellets– Colley et al., 2006; cowpea – Ajibola et. al., 2003)

Table 3.18 – Model coefficients and values for the standard error of estimate (SEE), mean relative deviation (MRD) and coefficient of determination (R^2) for the temperature range of 10-50°C

Coefficients			Statistics of fitting			
Equation	<i>a</i>	<i>b</i>	<i>c</i>	SEE	MRD	R^2
Halsey	3.4093	-0.0068	1.5359	0.0773	0.0718	0.999
Stdev	± 0.5490	± 0.0050	± 0.1968			
Henderson	1.020E-04	142.500	1.5065	0.0307	0.0265	0.999
Stdev	± 3.200E-05	± 50.006	± 0.0578			
Chung-Pfost	528.3000	136.7000	0.1313	0.0291	0.0245	0.999
Stdev	± 150.9000	± 46.8436	± 0.0048			
Oswin	12.2736	-0.0444	2.2105	0.0539	0.0508	0.999
Stdev	± 0.8161	± 0.0236	± 0.1611			

3.4. Conclusions

Compositional analysis of pecan shells indicated that energy content and ash content were significantly affected by particle size. Elemental analysis of pecan shells at different particle sizes indicated that there was significantly less carbon percentage in the fine fraction whereas the composition of nitrogen decreased as particle size increased. Hydrogen levels were statistically similar at a 95% confidence level. The structural carbohydrate analysis indicated that the cellulose, hemicelluloses and lignin percentages were significantly affected by particle size. Cellulose levels increased as particle size increased, however, there was no noticeable trend for the effect of particle size in hemicelluloses and lignin levels.

It can be concluded from this study that particle size and moisture content significantly affect the physical characteristics of pecan shells. Increasing particle size and moisture content resulted in decreases in the poured bulk, particle and tap bulk densities. Porosity of pecan shells indicated that the particles were irregular and non-spherical in shape and increased with particle size and moisture content. The Hausner ratio of the particle size fractions indicated that the coarse and raw samples can be easily fluidized as well as the samples at all moisture contents. The compressibility of pecan shells increased as particle size decreased, as moisture content and applied pressure increased. Flow characteristics of pecan shells were determined as free-flowing for the fine fraction and easy flowing for the medium and coarse particle size fractions. Cohesion was significantly affected by pressure and particle size. Cohesion of pecan shells increased as particle size increased. Angle of internal friction was also

significantly affected by particle size, where a 17% decrease was observed as particle size decreased by 10%.

Temperature and relative humidity had a significant effect on the moisture sorption rate (k), constant (n) and equilibrium moisture content (M_e). The Henderson and Chung-Pfost isotherm equations were determined to be the most appropriate fit to the experimental data whereas the Halsey equation was determined to be the least appropriate.

3.5. References

- Ajibola, O.O., Aviara, N.A., Ajetumobi, O.E. 2003. Sorption equilibrium and thermodynamic properties of cowpea (*Vigna unguiculata*). *Journal of Food Engineering* 58: 317-324.
- Akpınar, E.K., Bicer, Y. 2004. Modelling of the drying of eggplants in thin-layers. *International Journal of Food Science and Technology* 39: 1-9.
- Altunaş, E., Yildiz, M. 2007. Effect of moisture content of some physical and mechanical properties of faba bean (*Vicia faba* L.) grains. *Journal of Food Engineering* 78: 178-183.
- ASABE Standard. 2006. S593 Terminology and definitions for biomass production, harvesting and collection, storage, processing, conversion and utilization. St. Joseph, MI: ASABE.
- ASABE Standard. 2007. S269.4. Definition of Methods and Determining Density, Durability, and Moisture Content. St. Joseph, MI: ASABE
- ASABE Standard. 2008. S319.4 Method of determining and expressing fineness of feed materials by sieving. St. Joseph, MI: ASABE.
- ASTM Standard. 2005. B 527. Standard test method for determination of tap density of metallic powders and compounds. West Conshohocken, PA: ASTM.
- Aviara, N.A., Gwandzang, M.I., Haque, M.A. 1999. Physical properties of Guna Seeds. *Journal of Agricultural Engineering Research* 73: 105-111.
- Balasubramanian, D. 2001. Physical properties of raw cashew nut. *Journal of Agricultural Engineering Research* 78(3): 291-297.
- Barbosa-Canovas, G.V., Ortega-Rivas, E., Juliano, P., Yan, H. 2005. *Food Powders: Physical Properties, Processing, and Functionality*. New York, NY: Kluwer Academic/Plenum Pub.
- Bernhart, M., Fasina, O.O. 2009. Moisture effect of the storage, handling and flow properties of poultry litter. *Waste Management* 29: 1392-1398.
- Biagini, E., Barontini, F., Tognotti, L. 2006. Devolatilization of biomass fuels and biomass components studied by TG-FTIR technique. *Industrial and Engineering Chemistry Research* 45: 4486-4493.
- Chen, C. 2000. Factors which effect equilibrium relative humidity of agricultural products. *Transactions of the ASAE* (43)2: 673-683.

- Chen, C. 2003. Moisture sorption isotherms of pea seeds. *Journal of Food Engineering* 58: 45-51.
- Colley, Z., Fasina, O.O., Bransby, D., Lee, Y. 2006. Moisture effect of the physical characteristics of switchgrass pellets. *Transactions of the ASABE* (49)6: 1845-1851.
- Dadgar S., Tabil, L.G., Crerar, B. 2004. Moisture adsorption of field peas as a function of temperature and relative humidity during storage, An ASABE/CSAE Annual Meeting Presentation, Paper No. 046089, Sponsored by ASAE/CSAE, August 1-4, Ottawa, Ontario, Canada.
- Deshpande, S.D., Bal, S., Ojha, T.P. 1993. Physical properties of soybean. *Journal of Agricultural Engineering Research* 56(2): 89-98.
- Di Blasi, C., Signorelli, G., Di Russo, C., Rea, G. 1999. Product distribution from pyrolysis of wood and agricultural residues. *Industrial Engineering and Chemistry Research* 38: 2216-2224.
- Doymaz, I. 2007. Air-drying characteristics of tomatoes. *Journal of Food Engineering* 78: 1291-1297.
- Doymaz, I., Pala, M. 2002. Hot-air drying characteristics of red pepper. *Journal of Food Engineering* 55: 331-335.
- Erbaş, M., Ertugay, M., Certel, M. 2005. Moisture adsorption behavior of semolina and farina. *Journal of Food Engineering* 69: 191-198.
- Fasina, O.O., Ranatunga, T., Vaughan, B. 2007. Physical and chemical characteristics of biofuel feedstocks indigenous to southeastern United States, An ASABE Annual Meeting Presentation, Paper No. 076247, June 17-20, Minneapolis Convention Center, Minneapolis, MN.
- Fasina, O.O., Sokhansanj, S. 1992. Hygroscopic moisture absorption by alfalfa cubes and pellets. *Transactions of the ASAE* 35: 1615-1619.
- Fasina, O.O., Sokhansanj, S. 1993. Equilibrium moisture relations and heat of sorption of alfalfa pellets. *Journal of Agricultural Engineering Research* 56: 51-63.
- Fayed, M.E., Skocir, T.S. 1997. *Mechanical Conveyors: Selection and Operation*. Lancaster, PA: Technomic Publishing Company, Inc.
- Fitzpatrick, J.J., Barringer, S.A., Iqbal, T. Flow property measurement of food powders and sensitivity of Jenike's hopper design methodology to the measured values. *Journal of Food Engineering* 61: 399-405.

- Ganesan, V., Muthukumarappan, K., Rosentrater, K.A. 2008. Flow properties of DDGS with varying soluble and moisture contents using Jenike shear testing. *Powder Technology* 187: 130-137.
- Geisler, Malinda. 2009. Pecans. Agriculture Marketing Resource Center, Iowa State University. Available at: <http://www.agmrc.org>. Accessed 3 May 2010.
- Gupta, R.K., Das, S.K. 1997. Physical properties of sunflower seeds. *Journal of Agricultural Engineering Research* 66: 1-8.
- Haykiri-Acma, H. 2006. The role of particle size in the non-isothermal pyrolysis of hazelnut shells. *Journal of Analytical and Applied Pyrolysis* 75: 211-216.
- Igathinathane, C., Womac, A.R., Sokhansanj, S., Pordesimo, L.O. 2007. Moisture sorption thermodynamic properties of corn stover fractions. *Transactions of ASABE* 50(6): 2151-2160.
- Jenike, A.W. 1964. *Storage and flow of solids*. Bulletin No. 123. University of Utah, Salt Lake City, Utah: Engineering and Experiment Station.
- Joshi, D.C., Das, S.K., Mukherjee, R.K. 1993. Physical properties of pumpkin seeds. *Journal of Agricultural Engineering Research* 54(3): 219-229.
- Kashaninejad, M., Tabil, L.G. 2004. Drying characteristics of purslane (*Portulaca oleraceae* L.). *Drying Technology* 22: 2183-2200.
- Labuza, T.P. 1984. *Moisture sorption: practical aspects of isotherm measurement and use*. Minneapolis, MN: American Association of Cereal Chemist.
- Lam, P.S., Sokhansanj, S., Bi, X., Lim, C.J., Naimi, L.J., Hoque, M., Mani, S., Womac, A.R., Ye, X.P., Narayan, S. 2008. Bulk density of wet and dry wheat straw and switchgrass particles. *Applied Engineering in Agriculture* 24(3): 351-358.
- Mani, S., Tabil, L.G., Sokhansanj, S. 2004. Grinding performance and physical properties of wheat and barley straws, corn stover and switchgrass. *Biomass and Bioenergy* 27: 339-352.
- Mani, S., Tabil, L.G., Sokhansanj, S. 2006. Effects of compressive force, particle size and moisture content on mechanical properties of biomass pellets from grasses. *Biomass and Bioenergy* 30: 648-654.
- McMullen, J., Fasina, O.O., Wood, C.W., Feng, Y. 2004. Storage and handling characteristics of pellets from poultry litter. *Applied Engineering in Agriculture* 21: 645-651.

- Mozammel, H., Shahab, S., Bi, T., Sudhagar, M., Ladan, J., Lim, J. 2006. Interaction of particle size, moisture content, and compression pressure on the bulk density of wood chip and straw, An SCBE/SCGAB Annual Meeting Presentation, Paper No. 06-100, Sponsored by CSBE/SCGAB, July 16-19, Edmonton, Alberta, Canada.
- Nimkar, P.M., Chattopadhyay, P.K. 2001. Some physical properties of green gram. *Journal of Agricultural Engineering Research* 80: 183-189.
- NREL. 2005. Laboratory Analytical Procedure - Determination of Ash in Biomass. United States Department of Energy, Washington, D.C.
- Pagano, A.M., Mascheroni, R.H. 2004. Sorption isotherms for amaranth grains. *Journal of Food Engineering* 67: 441-450.
- Sun, D., Byrne, C. 1998. Selection of EMC/ERH isotherm equations for rapeseed. *Journal of Agricultural Engineering Research* 69: 307-315.
- Suthar, S.H., Das, S.K. 1996. Some physical properties of Karingda [*Citrullus lanatus* (Thumb) Mansf] seeds. *Journal of Agricultural Engineering Research* 65: 15-22.
- Tabil, L.G., Sokhansanj, S. 1997. Bulk properties of alfalfa grind in relation to its compaction characteristics. *Applied Engineering in Agriculture* 13(4): 499-505.
- Teunou, E., Fitzpatrick, J.J. 1999. Effect of relative humidity and temperature on food powder flowability. *Journal of Food Engineering* 42: 109-116.
- USDA-ERS. 2003. Fruit and Tree Nuts Outlook: 28 May 2003. USDA - Economic Research Service, Washington DC.
- USDA-NASS. 2008. Noncitrus Fruits and Nuts Summary. Washington, DC.: USDA National Agricultural Statistics Service.
- Van Soest, P.J., Robertson, J.B. 1985. *Analysis of forages and fibrous foods*. A Laboratory Manual for Animal Science 613. Cornell University, Ithaca, NY.
- Woodcock, C.R., Mason, J.S. 1987. *Bulk Solids Handling: An Introduction to the Practice and Technology*. Glasgow, Scotland: Blackie and Son, Ltd.
- Zou, Y., Bruswitz, G.H. 2002. Flowability of uncompacted marigold powder as affected by moisture content. *Journal of Food Engineering* 55: 165-171.

CHAPTER 4: TG-FTIR ANALYSIS OF PECAN SHELLS DURING THERMAL DECOMPOSITION

4.1. Introduction

Biomass can be converted to energy via biological and thermochemical conversion platforms. Biological conversion processes typically use fermentation to produce ethanol. High conversion efficiency is only possible if the biomass feedstock contain high concentrations of starch or sugar compounds (that are easily accessible) and low concentrations of lignin (e.g. maize or sugar cane). Pecan shells do not contain easily accessible cellulose chains because of a significant amount of lignin concentration (see Chapter 3, Section 3.3.2). Thermochemical conversion processes are the preferred conversion process for biomass feedstocks that have high amounts of lignin, such as wood chips or pecan shells. Combustion, gasification and pyrolysis are the main thermochemical conversion processes that can be used to convert biomass to value-added products, such as heat, syngas, bio-oil or bio-char. Gasification and pyrolysis are considered the most promising because of high energy efficiencies and the ability to handle most biomass materials (Yang et al., 2004; Yaman, 2004). Thermogravimetric analysis (TGA) is the most common thermo-analytical method for quantifying thermal decomposition of biological materials (Vamvuka et al., 2003; Vuthaluru et al., 2003). The fast, repeatable and accurate data collection from TGA enables in-depth analysis of mass loss and determination of kinetic parameters (Yang et al., 2004).

In addition to TGA, other thermo-analytical methods used to study the thermal decomposition of biological materials include: differential scanning calorimetry (DSC) and differential thermal analysis (DTA). TGA, DSC and DTA are all able to provide valuable information on the rate of decomposition. However, they are unable to provide information about the composition and rate of the gas compounds volatilized during thermal decomposition. Thus, it is advantageous to use TGA in conjunction with other analytical tools which can identify and quantify the evolved gas products, or 'real-time analysis', during thermal decomposition. TGA is currently the only thermo-analytical method that can be coupled to other gas analytical instruments, such as a gas chromatogram (GC), mass spectrometer (MS) and Fourier transform infrared (FTIR) spectrometer. These gas analytical instruments are used for 'real-time' analysis of the gases produced during thermochemical analysis (Butterman et al., 2009; Arias et al., 2006; Yang et al., 2007; Bahng et al., 2009).

Therefore, the objectives of this study were to:

- (1) Quantify the rate of thermal decomposition of pecan shells and
- (2) Quantify the composition of the gases evolved during the thermal decomposition process.

4.2. Methods and Materials

4.2.1. Sample Preparation

The pecan shells used in this study were obtained from the Louisville Pecan Company, Louisville, AL. The samples were stored in the Biosystems Process Engineering Laboratory (average temperature of 25°C). Before use, the pecan shells were ground in a Wiley mill to pass through a standard 40-mesh screen. Energy content, ash content and ultimate analysis of pecan shells were previously discussed in Section 3.3.2 and values given in Tables 3.2 and 3.3, respectively.

4.2.2. Thermal Decomposition Study

The thermal decomposition for pecan shells was carried out in a thermogravimetric analyzer (TGA) (Pyris 1, Perkin-Elmer, Shelton, CT). A sample mass of approximately 5 mg was used for thermogravimetric analysis. Samples were heated at rates of 5°C/min, 10°C/min, 20°C/min, 30°C/min and 40°C/min within the temperature range of 30°C to 800°C. Nitrogen and air were used as carrier gases, each at a flow rate of 20 ml/min. Prior to use, the TGA was calibrated for temperature and mass according to the manufacturer's procedure. Temperature calibration was performed using the Curie point of four magnetic standards – alumel (T_{Curie} of 154.2°C), nickel (T_{Curie} of 355.3°C), perkalloy (T_{Curie} of 596.0°C) and iron (T_{Curie} of 780.0°C). Calibration for mass was performed using a 100 mg calibration mass provided by the manufacturer.

4.2.3. Fourier Transform Infrared Spectroscopy

A Fourier Transform infrared (FTIR) spectrometer (Model 100, Perkin-Elmer, Shelton, CT) was used to identify and quantify the gases volatilized from the TGA. A transfer line (heated to 220°C) was used to connect the FTIR to the TGA. The transfer line was heated to eliminate condensation of the volatile gases or adsorption of semi-volatile products produced during pyrolysis (Yang et al., 2004). The software provided by the FTIR manufacturer was used to obtain spectra of the gas flowing through the measurement cell at 20 second intervals within the wavelength number range of 4000 to 700 cm^{-1} . Quantitative analysis of the spectra was performed in two steps: (a) identification of peaks by matching spectra against a library software package (QASOFT, Infrared Analysis Inc., Anaheim, CA) and (b) using the software to quantify the concentration of the identified gases in ppm. Thermogravimetric analysis and FTIR experiments were run simultaneously in triplicate.

4.2.4. Data Analysis

Concentration of volatile gases was determined using library software (QASOFT, Infrared Analysis Inc., Anaheim, CA) and plotted as a function of temperature using Microsoft Excel (Microsoft Office XP Professional, 2007). Analysis of variance (ANOVA) and Studentized t-tests were performed using the Proc anova and Proc ttest functions in SAS statistical software package (Version 9.3, SAS Institute Inc., Cary, NC, 2008-2009), respectively.

4.3. Results and Discussion

4.3.1. Thermal Decomposition of Pecan Shells in Nitrogen Atmosphere

Observed thermal behavior (TG curve) of pecan shells during thermal decomposition is shown in Figure 4.1. For each heating rate, there was an initial mass loss (approximately 14% of total weight) recorded between 30°C and 150°C due to the release of moisture (Fang et al., 2006; de Jong et al., 2007; Baker et al., 2005). The thermal decomposition of pecan shells was therefore determined to begin at 180°C, similar to other reported biological materials (wood lignin – Liu et al., 2008; sugar cane and coconut fibers – Mothe and Miranda; 2009; coconut shells, sugarcane bagasse, corn stalks and peanut shells – Souza et al., 2009). The figure also showed that significant loss in sample mass (40% original weight) occurred between the temperature range of 180°C and 400°C, and thermal decomposition was essentially complete at 600°C. There was a residual weight of 30% after the thermal decomposition procedure. This residue is typically referred to as bio-char. In general, there was an increase in mass loss as heating rate decreased within the temperature range of 180°C to 400°C. Similar results were reported for textile wastes (Miranda et al., 2007), seaweed (Wang et al., 2007) and rice straw, camphor branch, rice husk, cherry bay branch, cotton and maize straw (Hu et al., 2007). For temperatures higher than 600°C, mass losses of 5.72% and 6.16% were obtained at heating rates of 5°C/min and 40°C/min, respectively. Therefore, the amount of gases volatilized at temperatures higher than 600°C may not justify the amount of energy required to maintain the high temperatures (Biagini et al., 2006).

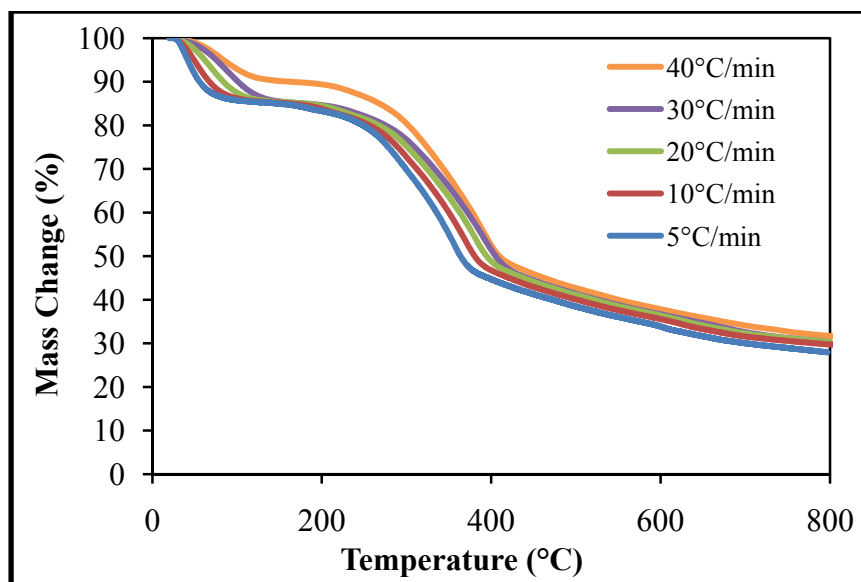


Figure 4.1 – Mass loss from thermal decomposition of pecan shells at different heating rates with nitrogen as carrier gas

Figure 4.2 shows the mass loss rate (da/dt) curves (derivative thermogram – DTG curves) within the temperature range of 150°C to 800°C. Mass loss rate at temperatures lower than 150°C was not shown in order to isolate peaks caused by the thermal decomposition of the hemicelluloses and cellulose compounds in the pecan shell samples. The mass loss fraction (α) was calculated using the equation below:

$$\alpha = \frac{m - m_o}{m_f - m_o} \quad (4.1)$$

Where: m is instantaneous mass (g), m_o is initial mass (at 30°C, g) and m_f is final mass (at 800°C, g). The DTG curve provides a clear representation of the general trend of increasing mass loss with heating rate. Thermal decomposition of biomass frequently presents overlapping peaks; one large peak with a shoulder peak on the left side, which represents the thermal decomposition of hemicelluloses and cellulose. The shoulder peak on the left side is attributed to the peak of hemicelluloses thermal decomposition while

the larger peak is regarded as the peak decomposition for cellulose. The hemicelluloses shoulder and the cellulose peak phenomena has been shown in other biological materials, such as dry distiller's grains with solubles (DDGS) - Giuntoli et al., 2009; sugarcane bagasse – Mothe and Miranda, 2009; palm oil waste – Yang et al., 2004; coconut shells - Souza et al., 2009; seaweed – Wang et al., 2007; and coconut and cashew nut shells - Tsamba et al., 2006. The flat, tailing section of the DTG curves at higher temperatures indicates the thermal degradation of lignin.

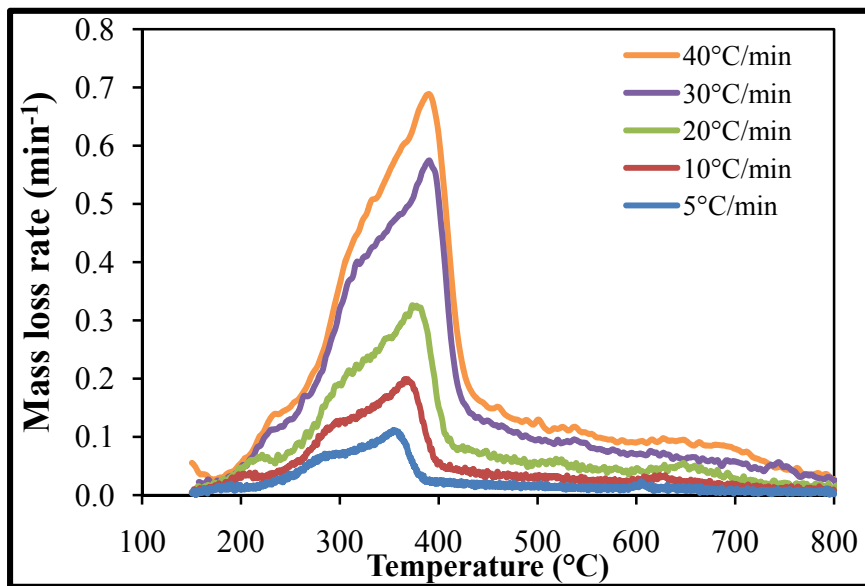


Figure 4.2 – Mass loss rate from the thermal decomposition of pecan shells at different heating rates with nitrogen as carrier gas

The cellulose peaks increased as heating rates increased, occurring at temperatures of 348, 360, 371, 385 and 386°C at heating rates of 5, 10, 20, 30 and 40°C, respectively. Hemicelluloses decomposition peaks were at 275, 285, 305, 315 and 330°C at heating rates of 5, 10, 20, 30 and 40°C, respectively. Hemicelluloses decompose at lower temperatures than cellulose due to the amorphous structure and composition of shorter,

branched 5 carbon chains. In contrast, cellulose consists of a long polymer of glucose without branches, hence the higher thermal stability of cellulose when compared to hemicelluloses (Yang et al., 2007). The temperature ranges observed during decomposition of hemicelluloses and cellulose in pecan shells is consistent with other agricultural waste materials (cotton cocoon shells – Çağlar and Demirbaş; hazelnut shells – Demirbaş, 1998; grape residues, olive and rice husk – Di Blasi et al., 1999; coconut and cashew shells – Tsamba et al., 2006; olive kernel, cotton waste and forest residue – Vamvuka et al., 2003). There was no identifiable mass loss peak for lignin decomposition. Previous researchers have determined that lignin decomposition occurs throughout the thermal decomposition temperature range (180-800°C). This is because of the large molecular composition of lignin that consists of many aromatic rings with various branches and that the activities of the chemical bonds are covered in an extremely wide range (Yang et al., 2007; Gronli et al., 1999; Vamvuka et al., 2003).

4.3.2. Thermal Decomposition of Pecan Shells in Air Atmosphere

The reduction in mass of pecan shells during thermal decomposition in air is shown in Figure 4.3. The trend of reducing mass loss as heating rate increased that was observed during thermal decomposition in nitrogen was also obtained when pecan shells was thermal decomposed in air. However, the oxygen content in the air caused the pecan shells to experience total oxidation, meaning total decomposition of all the hemicelluloses, cellulose and lignin compounds. In contrast to the thermal decomposition of pecan shells in nitrogen where there was a 30% (of original weight) residual ‘bio-char’ left over after the process, the air thermal decomposition yielded ash as residual material consisting of less than 2% (of original weight). The rate of

decomposition in air atmosphere is much faster than that of the nitrogen atmosphere. The oxygen content in the air promoted the combustion of the char residue generated from thermal decomposition at lower temperatures (Liu et al., 2002). The morphology of the char formed by the thermochemical conversion of pecan shells in an air atmosphere also aids in the total oxidation phenomena observed (Gani and Naruse, 2007).

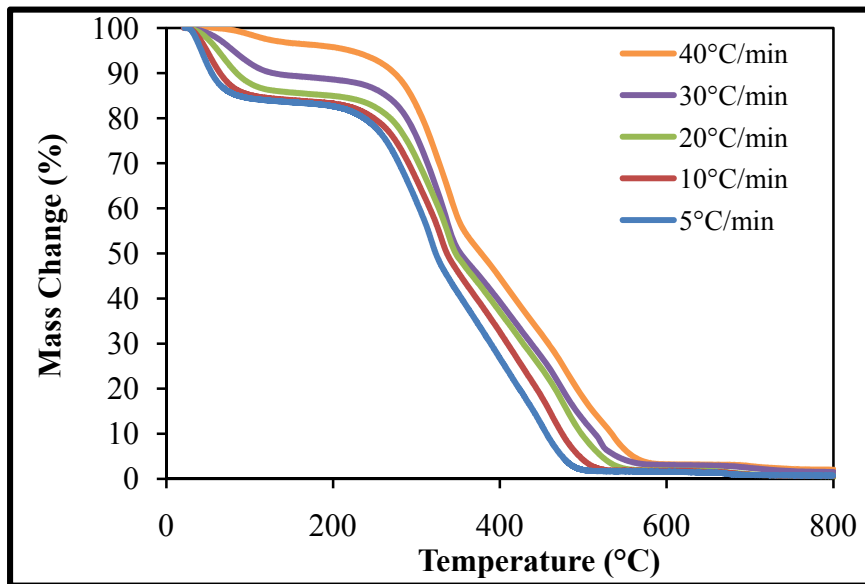


Figure 4.3 – Mass loss from the thermal decomposition of pecan shells at different heating rates with air as carrier gas

The mass loss curves for pecan shell thermal decomposition in air were similar to those obtained when thermally decomposed in nitrogen. Moisture release occurred between the temperature ranges of 30°C to 150°C (12.58% - 16.01%). Thermal decomposition of pecan shells during combustion was determined to start at 180°C and considered essentially finished at 600°C. Figure 4.4 shows the mass loss rate (da/dt) of pecan shells (DTG curve), calculated using the mass loss fraction (Equation 4.1). Similar to the thermal decomposition in nitrogen results, the hemicelluloses-cellulose shoulder

peaks were observed. Peak thermal degradation for hemicelluloses occurred at 270°C, 292°C, 309°C, 318°C and 331°C for heating rates of 5, 10, 20, 30 and 40°C/min, respectively. Temperatures at which cellulose decomposition peaked were 315°C, 327°C, 334°C, 336°C and 339°C for heating rates of 5, 10, 20, 30 and 40°C/min respectively. Unlike the thermal decomposition in nitrogen, an additional peak in the temperature range of 430°C-600°C was observed. This can be attributed to the combustion of the char residue formed from decomposition at lower temperatures. Mass loss during the range of thermal decomposition of the char increased from 16.53% to 29.31% (of total mass), increasing as heating rate increased from 5-40°C/min.

It should be noted that the mass loss rate is higher during air decomposition (Figure 4.4) compared to the rate obtained during nitrogen decomposition (Figure 4.2). The total oxidation of the pecan shells in an air atmosphere (e.g. combustion) allows for total decomposition of the cellulose, hemicelluloses and lignin compounds. Sufficient amounts of oxygen in the air atmosphere allow for the decomposition of the char residue whereas under the nitrogen atmosphere, the nitrogen environment does not promote the further degradation of the lignin-rich bio-char (Liu et al., 2002). The aromatic rings and complex structure of lignin must have sufficient amounts of oxygen in the air to cleave the C-O bonds to experience total decomposition of biological materials (Demirbas, 2002). Peak temperatures of mass loss rate of hemicelluloses and cellulose during thermal decomposition in air and nitrogen are given in Table 4.1. Although the peak temperatures of hemicelluloses decomposition were similar in nitrogen and air atmospheres, cellulose peak decomposition temperatures in air were lower than that of the nitrogen environment. This suggests that the oxygen content in the air atmosphere

has a more significant effect on the activation energy of pecan shells during cellulose decomposition than hemicelluloses decomposition (Fang et al., 2006).

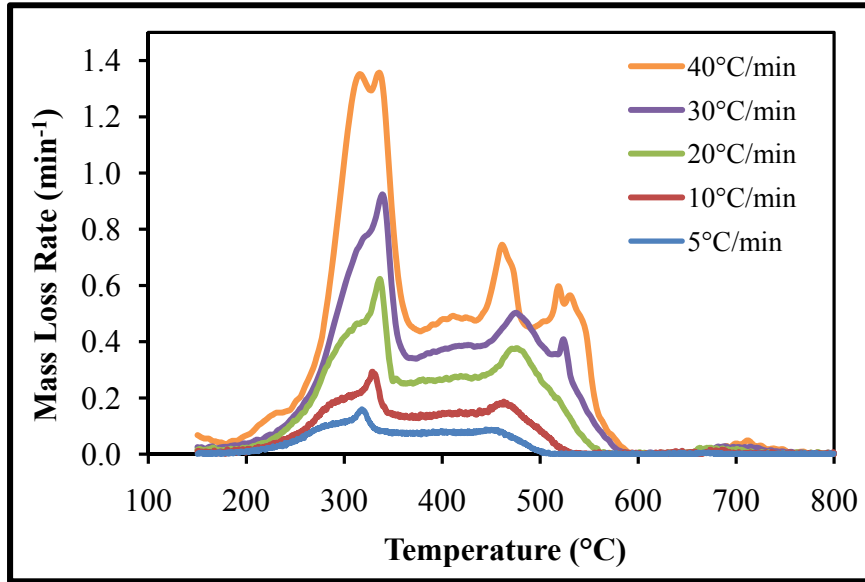


Figure 4.4 – Mass loss rate from the thermal decomposition of pecan shells at different heating rates with air as carrier gas

Table 4.1 –Temperature (°C) peaks in mass loss rate for the main chemical constituents of pecan shells when thermally degraded in nitrogen and air

Thermal Decomposition Atmosphere	Chemical Constituent	Heating Rates (°C/min)				
		5	10	20	30	40
Nitrogen	hemicelluloses	275	285	305	315	330
	cellulose	348	360	371	385	386
Air	hemicelluloses	270	292	309	318	331
	cellulose	315	327	334	336	339

4.3.3. FTIR Analysis

4.3.3.1. Thermal Decomposition in Nitrogen Atmosphere

A typical 3-dimensional plot of the spectral obtained from the gas volatilized during thermal degradation of pecan shells in nitrogen atmosphere is shown in Figure 4.5.

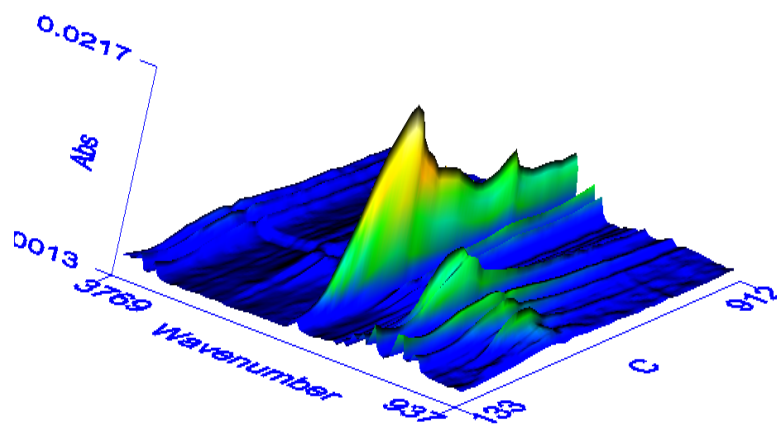


Figure 4.5 – Three-dimensional spectral plot of the gases produced from the thermal degradation of pecan shells in nitrogen at a heating rate of 30°C/min

Generally the thermal decomposition of biomass results in gas compounds evolving from volatilization of hemicelluloses, cellulose and lignin, the main organic constituents of biomass (Basilakis et al., 2001; Baker et al., 2005; Yang et al., 2004). The following 15 gas compounds were identified from the FTIR spectra: acetic acid (CH_3COOH), ammonia (NH_3), carbon dioxide (CO_2), carbon monoxide (CO), carbonyl sulfide (COS), ethanol ($\text{CH}_2\text{CH}_3\text{OH}$), ethylene (C_2H_4), formaldehyde (CH_2O), hydrogen cyanide (HCN), isocyanic acid (HCNO), formic acid (HCOOH), methane (CH_4), methanol (CH_3OH), methyl isocyanate ($\text{C}_2\text{H}_3\text{NO}$) and nitrous oxide (N_2O) (Basilakis et al., 2001; Yang et al., 2004; Gronli et al., 1999). Of the gas compounds analyzed, four were determined to volatilize in higher concentrations. These four compounds were carbon dioxide, carbon

monoxide, ethanol and acetic acid and are referred to as major gases. Carbon dioxide demonstrated a wide concentration peak ranging from 360-425°C that is representative of the degradation of hemicelluloses. The concentration of CO₂ at this thermal degradation range is attributed to the cracking and cutting of C-C and C-O bonds connected with the main branch of hemicelluloses, thus leading to the high thermal decomposition reactivity of hemicelluloses. The degradation of lignin was also responsible for the volatilization of CO₂, occurring at temperatures 400-600°C (Yang et al., 2007). Lower concentrations of isocyanic acid, carbonyl sulfide, methane and methyl isocyanate were also found (referred as minor gases). A general trend of increased concentration of these gases increased with heating rate. Acetic acid, ethanol and carbon dioxide peak concentrations were found to correspond with the hemicelluloses-cellulose shoulder-peak phenomena observed in the mass loss rate peaks during the pyrolysis procedure previously discussed. The major and minor gaseous products volatilized during nitrogen thermal decomposition are shown in Figures 4.6 and 4.7.

The shoulder peak phenomenon was not observed for carbon monoxide. Carbon monoxide volatilization resulted in a peak, at approximately 400°C, due to the cracking of carbonyl (C-O-C) and carboxyl (C=O) bonds. At higher temperatures (> 475°C) lignin degradation resulted in concentration peaks of carbon monoxide. However, carbon monoxide concentrations increased in the temperature region beyond hemicelluloses and cellulose decomposition, known as the char combustion region (Baker et al., 2005). The increased concentrations of carbon monoxide and carbon dioxide in the char combustion region has been attributed to thermal cracking of residue in the sample, to oxidation of

the carbonized char and to high temperature reaction that is given by: (Yang et al., 2007, Baker et al., 2005; Lee and Fasina, 2009):



Total volume of the gaseous products volatilized during the nitrogen thermal decomposition of pecan shells was obtained by the following equation:

$$V = \frac{10^{-6}IF}{60} \quad (4.3)$$

Where, I is the value obtained by integrating the concentration-time curve (using Simpson's Rule, ppm) and F is the flow rate of nitrogen carrier gas through the infrared spectrometer (20 ml/min). Table 4.2 shows the total volume of each gaseous compound analyzed during the course of the thermal decomposition experiment. Analysis of variance of total volume of carbon monoxide, carbon dioxide and ethanol were determined to significantly ($P < 0.05$) decrease with increased heating rate. There was not a significant trend identified in the other gases analyzed. The total volumes of all gases quantified were also found to be significantly ($P < 0.05$) decreasing as heating rate decreased. This is due to the shorter residence times in higher heating rates resulted in higher residue during the thermal decomposition process (Lee and Fasina, 2009). There was not sufficient time for the residue in higher heating rates for the oxidation of carbon containing gases to carbon dioxide during thermal decomposition, thus the reduction in carbon concentration as heating rate increased.

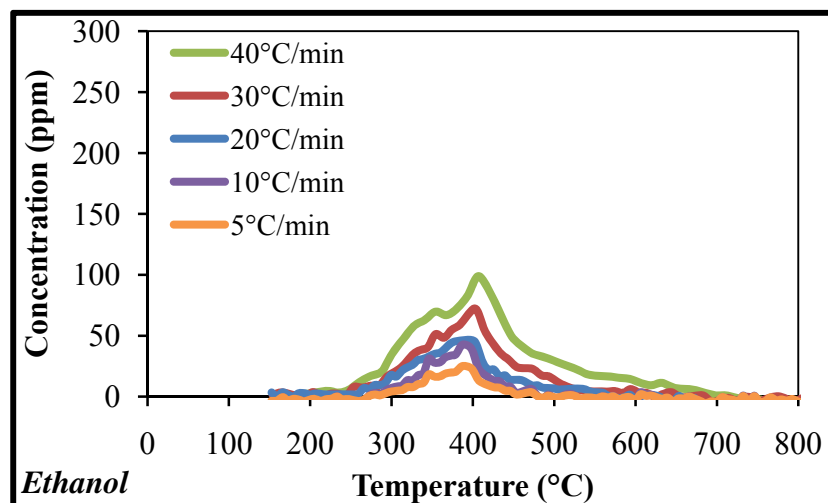
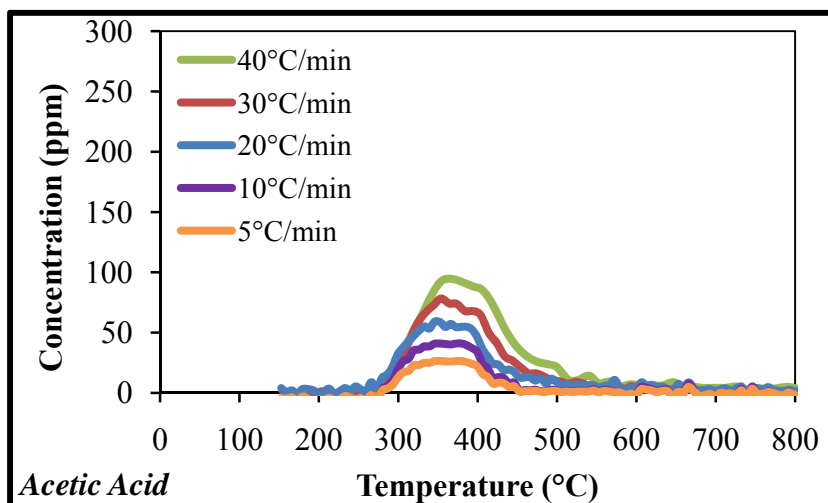
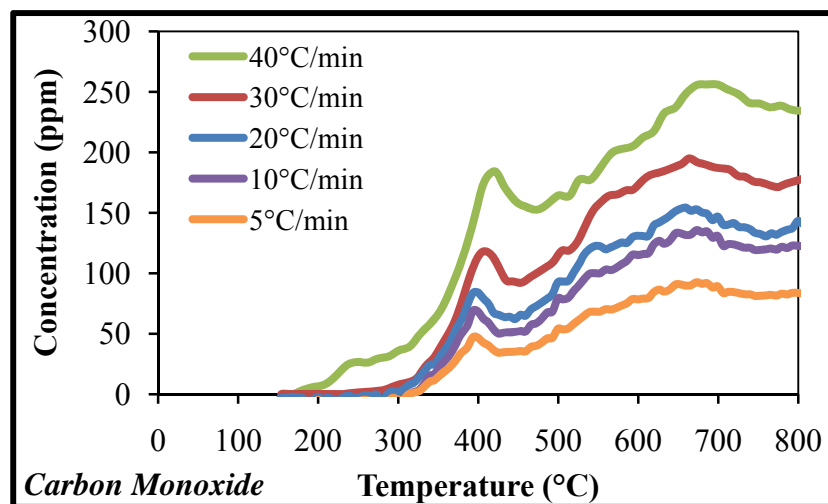
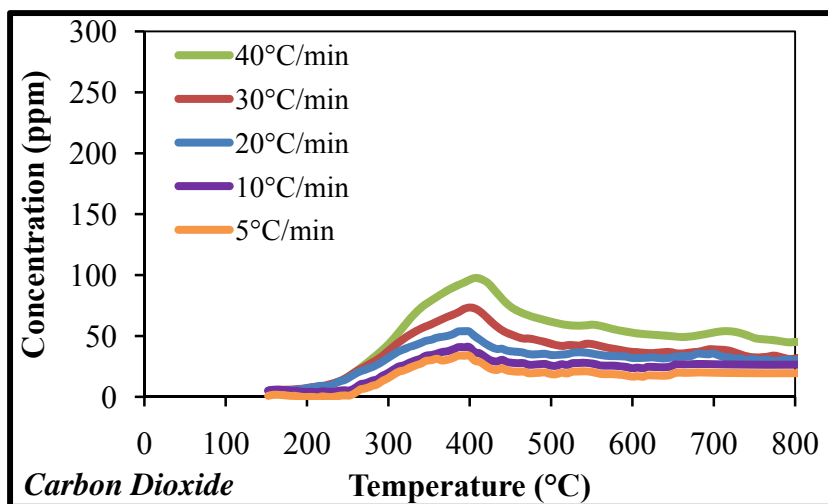


Figure 4.6 – Concentration of the major gases volatilized during nitrogen thermal decomposition of pecan shells at heating rates of 5-40°C/min

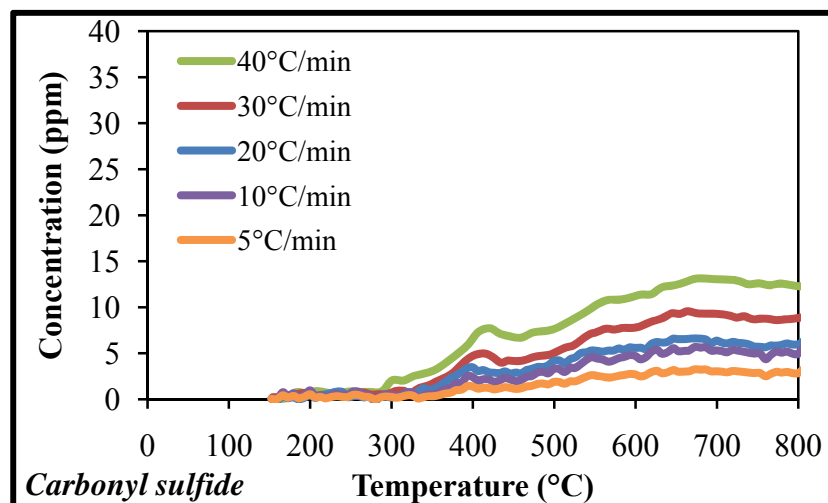
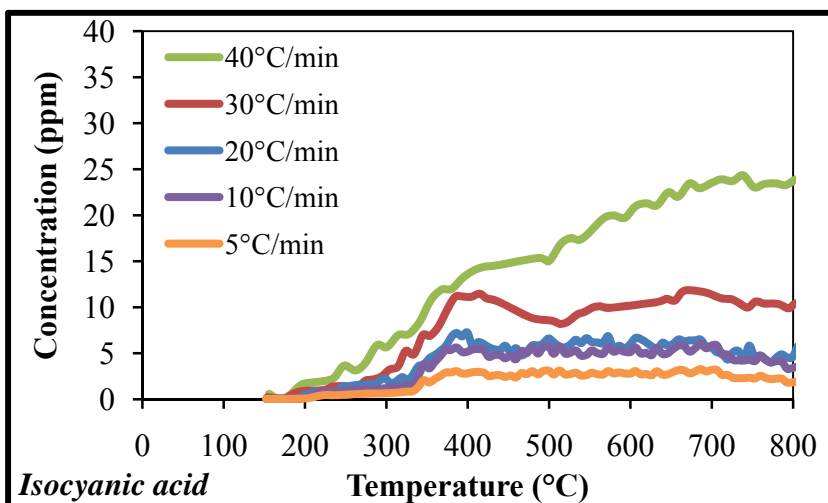
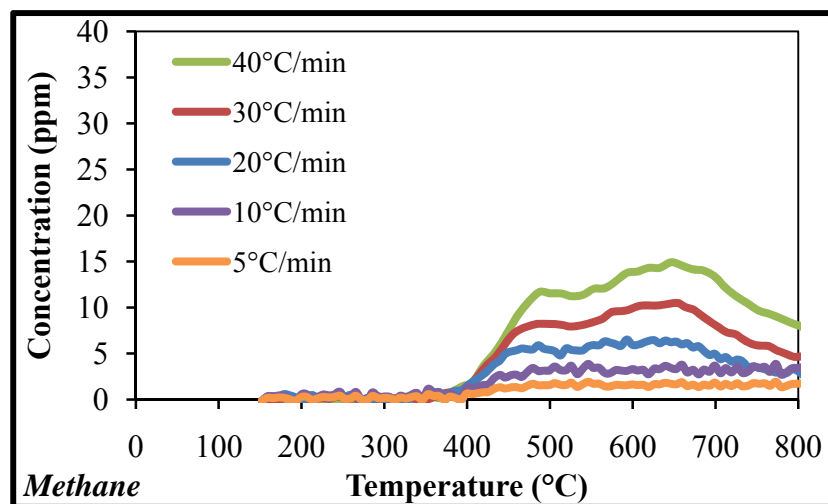
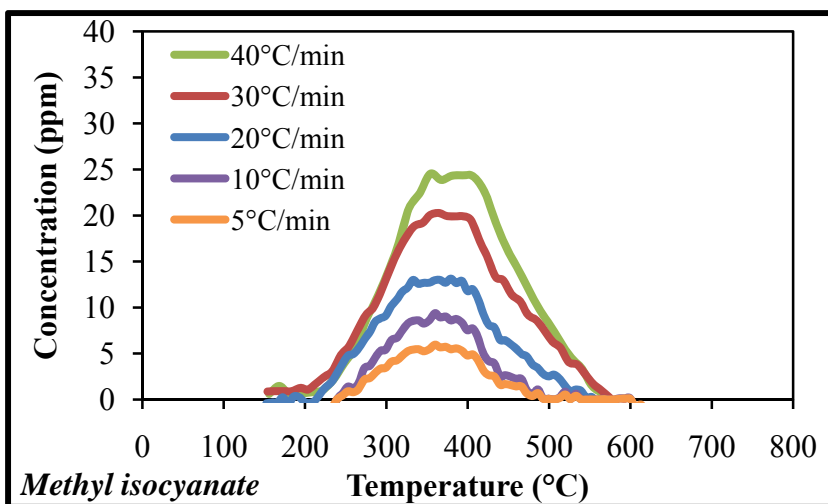


Figure 4.7 – Concentration of the minor gases volatilized during nitrogen thermal decomposition of pecan shells at heating rates of 5-40°C/min

Table 4.2 – Effect of heating rate on the concentration (ml) of gases produced during thermal decomposition of pecan shells in nitrogen atmosphere

Gas Type	Heating rate (°C/min)				
	5	10	20	30	40
Carbon dioxide	0.0129	0.0146	0.0118	0.0093	0.0069
Carbon monoxide	0.0349	0.0331	0.0328	0.0314	0.0294
Isocyanic acid	0.0062	0.0049	0.0017	0.0020	0.0039
Carbonyl sulfide	0.0015	0.0012	0.0014	0.0012	0.0010
Acetic acid	0.0041	0.0035	0.0047	0.0034	0.0046
Nitrous oxide	0.0004	0.0001	0.0002	0.0001	0.0001
Methane	0.0034	0.0026	0.0012	0.0012	0.0010
Ethylene	0.0002	0.0003	0.0001	0.0002	0.0001
Ammonia	0.0004	0.0006	0.0004	0.0002	0.0002
Hydrogen cyanide	0.0001	0.0003	0.0001	0.0004	0.0001
Formic acid	0.0001	0.0007	0.0003	0.0001	0.0001
Formaldehyde	0.0003	0.0001	0.0001	0.0001	0.0002
Methyl isocyanate	0.0006	0.0007	0.0014	0.0007	0.0001
Ethanol	0.0173	0.0149	0.0148	0.0098	0.0054
Methanol	0.0010	0.0012	0.0007	0.0005	0.0003
Total	0.0834	0.0788	0.0716	0.0605	0.0533

4.3.3.2. Thermal Decomposition in Air Atmosphere

Figure 4.8 shows a 3-dimensional plot of the spectra obtained from the gas volatilized during thermal decomposition of pecan shells in air. The major gases identified from the spectra were carbon dioxide, carbon monoxide and methyl isocyanate and are shown in Figure 4.9 below:

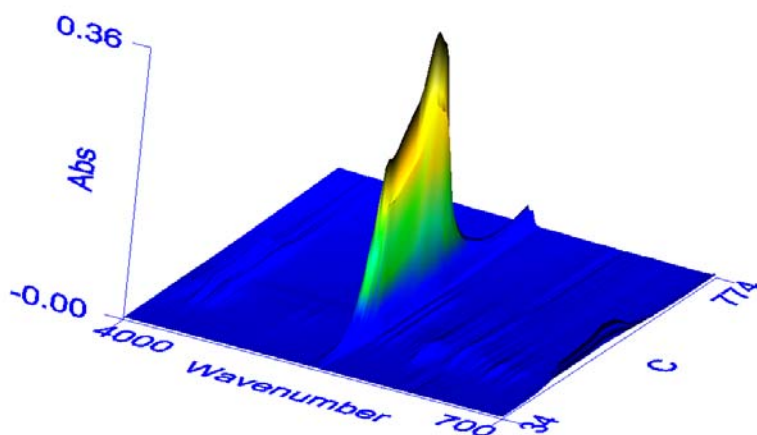


Figure 4.8 – Three-dimensional spectral plot of the gases produced from the thermal decomposition of pecan shells in air atmosphere at a heating rate of 30°C/min

The concentration-temperature curves of carbon dioxide and carbon monoxide gases demonstrated the shoulder peak trend previously shown in the mass loss rate curves in air thermal decomposition (Figure 4.4). It should be mentioned that the concentration of carbon dioxide was higher in temperatures beyond the hemicelluloses-cellulose decomposition region. Similar to the nitrogen decomposition, carbon monoxide and carbon dioxide were volatilized due to the abscission of C-C and C-O complexes in these organic compounds. The additional CO₂ peak observed at temperatures beyond hemicelluloses and cellulose decomposition range can be attributed to the thermal degradation of lignin present in the char residue. The released CO₂ was caused by the cracked C-O and COOH bonds in the lignin-rich char (Chouchene et al., 2010). Thus, carbon from the lignin compound reacts with the oxygen to form CO₂ and CO, as previously shown in Equation 4.2. Similar results were also reported by Chouchene et al. (2010) with olive solid waste. Similar to the FTIR results in a nitrogen atmosphere, at any temperature, the concentration of the main gases volatilized increased as heating rate increased during air

thermal decomposition. Lower concentrations of isocyanic acid, carbonyl sulfide and acetic acid were found and shown in Figure 4.10.

Equation 4.3 was utilized to calculate the total volumes of the gas products volatilized from the combustion of pecan shells are located in Table 4.3. Statistical testing of total volume of gas products evolved from the combustion of pecan shells indicated that total volume was significantly ($P < 0.05$) affected by heating rate. As the heating rate increased, total volume of carbon monoxide, isocyanic acid, carbonyl sulfide and acetic acid decreased significantly ($P < 0.05$). It is postulated that the residence times in all heating rates was sufficient for complete oxidation of carbon containing gases into carbon dioxide and carbon monoxide.

Table 4.3 – Effect of heating rate on the concentration (ml) of gases produced during thermal decomposition of pecan shells in air atmosphere

Gas Type	Heating rate (°C/min)				
	5	10	20	30	40
Carbon dioxide	0.0924	0.0994	0.0903	0.0826	0.0889
Carbon monoxide	0.0197	0.0164	0.0110	0.0053	0.0031
Isocyanic acid	0.0128	0.0098	0.0083	0.0070	0.0012
Carbonyl sulfide	0.0041	0.0028	0.0018	0.0007	0.0004
Acetic acid	0.0032	0.0034	0.0043	0.0025	0.0007
Nitrous oxide	0.0002	0.0003	0.0003	0.0004	0.0005
Methane	0.0004	0.0003	0.0002	0.0001	0.0003
Ethylene	0.0005	0.0003	0.0009	0.0001	0.0001
Ammonia	0.0006	0.0009	0.0003	0.0004	0.0003
Hydrogen cyanide	0.0022	0.0021	0.0023	0.0016	0.0011
Formic acid	0.0010	0.0001	0.0003	0.0001	0.0001
Formaldehyde	0.0002	0.0004	0.0007	0.0002	0.0002
Methyl isocyanate	0.0385	0.0379	0.0274	0.0346	0.0348
Ethanol	0.0057	0.0059	0.0052	0.0049	0.0051
Methanol	0.0003	0.0002	0.0002	0.0003	0.0001
Total	0.1818	0.1801	0.1535	0.1409	0.1370

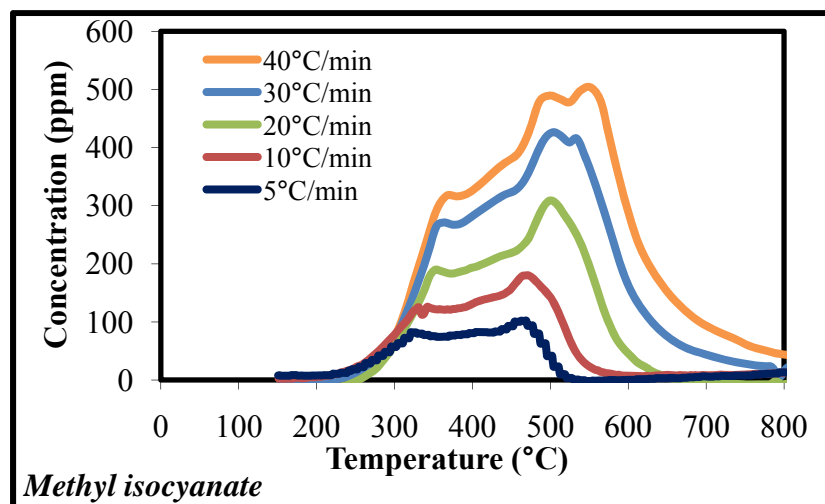
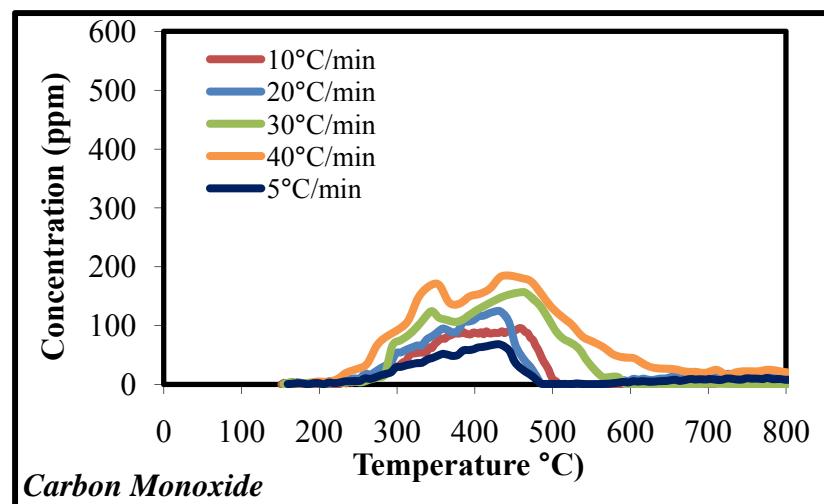
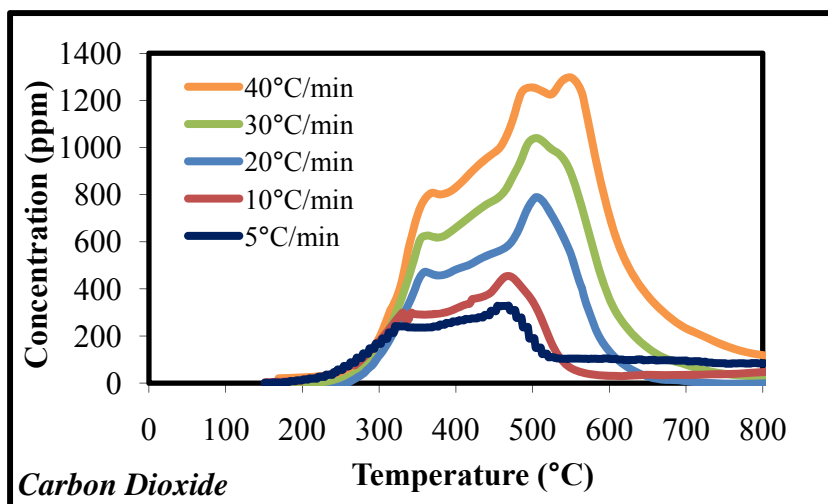


Figure 4.9 – Concentration of the major gases volatilized during air thermal decomposition of pecan shells at heating rates of 5-40°C/min

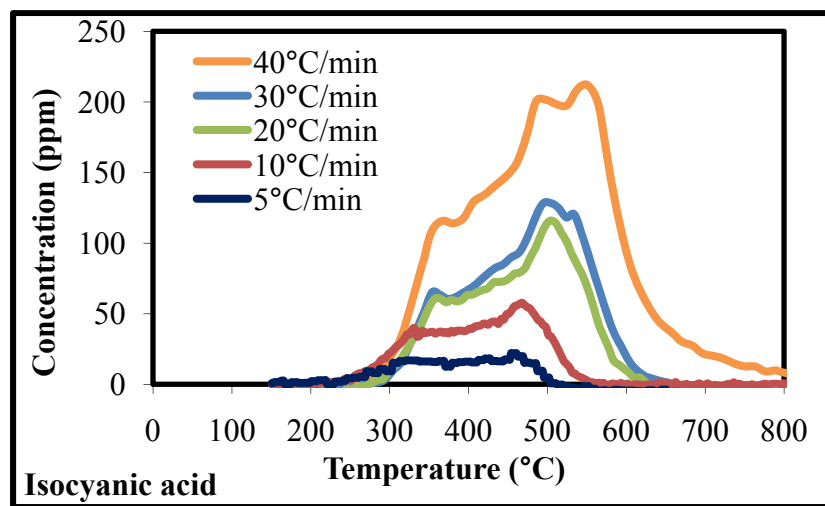
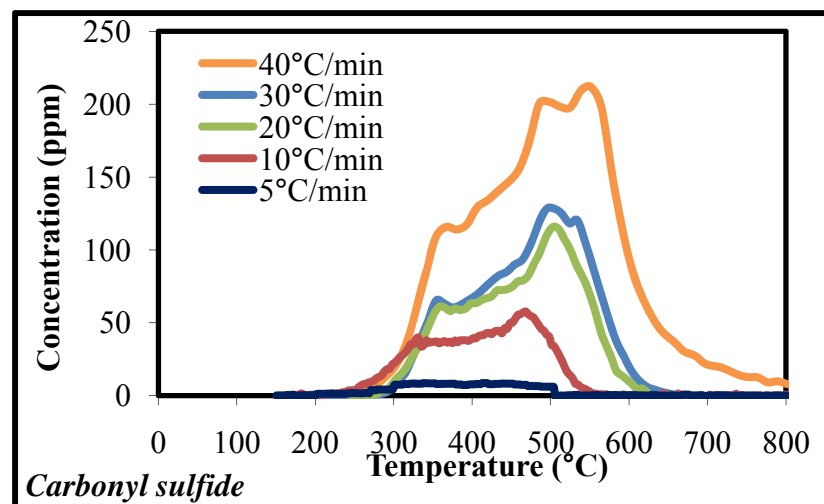
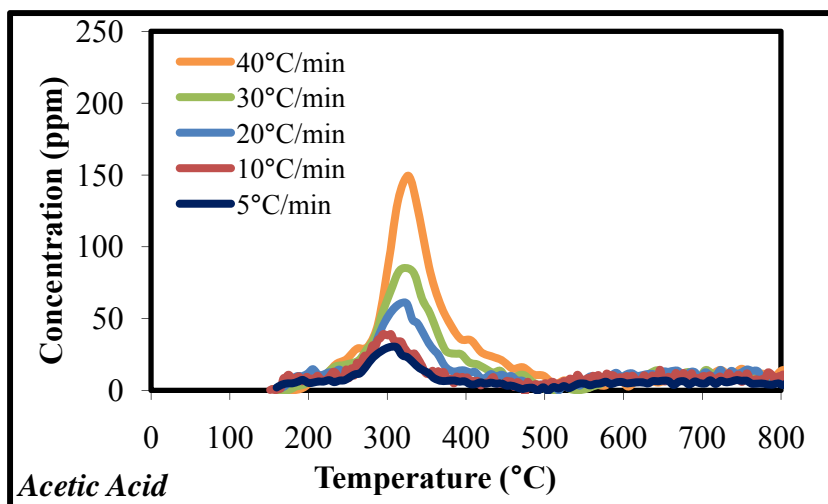


Figure 4.10 - Concentration of the minor gases volatilized during air thermal decomposition of pecan shells at heating rates of 5-40°C/min

4.4. Conclusions

The thermal decomposition of pecan shells in nitrogen and air atmospheres were observed at five different heating rates. There was evidence of the thermal degradation of the major chemical constituents of pecan shells (i.e. hemicelluloses, cellulose and lignin). The four main stages of mass loss were observed to be moisture evaporation, hemicelluloses and cellulose decomposition and lignin degradation. Moisture was released in the temperature range of 30 to 150°C in both atmospheres. Mass loss rate increased as heating rate increased in both nitrogen and air atmospheres.

During thermal decomposition under nitrogen, hemicelluloses and cellulose decomposition peaks were observed. Mass loss rate peaks at temperatures of 275, 285, 305, 315 and 330°C at heating rates of 5, 10, 20, 30 and 40°C/min were determined to attribute to hemicelluloses decomposition. Cellulose nitrogen decomposition demonstrated mass loss rate peaks at temperatures of 348, 360, 371, 385 and 386°C for heating rates of 5-40°C/min, respectively. The nitrogen decomposition of hemicelluloses, cellulose and some of the lignin resulted in approximately 40% mass loss of total weight of the pecan shell sample. Similar to other researchers, a thermal degradation mass loss rate peak was not observed for lignin. However, similar to other researchers, a flat, tailing section of mass loss rate at higher temperatures indicated thermal degradation of lignin. The nitrogen thermal degradation of pecan shells was determined to be essentially complete at 600°C, with a residual content of 30% of original weight.

The thermal decomposition of pecan shells in an air atmosphere was similar to the thermal degradation observed under nitrogen atmosphere in that the mass loss rate

increased with increased heating rate and the hemicelluloses-cellulose decomposition shoulder-peaks were observed. However, mass loss rate in the air atmosphere was higher compared to nitrogen thermal decomposition due to the oxidation of the char residue generated during lower temperature decomposition. Mass loss rate during hemicelluloses decomposition exhibited peaks at temperatures of 270, 292, 309, 318, 331°C for heating rates of 5, 10, 20, 30 and 40 °C min⁻¹, respectively. Cellulose decomposition mass loss rate peaks also increased with increased heating rate. Cellulose mass loss rate peaks (in air atmosphere) were observed at temperatures of 315, 327, 334, 336, 333°C for heating rates of 5 – 40°C/min, respectively. Combustion of the char residue demonstrated peaks at temperatures of 450, 456, 467, 469 and 517°C at heating rates of 5, 10, 20, 30 and 40°/min, respectively.

Heating rate significantly ($P < 0.05$) affected the total volume of gaseous products volatilized from the thermal decomposition of pecan shells in nitrogen and air atmospheres. The major gases evolved from nitrogen thermal decomposition of pecan shells were carbon dioxide, carbon monoxide, ethanol and acetic acid. The major gases volatilized from air thermal decomposition of pecan shells were carbon dioxide, carbon monoxide and methyl isocyanate.

4.5. References

- Arias, M.E., Polvillo, O., Rodriguez, J., Hernandez, M., Gonzalez-Perez, J.A., Gonzalez-Vila, F.J. 2006. Thermal transformations of pine wood components under pyrolysis-gas chromatography/mass spectrometry conditions. *Journal of Analytical and Applied Pyrolysis* 77: 63-67.
- ASABE *Standard*. 2006. S593 Terminology and definitions for biomass production, harvesting and collection, storage, processing, conversion and utilization. St. Joseph, MI: ASABE.
- Bahng, M.K., Mukarakate, C., Robichaud, D., Nimlos, M. 2009. Current technologies for the analysis of biomass thermochemical processing: a review. *Analytica Chimica Acta* 651: 117-138.
- Baker, R.R., Coburn, S., Liu, C., Tetteh, J. 2005. Pyrolysis of saccharide tobacco ingredients: a TGA-FTIR investigation. *Journal of Analytical and Applied Pyrolysis* 74: 171-180.
- Bassilakis, R., Carangelo, R.M., Wojtowicz, M.A. 2001. TG-FTIR analysis of biomass pyrolysis. *Fuel* 80: 1765-1786.
- Biagini, E., Barontini, F., Tognotti, L. 2006. Devolatilization of biomass fuels and biomass components studied by TG-FTIR technique. *Industrial and Engineering Chemistry Research* 45: 4486-4493.
- Butterman, H., Castildi, M.J. 2009. CO₂ as a carbon neutral fuel source via enhanced biomass gasification. *Environmental Science and Technology* 43(23): 9030-9037.
- Çağlar, A., Demirbaş, A. 2002. Conversion of cotton cocoon shells to hydrogen rich gaseous products by pyrolysis. *Energy Conversion and Management* 43: 489-497.
- Chouchene, A., Jeguirim, M., Khiari, B., Zagrouba, F., Trouve, G. 2010. Thermal degradation of olive solid waste: Influence of particle size and oxygen concentration. *Resources, Conservation and Recycling* 54: 271-277.
- de Jong, W., Di Nola, G., Venneker, B.C.H., Spliethoff, H., Wojtowicz, M.A. 2007. TG-FTIR pyrolysis of coal and secondary biomass fuels: determination of pyrolysis kinetic parameters for main species and NO_x precursors. *Fuel* 86: 2367-2376.
- Demirbaş, A., Hyan. 1998. Kinetics for non-isothermal flash pyrolysis of hazelnut shells. *Bioresource Technology* 66: 247-252.

- Di Blasi, C., Signorelli, G., Di Russo, C., Rea, G. 1999. Product distribution from pyrolysis of wood and agricultural residues. *Industrial Engineering and Chemistry Research* 38: 2216-2224.
- Fang, M.X., Shen, D.K., Li, Y.X., Yu, C.J., Luo, Z.Y., Cen, K.F. 2006. Kinetic study on pyrolysis and combustion of wood under different oxygen concentrations by using TG-FTIR analysis. *Journal of Analytical and Applied Pyrolysis* 77: 22-27.
- Gani, A., Naruse, I. 2007. Effect of cellulose and lignin content on pyrolysis and combustion characteristics for several type of biomass. *Renewable Energy* 32: 649-661.
- Gronli, M., Antal Jr., M., Varhegyi, G. 1999. A round-robin study of cellulose pyrolysis kinetics by thermogravimetry. *Industrial Engineering and Chemical Research* 38: 2238-2244.
- Guintoli, H., de Jong, W., Arvelakis, S., Spliethoff, H., Verkooijen, A.H.M. 2009. Quantitative and kinetic TG-FTIR study of biomass residue pyrolysis: dry distiller's grains with solubles (DDGS) and chicken manure. *Journal of Analytical and Applied Pyrolysis* 85: 301-312.
- Hu, S., Jess, A., Xu, M. 2007. Kinetic study of chinese biomass slow pyrolysis: comparison of different kinetic models. *Fuel* 86: 2778-2788.
- Lee, S-B, Fasina, O. 2009. TG-FTIR analysis of switchgrass pyrolysis. *Journal of Analytical and Applied Pyrolysis* 86: 39-43.
- Liu, Q., Wang, S., Zheng, Y., Luo, Z., Cen, K. 2008. Mechanism study of wood lignin pyrolysis by using TG-FTIR analysis. *Journal of Analytical and Applied Pyrolysis* 82: 170-177.
- Miranda, R., Sosa_Blanco, C., Bustos-Martinez, D., Vasile, C. 2007. Pyrolysis of textile wastes I. Kinetics and yields. *Journal of Analytical and Applied Pyrolysis* 80: 489-495.
- Mothe C.G., Miranda, I.C. 2009. Characterization of sugarcane and coconut fibers by thermal analysis and FTIR. *Journal of Thermochemical and Analytical Calorimetry* 97:661-665.
- Rao, T.R., Sharma, A. 1998. Pyrolysis rates of biomass materials. *Energy* (23) 11: 973-978.
- Souza, B.S., Moreira, A.P., Teixeira, A.M. 2009. TG-FTIR coupling to monitor the pyrolysis products from agricultural residues. *Journal of Thermal Analysis and Calorimetry* 97: 637-642.
- Tsamba, A., Yang, W., Blasiak, W. 2006. Pyrolysis characteristics and global kinetics of coconut and cashew nut shells. *Fuel Processing Technology* 87: 523-530.

Wang, S., Jian, X.M., Wang, N., Yu, Y.J., Li, Z., He, P.M. 2007. Research on pyrolysis characteristics of seaweed. *Energy and Fuels* 21: 3723-3729.

Vamvuka, D., Kakaras, E., Kastanaki, E., Grammelis, P. 2003. Pyrolysis characteristics and kinetics of biomass residuals mixtures with lignite. *Fuel* 82: 1949-1960.

Vuthaluru, H.B. 2003. Thermal behavior of coal/biomass blends during co-pyrolysis. *Fuel Processing Technology* 85: 141-155.

Yang, H., Yan, R., Chin, T., Lian, D.T., Chen, H., Zheng, C. 2004. Thermogravimetric analysis - Fourier transform infrared analysis of palm oil waste pyrolysis. *Energy and Fuels* 18: 1814-1821.

Yang, H., Yan, R., Chen, H., Lee, D.H., Sheng, C. 2007. Characteristics of hemicellulose, cellulose and lignin pyrolysis. *Fuel* 86: 1781-1788.

CHAPTER 5. DETERMINATION OF ENERGY REQUIREMENT AT DIFFERENT THERMAL DEGRADATION TEMPERATURES

5.1. Introduction

Thermal degradation of biomass in the absence of an oxidizing agent is the first step in the thermochemical conversion of biomass into char, bio-oil and synthesis gas (Garcia-Nunez et al., 2008; Chen et al., 2003; Yaman, 2004; Guo and Lua, 2001). The economics of thermochemical conversion of biomass into value-added products depends on the amount of energy consumed and produced during the process (He et al, 2006). Enthalpy is therefore defined as the energy required to raise biomass from room temperature to the reaction temperature and convert the solid biomass into gas, liquid and solid (char) products (Daugaard and Brown, 2003). Enthalpy needed for thermal degradation can vary with different types of biomass. Enthalpy will therefore play an important role in reactor design, specification of operation parameters, energy balance analysis and the analysis of biomass pyrolysis, gasification and combustion (He et al., 2006; Daugaard and Brown, 2003).

Therefore, the objective of this study was to quantify the energy required to thermally degrade pecan shells.

5.2. Materials and Methods

5.2.1. Sample Preparation

The pecan shells used in this study were obtained from the Louisville Pecan Company, Louisville, AL. The samples were stored in the Biosystems Engineering Process Engineering Laboratory with an average temperature of 25°C. Before use, the pecan shells were ground in a Wiley mill to pass through a standard 40-mesh screen. Energy content, ash content and ultimate analysis of pecan shells were previously discussed in Section 3.3.2 and values given in Tables 3.2 and 3.3, respectively.

5.2.2. Differential Scanning Calorimetry

The differential scanning calorimeter (DSC) used in this study was a DSC Q200 (Perkin-Elmer, Shelton, CT) that was operated under nitrogen atmosphere at a flow rate of 20 ml/min. Samples (approximately 5 mg) were equilibrated at 30°C for 2 minutes, then heated to 550°C at five different heating rates (5, 10, 20, 30 and 40°C/min) and then held at 550°C for 2 minutes. Temperature (°C), time (min), heat flow (W/g) and sample purge flow (ml/min) were all recorded by the software provided by the manufacturer of the DSC. The equipment was calibrated before use according to manufacturer's specifications.

5.2.3. Data Analysis

Statistical analysis was performed using SAS statistical package (Version 9.2, SAS Institute Inc., Cary, NC, 2008-2009) at the 95% confidence interval. The

experimental data was plotted using Microsoft Excel (Microsoft Office XP Professional, 2007).

5.3. Results and Discussion

Moisture evaporation typically occurs between ambient (30°C) and 150°C.

Figure 5.1 below shows the heat flow (W/g) of pecan shells pyrolysis from 30°C to 550°C at heating rates of 5, 10, 20, 30 and 40°C/min. The negative values of heat flow indicate endothermic reactions. The large endothermic peaks at temperatures around 100°C are due to moisture evaporation from the pecan shells samples (He et al., 2006; Gomez et al., 2009).

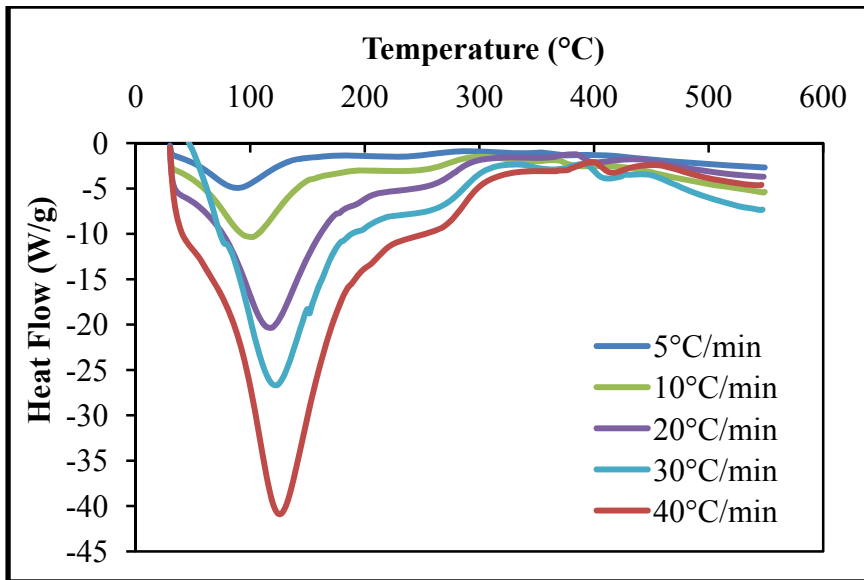


Figure 5.1 – Heat flow (W/g) of pecan shells pyrolysis at different heating rates

Since the thermal decomposition of pecan shells begin at approximately 180°C (as reported in Section 4.3.1. of this thesis), the energy requirement to thermally degrade

pecan shells was divided into two zones: a) the energy required to evaporate moisture in the sample and b) the energy required to heat the now moisture-free pecan shells. Based on the DSC curves obtained at the different heating rates, the temperature that was used to divide the two zones was 175°C. Therefore, the moisture evaporation temperature zone was calculated from 30-175°C and the thermal decomposition energy was calculated from 175-550°C. The energy required in these two temperature zones were calculated based on sigmoidal tangent baseline calculation where two tangent lines were fit within the selected limits (30-175°C and 175-550°C) and a sigmoidal curve joined the tangent lines together and the area under the curve was calculated via the integration equation below (He et al., 2006):

$$\frac{Q}{m_{s,0}} = \int_0^t \frac{(m_s c_p \frac{dT}{dt} + m_s \dot{H}_p)}{m_{s,0}} dt \quad (5.1)$$

Where, Q is caloric requirement of pecan shells pyrolysis (J), $m_{s,0}$ is initial mass of sample (g), m_s is mass of sample during experiment (g), c_p is specific heat of sample (J/g °C), dT/dt is the ratio of the sample temperature and time of DSC run (°C/s) and \dot{H}_p is heat flow caused by the reaction heat of pecan shells thermal decomposition.

Table 5.1 shows the energy required to evaporate moisture and the thermally degrade pecan shells. The energy required to remove moisture from the sample was significantly higher ($P < 0.05$) than that required for thermal degradation of pecan shells. Similar results were reported by Park et al. (2007) for wood cellulose fibers and Daugaard and Brown (2003) for oak, oat hulls, corn stover and pine.

Table 5.1 – Energy requirements for moisture evaporation and thermal degradation of pecan shells at different heating rates

Temperature Zones	Heating rates(°C/min)					Energy (MJ/kg)
	5	10	20	30	40	
0 - 175°C	3.16	3.41	3.24	3.47	2.94	
175 - 550°C	2.93	3.22	2.62	2.72	2.78	
% of Energy in Raw* Pecan Shells	30.38	33.04	29.19	30.86	28.53	
% of Energy in Dry* Pecan Shells	14.61	16.05	13.06	13.56	13.86	

*Raw pecan shells energy calculation based on moisture content level of 15.02% (w.b.)

*Dry pecan shells energy calculation based on moisture-free or 0% moisture content.

Statistical analysis indicated that the energy required to remove moisture (30-175°C) and pyrolysis temperatures (175-550°C) were not significantly ($P > 0.05$) affected by heating rate. It should be mentioned that the energy required to drive off moisture and raise the temperature of the pecan shells (moisture content of 15.02%, w.b.) to the thermal decomposition temperature range was approximately 6 MJ/kg. As previously reported in Section 3.3.2.1. of this thesis, the energy content of raw pecan shells was 20.06 MJ/kg. Therefore, the energy calculated in the two temperature zones of pyrolysis required approximately 30% of the energy available in pecan shells. However, if the pecan shells are bone-dry (or 0% moisture) the energy to thermally degrade the pecan shells is approximately 14%. This is an important logistical and economic parameter for the potential use of pecan shells for value-added applications. Ideal biomass feedstocks for the conversion to value-added products have to contain more energy than the conversion process requires. If not, the conversion process will not be economically feasible.

5.4. Conclusions

This study found that the energy requirement to remove moisture during thermal degradation of pecan shells under nitrogen is significantly greater than the energy required to thermally degrade pecan shells. The energy required in the moisture evaporation and the thermal degradation stages were not significantly affected by heating rate. The energy required to drive off moisture and raise the temperature of raw pecan shells to thermal degradation temperatures was approximately 30% of the energy available in the sample. However, if the pecan shells are dried to 0% moisture, the thermal degradation of the material uses approximately 14% of the energy available.

5.5. References

- Cai, J., Liu, R. 2007. Research on water evaporation in the process of biomass pyrolysis. *Energy and Fuels* 21: 3695-3697.
- Cai, J., Chen, S. 2008. Determination of drying kinetics for biomass by thermogravimetric analysis under nonisothermal conditions. *Drying Technology* 26: 1464-1468.
- Cozzani, V., Petarca, L., Tognotti, L. 1995. Devolatilization and pyrolysis of refuse derived fuels: characterization and kinetic modelling by a thermogravimetric and calorimetric approach. *Fuel* 74(6): 903-912.
- Daugaard, D., Brown, R. 2003. Enthalpy for pyrolysis for several types of biomass. *Energy and Fuels* 17: 934-939.
- Garcia-Nunez, J.A., Garcia-Perez, M., Das, K.C. 2008. Determination of kinetic parameters of thermal degradation of palm oil mill by-products using thermogravimetric analysis and differential scanning calorimetry. *Transactions of the ASABE* 51(2): 547-557.
- Gomez, C., Velo, E., Barontini, F., Cozzani, V. 2009. Influence of secondary reactions on the heat of pyrolysis of biomass. *Industrial Engineering and Chemical Research* 48: 10222-10233.
- He, F., Yi, W., Bai, X. 2006. Investigation on caloric requirement of biomass pyrolysis using TG-DSC analyzer. *Energy Conversion and Management* 47: 2461-2469
- Murugan, P, Mahinpey, N., Johnson, K.E., Wilson, M. 2008. Kinetics of the Pyrolysis of Lignin Using Thermogravimetric and Differential Scanning Calorimetry Methods. *Energy and Fuels* 22: 2720-2724.
- Park, S., Venditti, R., Jameel, H., Pawlak, J. 2007. Studies of the heat of vaporization of water associated with cellulose fibers characterized by thermal analysis. *Cellulose* 14: 195-204.
- Stenseng, M., Jensen, A., Dam-Johnson, K. 2001. Investigation of biomass pyrolysis by thermogravimetric analysis and differential scanning calorimetry. *Journal of Analytical and Applied Pyrolysis* 58-59: 765-780.
- Yang, H., Yan, R., Chen, H., Lee, D.H., Sheng, C. 2007. Characteristics of hemicellulose, cellulose and lignin pyrolysis. *Fuel* 86: 1781-1788.

CHAPTER 6. CONCLUSION

It can be concluded from this study that particle size and moisture content significantly affected the physical properties of pecan shells. Increases in particle size and moisture content resulted in decreases in bulk, tap and density. The porosity of pecan shells separated by particle size indicated that the particles were irregular and non-spherical in shape. Compressibility of pecan shells increased with increased pressure and decreased particle size or increased moisture content. Flow characterizations of particle sizes fractions ranged from free-flowing to easy-flowing as particle size increased and from easy flowing at a moisture content of 4.11% (w.b.) to cohesive at a moisture content of 24.70% (w.b.). Cohesion of particle sizes increased as particle size and moisture content increased. Average angle of internal friction for the particle sizes were determined to be 36.87, 42.56 and 44.87° for the fine, medium and coarse particle size fractions (for all pressures), respectively.

The rate of moisture sorption was determined. The Page model gave a good fit to the experimental data at three relative humidity levels of 50, 65 and 80% and temperatures of 15, 25 and 35°C. The Henderson and Chung-Pfost equations were the best fit to the EMC-ERH data.

Thermal decomposition of pecan shells was carried out at 5 different heating rates (5, 10, 20, 30 and 40°C/min). Four stages of thermal degradation were observed. The stages include: moisture evaporation, hemicelluloses decomposition, cellulose

decomposition and lignin degradation. During nitrogen thermal decomposition, peak hemicelluloses decompositions were found to occur at 275-330°C, whereas cellulose decomposition peaks were determined to occur at temperatures ranging from 348-386°C. No identifiable peak was determined for lignin degradation in the nitrogen atmosphere. Thermal decomposition under air demonstrated hemicelluloses decomposition peaks at temperatures of 270-331°C. Cellulose decomposition in an air atmosphere occurred at temperatures of 315-339°C. Oxidation of the char residue demonstrated peaks at temperatures of 450-517°C. Mass loss rate and thermal decomposition peaks of hemicelluloses, cellulose and char increased with increases in heating rate in both atmospheres.

Fifteen gases were identified to evolve during thermal decomposition of pecan shells. The major gases evolved from the nitrogen decomposition process were carbon dioxide, carbon monoxide, acetic acid and ethanol while the major gases volatilized during the air decomposition process were carbon dioxide, carbon monoxide and methyl isocyanate. For each gas analyzed, concentration increased at all temperatures as heating rate increased. The total volume of gaseous products volatilized during thermal decomposition in air and nitrogen atmospheres decreased as heating rate increased.

The energy requirement for the thermal decomposition of pecan shells was determined in two stages; moisture evaporation and the thermal degradation. It was determined that the energy required to remove moisture from pecan shells was greater

than the energy required to heat pecan shells to the thermal decomposition temperature range. Heating rate did not affect the energy requirements at the two temperature zones examined. The energy consumed to drive off moisture and raise the raw pecan shells to thermal degradation temperatures was approximately 30% of the energy content of the pecan shell sample.

CHAPTER 7. FUTURE WORK

This study provides useful information regarding particle size and moisture content and their effect on physical properties, compressibility and flowability of pecan shells. This will aid in the efficient design and selection of proper equipment for the storage, handling and transportation of pecan shells. The thermal decomposition characteristics were also examined, providing useful data to develop thermochemical conversion techniques specific for pecan shells. However, more research can be done to gain further understanding of the material.

In order for pecan shells to be considered as a biomass feedstock for value-added applications, a form of densification must be determined to increase bulk density. Pelletizing has been developed for other biomass materials, such as switchgrass and wood chips. Research into optimal moisture content and particle size for the pelletization of pecan shells should be considered to make transportation of the raw material as economically advantageous as possible.

Additional tests on the flowability of pecan shells should be completed. As observed in the present data, pecan shells at a moisture content of 19 % (w.b.) were characterized as an easy flowing material, whereas shells at a moisture content of 24% were characterized as a cohesive material. The point at which the material changes from easy flow to cohesive must be examined in order to determine the specific moisture content at which the pecan shells gain cohesive properties. In addition, the effect of

moisture content on the pecan shells was carried out on a single particle size. Further physical property measurements must be determined for the other particle sizes used in the effect of particle size.

The data in Chapter 4 could be added to additional tests run in order to determine the kinetic parameters of pecan shells thermal decomposition. For example, activation energy of pecan shells (determined by a DSC) is necessary to fit mass loss data to mathematical kinetic models. The knowledge of kinetic parameters of the thermal decomposition of pecan shells will allow better design and higher efficiencies of energy products produced. A further study of the feasibility of pecan shells to be used in the formation of bio-oil should also be considered.

Therefore, future research objectives could include:

- (a) Determination of optimal conditions for the pelleting of pecan shells,
- (b) Characterization of the effect of moisture content on the other particle sizes determined in the sieve analysis of the bulk material, and
- (c) Application of the thermal decomposition characteristics to determine kinetic parameters for pecan shells thermal decomposition.

APPENDICES

Appendix A. Effect of Particle Size Physical Property Data

Table A.1. Particle size distribution of pecan shells

<u>Raw ($D_{gw} = 1.200$ mm)</u>		
Sieve		
U.S. Sieve No.	Aperture Size (mm)	Distribution (%)
4	4.75	6.40
5	4.00	6.47
6	3.36	10.27
8	2.36	26.53
10	2.00	12.92
14	1.40	16.98
25	0.71	10.59
140	0.11	6.70
pan	0	3.14

<u>Medium ($D_{gw} = 1.241$ mm)</u>		
Sieve		
U.S. Sieve No.	Aperture Size (mm)	Distribution (%)
10	2	0.89
12	1.7	16.50
14	1.4	37.04
16	1.18	25.01
18	1	14.16
20	0.85	3.97
60	0.25	0.99
140	0.106	0.17
pan	0.09	1.27

<u>Dust ($D_{gw} = 0.212$ mm)</u>		
Sieve		
U.S. Sieve No.	Aperture Size (mm)	Distribution (%)
20	0.85	9.41
25	0.71	13.47
35	0.50	16.55
60	0.25	17.89
80	0.18	5.72
120	0.13	4.81
230	0.06	15.53
325	0.05	5.32
pan	0.04	11.27

<u>Coarse ($D_{gw} = 2.194$ mm)</u>		
Sieve		
U.S. Sieve No.	Aperture Size (mm)	Distribution (%)
4	4.75	13.88
5	4	10.46
6	3.36	15.78
8	2.36	35.33
10	2	17.03
12	1.7	6.09
18	1	0.93
25	0.71	0.08
50	0.3	0.04
pan	0.25	0.37

Table A.2. Bulk density

d_{gw} (mm)	ρ_b (kg/m ³)	Mean (kg/m ³)	St.dev.
fine	464.439	459.935	7.022
	451.844		
	463.522		
medium	427.562	434.860	6.441
	439.748		
	437.269		
coarse	422.704	417.394	5.228
	412.252		
	417.228		

Table A.3. Tap density

d_{gw} (mm)	ρ_t (kg/m ³)	Mean (kg/m ³)	St.dev.
fine	613.000	601.667	9.866
	595.000		
	597.000		
medium	551.000	546.333	5.033
	541.000		
	547.000		
coarse	485.000	486.000	2.646
	484.000		
	489.000		

Table A.4. Particle density

d_{gw} (mm)	ρ_p (kg/m ³)	Mean (kg/m ³)	St.dev.
fine	1497.654	1498.512	2.398
	1496.662		
	1501.221		
medium	1452.304	1456.984	4.243
	1460.580		
	1458.068		
coarse	1440.521	1439.110	2.745
	1435.946		
	1440.862		

Table A.5 Porosity

d_{gw} (mm)	ϵ	Mean	St.dev.
fine	0.690	0.693	0.004
	0.698		
	0.691		
medium	0.706	0.702	0.004
	0.699		
	0.700		
coarse	0.707	0.710	0.003
	0.713		
	0.710		

Table A.6. Hausner Ratio

d_{gw} (mm)	H_R	Mean	St.dev.
fine	1.269	1.270	0.006
	1.277		
	1.265		
medium	1.300	1.281	0.017
	1.276		
	1.266		
coarse	1.136	1.145	0.012
	1.142		
	1.159		

Table A.7. Compressibility of pecan shells

d_{gw} (mm)	P (kPa)	C (%)	d_{gw} (mm)	P (kPa)	C (%)	d_{gw} (mm)	P (kPa)	C (%)
0.212	1.5	3.740	1.241	1.5	2.180	2.194	1.5	1.538
0.212	1.5	3.480	1.241	1.5	1.846	2.194	1.5	1.388
0.212	1.5	3.466	1.241	1.5	1.253	2.194	1.5	1.331
0.212	3	5.028	1.241	3	2.665	2.194	3	1.815
0.212	3	4.982	1.241	3	3.302	2.194	3	1.982
0.212	3	4.977	1.241	3	3.242	2.194	3	2.399
0.212	6	7.015	1.241	6	3.906	2.194	6	3.377
0.212	6	7.604	1.241	6	4.679	2.194	6	3.228
0.212	6	7.429	1.241	6	4.252	2.194	6	4.028
0.212	9	8.374	1.241	9	4.645	2.194	9	4.020
0.212	9	8.604	1.241	9	4.645	2.194	9	3.573
0.212	9	8.429	1.241	9	5.164	2.194	9	3.741
0.212	12	9.658	1.241	12	5.428	2.194	12	4.655
0.212	12	9.723	1.241	12	5.838	2.194	12	4.337
0.212	12	9.337	1.241	12	5.625	2.194	12	4.214
0.212	15	10.375	1.241	15	6.631	2.194	15	5.359
0.212	15	10.392	1.241	15	6.156	2.194	15	5.102
0.212	15	10.452	1.241	15	6.670	2.194	15	4.572

Table A.8. Flow function data

d_{gw} (mm)	0.212		1.241		2.194	
P (kPa)	M.C.S. (kPa)	U.Y.S. (kpa)	M.C.S. (kPa)	U.Y.S. (kpa)	M.C.S. (kPa)	U.Y.S. (kpa)
3	8.31	1.215	5.05	1.839	5.15	2.661
3	7.29	0.977	4.32	0.870	8.74	1.869
3	8.66	1.459	6.24	1.703	6.99	2.724
6	17.48	1.246	9.45	2.764	15.36	2.422
6	15.75	3.589	9.88	2.606	17.23	3.744
6	15.62	2.407	13.82	1.562	16.04	2.803
9	24.85	3.243	27.28	2.843	24.89	6.029
9	24.27	2.311	23.04	5.888	27.56	4.958
9	26.29	5.173	13.55	4.148	21.97	8.564
12	33.34	2.501	32.18	1.829	32.98	3.363
12	32.17	5.742	28.53	4.587	24.22	2.254
12	33.33	2.039	21.55	5.249	33.71	8.169
15	40.46	3.070	29.14	4.514	52.69	2.824
15	44.96	3.335	30.09	12.410	45.92	1.146
15			34.21	7.829	46.61	6.675
21			31.80	11.486	64.63	12.144
21			41.72	10.626	45.92	13.994
21			57.67	13.255	61.39	6.929

Table A.9. Cohesion and angle of internal friction

d_{gw} (mm)	0.212		1.241		2.194	
P (kPa)	c (kPa)	φ (°)	c (kPa)	φ (°)	c (kPa)	φ (°)
3	0.26	43.66	0.54	29.16	0.43	28.54
3	0.22	41.52	0.24	32.23	0.48	35.63
3	0.30	45.29	0.42	37.51	0.41	31.00
6	0.25	46.28	0.76	32.39	0.52	43.52
6	0.72	43.54	0.65	36.98	0.93	37.17
6	0.51	44.07	0.33	44.19	0.57	45.73
9	0.65	46.31	1.81	38.14	1.34	42.07
9	0.50	43.21	1.26	43.66	0.83	46.87
9	1.16	41.69	1.39	22.34	2.03	39.27
12	0.54	43.29	0.35	48.12	0.61	50.12
12	1.21	44.29	0.98	43.73	0.50	42.15
12	0.41	46.18	1.36	35.21	1.79	42.67
15	0.63	46.66	1.16	35.60	0.48	52.45
15	0.70	44.46	1.93	37.51	0.34	43.31
15					1.16	51.67
21			3.23	31.29	2.58	43.96
21			2.71	35.95	3.02	43.31
21			2.61	47.01		

Appendix B. Effect of moisture content on physical properties

Table B.1. Particle size distribution

US Sieve No.	Aperture size (mm)	Distribution (%)				
		MC = 4.21%	MC = 8.96%	MC = 14.59%	MC = 18.36%	MC = 24.56%
10	2.00	0.68	0.75	0.98	2.91	5.07
12	1.70	13.10	16.52	20.19	26.94	30.90
14	1.40	36.83	36.56	36.87	36.73	35.28
16	1.18	27.66	26.78	25.08	22.20	20.52
18	1.00	14.36	14.27	13.18	8.88	6.87
20	0.85	5.71	3.28	2.45	1.41	0.67
60	0.25	0.22	0.63	0.31	0.52	0.27
140	0.11	0.42	0.11	0.30	0.14	0.16
pan		1.01	1.09	0.63	0.28	0.26

Table B.2. Bulk density

M.C. (% wb)	ρ_b (kg/m ³)	Mean (kg/m ³)	St.dev.
4.42	460.480	460.837	1.468
	459.581		
	462.450		
8.41	462.078	458.978	4.160
	460.607		
	454.250		
14.73	434.790	436.089	1.172
	436.407		
	437.069		
19.36	437.778	434.684	2.719
	432.674		
	433.601		
24.70	398.376	396.369	1.826
	395.924		
	394.807		

Table B.3. Tap Density

M.C. (%_{wb})	ρ_t (kg/m³)	Mean (kg/m³)	St.dev.
4.42	537.000	537.000	1.000
	536.000		
	538.000		
8.41	526.000	536.333	8.963
	541.000		
	542.000		
14.73	510.000	514.333	4.041
	518.000		
	515.000		
19.36	506.000	508.667	2.517
	511.000		
	509.000		
24.70	471.000	472.667	1.528
	474.000		
	473.000		

Table B.4. Particle Density

M.C. (%_{wb})	ρ_p (kg/m³)	Mean (kg/m³)	St.dev.
4.42	1430.647	1429.833	0.993
	1428.727		
	1430.125		
8.41	1421.400	1421.747	0.375
	1421.694		
	1422.146		
14.73	1412.281	1412.409	0.390
	1412.098		
	1412.847		
19.36	1390.704	1390.944	0.265
	1391.229		
	1390.901		
24.70	1376.527	1375.651	0.858
	1375.614		
	1374.813		

Table B.5. Porosity

M.C. (%_{wb})	ϵ	Mean	St.dev.
4.42	0.678	0.678	0.001
	0.678		
	0.677		
8.41	0.675	0.677	0.003
	0.676		
	0.681		
14.73	0.692	0.691	0.001
	0.691		
	0.691		
19.36	0.685	0.687	0.002
	0.689		
	0.688		
24.70	0.711	0.712	0.001
	0.712		
	0.713		

Table B.6. Hausner Ratio

M.C. (%_{wb})	H_R	Mean	St.dev.
4.42	1.116	1.137	0.018
	1.147		
	1.147		
8.41	1.147	1.141	0.006
	1.141		
	1.136		
14.73	1.136	1.133	0.006
	1.136		
	1.126		
19.36	1.152	1.154	0.003
	1.152		
	1.157		
24.70	1.147	1.150	0.006
	1.147		
	1.157		

Table B.7. Compressibility of pecan shells

M.C. (%, w.b.)	P (kPa)	C (%)	M.C. (%, w.b.)	P (kPa)	C (%)	M.C. (%, w.b.)	P (kPa)	C (%)
4.42	1.5	1.957	8.41	1.5	0.769	14.73	1.5	2.180
4.42	1.5	1.398	8.41	1.5	1.057	14.73	1.5	0.846
4.42	1.5	0.977	8.41	1.5	0.541	14.73	1.5	1.253
4.42	3	2.197	8.41	3	1.383	14.73	3	2.665
4.42	3	2.277	8.41	3	2.097	14.73	3	3.302
4.42	3	2.504	8.41	3	1.845	14.73	3	3.242
4.42	6	3.728	8.41	6	2.880	14.73	6	3.906
4.42	6	3.234	8.41	6	3.111	14.73	6	3.679
4.42	6	3.037	8.41	6	2.807	14.73	6	4.252
4.42	9	4.697	8.41	9	4.824	14.73	9	4.645
4.42	9	3.714	8.41	9	4.917	14.73	9	4.645
4.42	9	4.765	8.41	9	4.622	14.73	9	4.164
4.42	12	4.908	8.41	12	4.963	14.73	12	5.428
4.42	12	4.674	8.41	12	5.125	14.73	12	5.838
4.42	12	5.046	8.41	12	5.175	14.73	12	5.625
4.42	15	4.627	8.41	15	6.571	14.73	15	6.631
4.42	15	4.759	8.41	15	5.678	14.73	15	6.156
4.42	15	4.930	8.41	15	5.048	14.73	15	6.670

M.C. (%, w.b.)	P (kPa)	C (%)	M.C. (%, w.b.)	P (kPa)	C (%)
19.36	1.5	1.510	24.7	1.5	3.559
19.36	1.5	1.869	24.7	1.5	4.163
19.36	1.5	1.917	24.7	1.5	3.491
19.36	3	3.642	24.7	3	5.444
19.36	3	2.839	24.7	3	5.826
19.36	3	2.869	24.7	3	5.164
19.36	6	4.354	24.7	6	7.252
19.36	6	4.728	24.7	6	7.459
19.36	6	3.832	24.7	6	7.227
19.36	9	5.328	24.7	9	8.317
19.36	9	5.409	24.7	9	7.165
19.36	9	5.025	24.7	9	8.535
19.36	12	5.778	24.7	12	9.494
19.36	12	6.478	24.7	12	8.946
19.36	12	6.256	24.7	12	10.316
19.36	15	6.264	24.7	15	10.792
19.36	15	6.996	24.7	15	10.337
19.36	15	6.244	24.7	15	10.928

Table B.8. Flow functions of pecan shells

M.C. (% w.b.)	4.11		8.53		14.57	
P (kPa)	U.Y.S. (kPa)	M.C.S. (kPa)	U.Y.S. (kPa)	M.C.S. (kPa)	U.Y.S. (kPa)	M.C.S. (kPa)
3	0.52	5.25	1.23	4.23	1.84	5.05
3	0.68	4.74	1.20	7.20	0.87	4.32
3	0.74	7.42	0.37	6.37	1.70	6.24
6	1.55	15.82	2.23	10.23	2.76	9.45
6	1.90	12.06	2.87	12.87	2.61	9.88
6	1.70	8.22	2.91	11.91	1.56	13.82
9	1.65	19.09	3.18	20.18	7.44	27.28
9	1.54	19.54	4.56	23.56	5.89	23.04
9	2.79	24.32	2.20	19.20	4.15	13.55
12	3.15	32.49	3.14	33.14	1.83	32.18
12	2.51	27.80	3.34	30.34	4.59	28.53
12	2.13	36.74	3.67	27.71	5.25	21.55
15			6.51	35.17	4.51	29.14
15			4.81	32.81	12.41	30.09
15			6.32	30.32	7.83	34.21
21			8.24	40.24	11.48	31.80
21			8.21	45.30	10.62	41.72
21			7.67	56.67	13.26	57.67
M.C. (% w.b.)	18.67		24.23			
P (kPa)	U.Y.S. (kPa)	M.C.S. (kPa)	U.Y.S. (kPa)	M.C.S. (kPa)		
3	1.09	5.42	1.341	6.79		
3	1.12	5.34	1.089	5.22		
3	0.53	5.77	3.549	8.14		
6	2.38	10.05	8.116	12.48		
6	2.57	10.08	6.33	9.59		
6	2.67	14.21	3.07	11.67		
9	2.42	17.61	6.754	19.44		
9	1.63	20.88	9.762	22.78		
9	4.63	27.86	4.242	28.11		
12	6.24	28.38	16.655	45.03		
12	6.69	30.30	10.04	33.21		
12	7.34	24.85				
15	8.91	33.09	16.885	54.19		
15	9.73	36.88	17.948	60.4		
15	3.88	38.87				
21	18.34	50.69	25.668	63.29		
21	8.66	57.33	20.162	66.7		
21	13.29	61.85	13.187	39		

Table B.9. Cohesion and angle of internal friction

M.C. (% <i>, w.b.</i>)	4.11		8.53		14.57	
P (kPa)	ϕ (kPa)	c (kPa)	ϕ (kPa)	c (kPa)	ϕ (kPa)	c (kPa)
3	40.12	0.12	37.89	0.3	29.16	0.54
3	28.77	0.2	39.97	0.28	32.23	0.24
3	42.19	0.16	43.71	0.08	37.51	0.42
6	54.21	0.25	35.84	0.57	32.39	0.76
6	34.39	0.5	34.23	0.76	36.98	0.65
6	10.32	0.71	39.31	0.69	44.19	0.33
9	42.94	0.36	40.64	0.73	38.14	1.81
9	45.84	0.11	34.27	1.15	43.66	1.26
9	38.78	0.19	40.34	0.51	22.34	1.39
12	46.29	0.23	39.52	0.74	48.12	0.35
12	40.94	0.8	41.78	0.3	43.73	0.98
12	41.21	0.71	27.7	1.11	35.21	1.36
15			31.35	2.67	35.6	1.16
15			46.03	0.77	32.7	3.39
15			42.56	0.73	37.51	1.93
21			33.36	2.76	31.29	3.23
21			34.08	3.24	35.95	2.71
21			39.08	2.54	47.01	2.61
M.C. (% <i>, w.b.</i>)	18.67		24.23			
P (kPa)	ϕ (kPa)	c (kPa)	ϕ (kPa)	c (kPa)		
3	37.16	0.27	34.86	0.35		
3	32.03	0.31	30.66	0.31		
3	41.53	0.12	41.35	0.35		
6	31.28	0.67	54.24	0.18		
6	31.5	0.72	25.52	1.05		
6	37.39	0.66	37.54	0.51		
9	39.47	0.57	43.21	2.11		
9	41.18	0.37	49.1	1.82		
9	40.37	1.07	54.04	2.08		
12	41.64	1.4	44.83	1.8		
12	41.96	1.49	44.42	2.21		
12	36	1.87				
15	49.6	1.64	55.71	2.46		
15	43.12	2.11	49.38	4.75		
15	46.22	0.78				
21	36.32	4.64	49.38	4.75		
21	50.61	1.55	54.16	3.26		
21	48.92	2.49	59.3	1.81		

Appendix C. Rate of Moisture Sorption of Pecan Shells

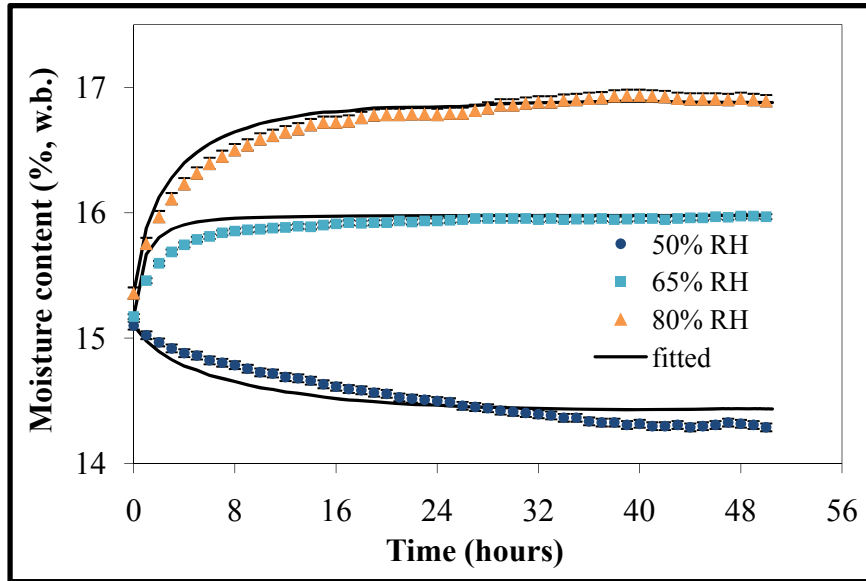


Figure C.1. Moisture change in pecan shells exposed to air at 25°C and relative humidity levels of 50, 65 and 80%. Initial moisture content was 15.02% (w.b.)

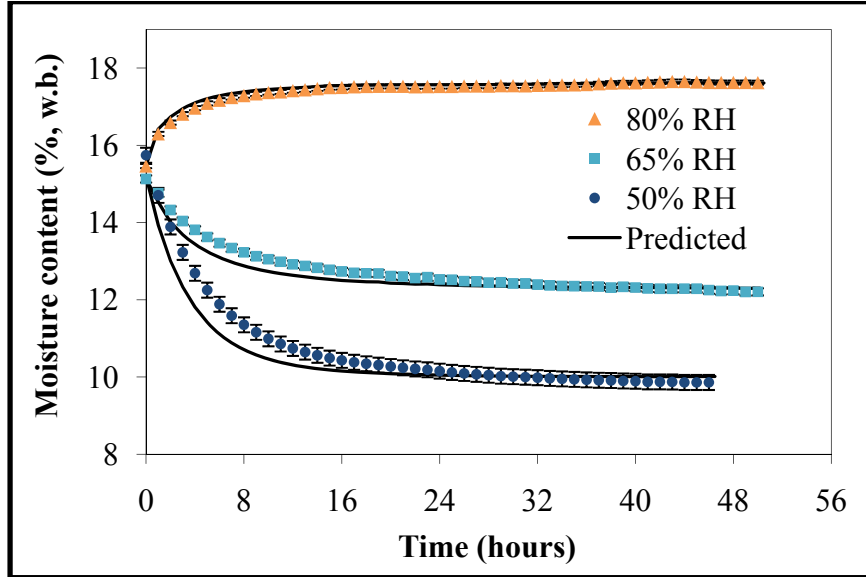


Figure C.2. Moisture change in pecan shells exposed to air at 35°C and relative humidity levels of 50, 65 and 80%.

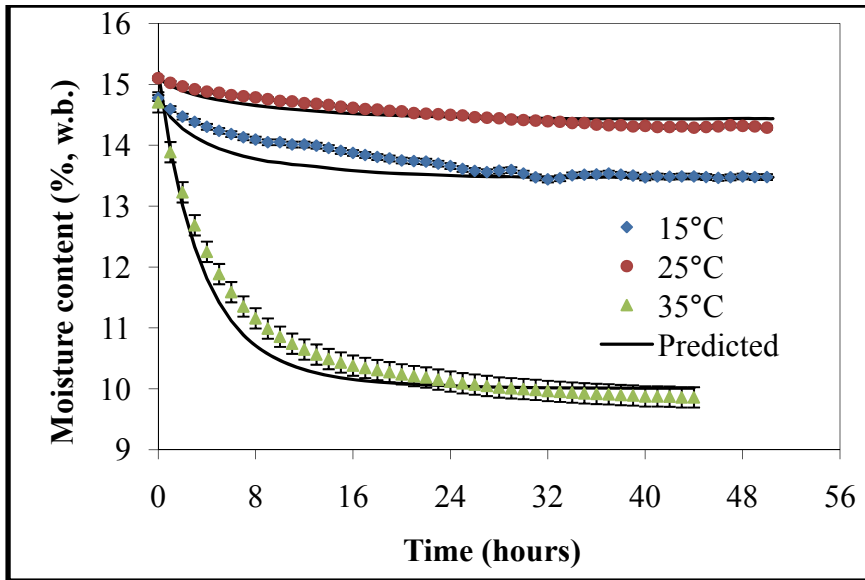


Figure C.3. Moisture change in pecan shells exposed to air at 50% relative humidity and temperatures of 15, 25 and 35°C.

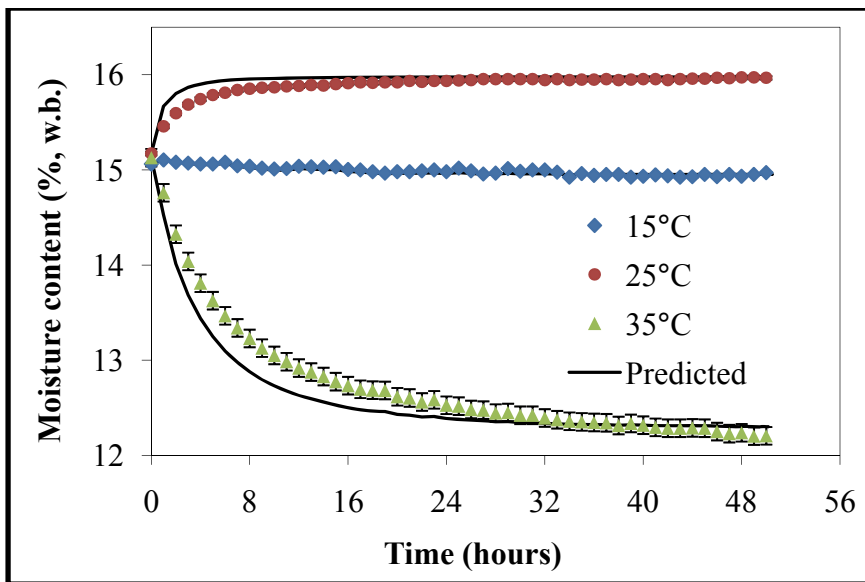


Figure C.4. Moisture change in pecan shells exposed to air at 65% relative humidity and temperatures of 15, 25 and 35°C.

Appendix D. Equipment Photos



Figure D.1. Annular shear cell



Figure D.2. Texture analyzer with compression cell and tight fitting piston



Figure D.3. Compression cell with tight fitting piston filled with fine, medium and coarse pecan shell samples (left to right)



Figure D.4. Thermogravimetric analyzer (right) connected to Fourier-transform infrared spectrometer (left) by heated Teflon tube.